UNIVERSITAT DE BARCELONA

Understanding the role of sensor diversity and redundancy to encode for chemical information in gas sensor arrays

Luis Fernández Romero

UNIVERSITAT DE BARCELONA

FACULTAT DE FÍSICA
Departament d'Electrònica

MEMÒRIA PER OPTAR AL TÍTOL DE DOCTOR PER LA UNIVERSITAT DE BARCELONA

Doctorat en Enginyeria i Tecnologies Avançades (RD 99/2011)

UNDERSTANDING THE ROLE OF SENSOR DIVERSITY AND REDUNDANCY TO ENCODE FOR CHEMICAL INFORMATION IN GAS SENSOR ARRAYS

Autor:
Luis Fernández Romero

Director:
Dr. Agustín Gutiérrez Gálvez

Tutor:
Dr. Santiago Marco Colás

Barcelona, 5 Octubre 2015

Elena es, probablemente, la persona que menos se parece a mí en este mundo. En verdad que su sonrisa es perenne y sus gestiones eléctricas. Parece inmune al desaliento. Es tan vital y corajuda (en sus dos acepciones) que enrojece el rostro abandonar cuando te escruta con sus ojos rasgados de oriente. Cualquiera la querría sólo por eso. Sin embargo, yo también la adoro por una razón más anodina y vanidosa: Elena no me comprende. Casi nunca. A veces, puedo provocarle una divertida extrañeza. Otras, un colorido rechazo. Las que más, una triste desespero. Es un hecho que no nos parecemos. Pero persevera. Persevera en mí con una fe que me sobrecoge, pues tampoco puedo comprenderla. Todo ese galimatías que soy quiere convertirlo en algo hermoso. Piensa que valgo la pena. Ni siquiera sé si lo merezco, pero de algún modo, ella lo sabe. Por todo esto, Elena es la primera. No puedo negociar este punto. Ella es la primera. Es la mujer que quiero y le dedico mi más profundo y sentido agradecimiento. Y en estas líneas queda escrito.

ABSTRACT

Electronic noses (e-noses) have been utilized during the past three decades as general purpose instruments for chemical sensing. These instruments are inspired by natural olfactory systems, where fine odour discrimination is performed without the necessity for highly specialized receptors. The key advantage provided by this approach is that odour representation is more efficient and robust when the encoding is performed by the population of receptors than by any of its individual elements. A population of receptors obtains its maximum performance in encoding odour stimulus features when it balances the benefits of sensory diversity and redundancy. Though, traditional electronic noses tend to exhibit a limited number of sensor units with very much correlated responses to odour stimuli. However, it has not been until recently that large arrays of cross-selective have become technologically available.

The objective of this dissertation is to develop one of these new generation arrays to investigate the advantages odour stimuli representation through population coding supported by sensor diversity and redundancy. In particular, we have built a chemical sensing system based on an array of metal oxide (MOX) gas sensors, and endowed with a high a degree of sensor diversity and redundancy.

We have used this bio-inspired sensing architecture alongside statistical pattern recognition techniques to cope with some of the unsolved problems in machine olfaction, namely, robustness to sensor failure, feature selection, and calibration transfer between e-nose instruments.

AGRADECIMIENTOS

Esta tesis que ahora lees no la pude escribir solo. Me ayudaron muchas manos a escribirla. Sujetaron el candil cuando el túnel era oscuro. Me colmaron de caricias. Me cedieron su paraguas en la lluvia. Y, por supuesto, me dieron la mano. Es tiempo dar gracias y que mis manos las aplaudan.

Permitidme empezar por mi familia. Hace poco sufrimos una gran pérdida. Mi padre falleció meses antes de finalizar esta memoria. Siempre es pronto para despedirse de un ser querido, pero yo no sabía que podía ser tan pronto. Fue un hecho tan brutal y despiadado que no admitió réplicas. Casi todo lo importante quedó por decirse. Me hubiera gustado agradecerle todos los buenos momentos que vivimos juntos: Los consejos, las charlas banales, incluso las discusiones. Que se sintiera reconocido y feliz. A mis hermanos, Javier y Víctor, y a mi madre, Araceli, les agradezco toda una vida de alegrías en familia. Hemos tenido nuestras risas y lágrimas, pero creo que más risas. Encajamos el golpe con entereza y todavía seguimos en pie. A mi cuñada Inma le agradezco ese balón de oxígeno que fue para nosotros el nacimiento de Clara. Nos enamoramos de ella a primera vista. También quiero agradecer a mi otra familia, Elena, Rafael, Carmen, Andrés y Nuria, todas las atenciones y fiestas que he recibido en su casa, especialmente las que llegaron a través de Júlia, que es la luz de mi vida. No hay palabras para agradecer la devoción que sienten por ella.

Me gustaría dar las gracias al Dr. Santiago Marco por ofrecerme la oportunidad de realizar esta tesis doctoral. Tengo que decir de él que le tengo por una persona justa, aunque no se prodigue en halagos. También que se preocupa activamente por el bienestar de quienes están a su cargo. Agradezco encarecidamente el soporte recibido por parte de mi supervisor, el Dr. Agustín Gutiérrez. Supo templar mis inseguridades y llevar esta tesis a buen puerto. Me quedo con muchas conversaciones interesantes (algunas fueron hasta divertidas) sobre la naturaleza de la diversidad y la redundancia sensorial. Realmente, la información estaba ahí. Al Dr. Antonio Pardo, le agradezco su bonhomía y pragmatismo. Todo lo soluciona, sin hacer ruido y con buena letra. Siempre estuvo en los momentos importantes y, en particular, en uno.

Durante los tres meses que estuve de estancia en la Universidad Manchester, me integré al grupo de trabajo del Profesor Krishna Persaud. Fue, en muchos aspectos, una gran experiencia. Quisiera recalcar que los componentes del grupo, Liviu, Mara, Elena, Daniella, Anna Maria y el propio Krishna se esforzaron mucho para hacerme sentir como en casa. Fueron muy considerados conmigo. Les quiero mostrar ahora todo mi agradecimiento.

A mis compañeros del IBEC y de la Facultad de Física quiero decirles que me siento muy afortunado de haber conocido a unas personas con caracteres tan dispares y, sin embargo, tan bien avenidas. Por ello, muchas gracias a: Marta, Jordi, Sergi, Víctor, Ana,

Miguel, Didier, Ariadna, Núria, Nil, Juanma, Raquel, Sergio, Elena, Oriol, Núria, Omar, Aïda, Adriana y Marina. Quisiera hacer mención especial a tres compañeros que por diferentes motivos han sido mi respaldo en tiempos de tribulación. No puedo dejar de agradecer a Erola sus increíbles ganas de vivir. Ella fue la primera persona que logró hacerme reír hasta llorar cuando creí que ya no volvería a hacerlo nunca. Inevitablemente, me hizo cosquillas en el alma. Me gustaría tenerla aún cerca, pues las horas con ella se llenaban de realismo mágico. Espero que siempre seamos amigos. Tampoco quiero olvidarme de Anita, con quién compartí muchas horas de clases y despacho, y a la que añoro tanto. Nos separa un océano pero la tengo muy cerca en el pensamiento. Le agradezco todo su coraje y empeño por sacar aquellas clases adelante, así como su desinteresada amistad. Finalmente, quiero agradecer a Sergio su gran corazón y total predisposición a ayudar a los demás. Muchas dificultades técnicas de esta tesis se resolvieron gracias a su mano experta y su actitud positiva. Es realmente difícil no sentirse en deuda con él. Le pido que acepte este pequeño regalo para su vanidad.

Para acabar, quiero nombrar aquí a una serie de personas que llevan mi existencia a la plenitud y suelen ir de la mano con mi esperanza. Algunas me conocen desde casi mi infancia. Otras llegaron mucho más tarde. Pero afortunadamente todas se quedaron, y se lo agradezco. Ellos son mis amigos y amigas: Carlos, David, Noelia, Tamer, Elvira, Dani, María Noel, Fernando y Álex.

TABLE OF CONTENTS

List of Tables

List of Figures

CHAPTER I

INTRODUCTION

Electronic noses (e-noses) have been utilized during the past three decades as general purpose instruments for chemical sensing. These instruments are inspired by natural olfactory systems, where fine odour discrimination is performed without the necessity for highly specialized receptors. Instead, odour information is extracted in these systems using arrays of broadly tuned receptors organized in a convergent pathway. Such a sensing architecture allows combining the responses of the array of receptors, giving rise to particular representations of the different odour stimuli. The key advantage provided by this approach is that odour representation is more efficient and robust when the encoding is performed by the population of receptors than by any of its individual elements (hyper-acuity).

A population of receptors obtains its maximum performance in encoding odour stimulus features when it balances the benefits of sensory diversity and redundancy. By *sensor diversity* we understand the number of different receptor types responsible for enhancing the variability of the array response to a collection of odours. Likewise, by *sensor redundancy* we refer to the average number of receptor replicates on a population. The role of sensory redundancy accounts for the robustness to receptor damage and noise exhibited by the odour stimuli representation. This variety of odour receptor types along

with its outstanding number of receptors is characteristic of natural olfactory systems. Though, traditional electronic noses tend to exhibit a limited number of sensor units with very much correlated responses to odour stimuli. Several strategies to enhance odour representation in gas sensor arrays are based on boosting sensor diversity and redundancy. However, it has not been until recently that large arrays of cross-selective have become technologically available.

The aim of this work is to develop one of these new generation arrays to investigate the advantages odour stimuli representation through population coding in artificial olfaction **(i)**. In particular, we propose to build a chemical sensing system based on an array of metal oxide (MOX) gas sensors, and endowed with a high a degree of sensor diversity and redundancy **(ii)**. We propose the use this bio-inspired sensing architecture alongside statistical pattern recognition techniques to cope with some of the unsolved problems in machine olfaction. Among others, this dissertation addresses the following issues: **(iii)** Robustness to sensor failure of highly redundant arrays, **(iv)** Feature selection in temperature modulated sensor arrays and, **(v)** Calibration transfer between replicate e-nose instruments.

I.1. CONTRIBUTIONS OF THIS WORK

As abovementioned, only a few large arrays of sensors have been developed for chemical sensing. This fact definitely limits the number of contributions that study odour stimuli representation using population coding with real data. We propose to enhance the

performance of our gas sensor array taking advantage of the population coding properties of sensor diversity and redundancy. The main contributions of this work research are summarized as follows:

(1) We propose a functional definition of sensor diversity and redundancy based on the clustering of the array features.

(2) We compare with a simple model the different way how natural and artificial olfactory systems encode for odour information. We model the encoding power of an array of sensors as a function of their molecular receptive range.

(3) We study the effect of sensor noise on odour concentration encoding. We propose to decrease the contribution of the independent sensor noise by means of sensor feature averaging and sensor array optimization.

(4) We perform a comprehensive to study the role of sensor redundancy in the robustness to sensor failure of an array of sensors. In particular, we investigate the effect of sensor failure dependency on the array's odour discrimination capabilities.

(5) We propose an update of feature selection technique based on maximizing the variability of the array response to a collection of odours. We use this technique to optimize the heater profile of an array of MOX sensors in terms of odour discrimination.

(6) We perform instrument standardization between temperature modulated gas sensor arrays to correct global shifts of temperature. A method to categorize the quality of the calibration transfer based on the bias-variance trade-off is presented.

I.2. ORGANIZATION OF THIS DISSERTATION

Chapter II introduces the e-nose instrument: definition, origin and evolution of the device. We present a review of the sensor technologies, pattern recognition techniques and odour delivery system mostly employed in artificial olfaction. We present the different large arrays of cross-reactive gas sensors arrays found in the literature. Also we include the description of the e-nose prototype developed and the datasets acquired using this instrument to address the experimental requirements of this dissertation. In Chapter III we revise the role of sensor diversity and redundancy, respectively, in enhancing odour discrimination and maintaining stable odour representations in spite of sensor noise. Also we propose a functional definition for sensor diversity and redundancy in an array of sensors. Chapter IV studies the role of sensor redundancy to assist the robustness to sensor damage in gas sensor arrays. In Chapter V we update a feature selection method to include the benefit of sensor redundancy in reducing sensor noise. Chapter VI is

practical case of study of instrument correction assisted by sensory redundancy. More specifically, this chapter devoted to instrument standardization between e-noses by means of calibration techniques. Chapter VII draws conclusions from this dissertation. Finally, we present in Chapter VIII a brief a summary of this work translated to Spanish.

CHAPTER II

THE ELECTRONIC NOSE

The breadth and discriminatory power exhibited by biological olfaction in chemical sensing was the source of inspiration for the field of machine olfaction (Persaud and Dodd, 2000). Machine olfaction- an automated simulation of the sense of smell- is an emerging application of engineering that aims to detect, identify and/or quantify odours. The iconic instrument for odour sensing is called the electronic nose or e-nose. This instrument comprises an array of partially selective sensors, combined with a pattern recognition system capable of determining certain odour properties, such as identity, composition and concentration (Gardner and Bartlett, 1994a).

The electronic nose has been successfully employed in many industrial production processes, for such a diverse product classes/areas as food industry (Mandenius et al., 1984; Barlett et al., 1997; Connell et al., 2001), quality control (Van Deventer et al., 2002; Hansen et al., 2005), cosmetics (Branca et al., 2007), security (Scorsone et al., 2003; Moore, 2004; Yinon, 2006, Haddi et al., 2011), environmental monitoring (Baby et al., 2000), and biomedical research (Di Natale et al., 2000; Di Natale et al. ,2003; Phillips et al., 2003; Hasegawa et al., 2004; Dragonieri et al. 2007, Bailey et al., 2008; Tran et al., 2010; Shih et al., 2010).

This chapter is devoted to study the electronic nose as a general purpose instrument for chemical sensing, and it is divided in five sections: Section II.1, where we present the biological olfactory system; Section II.2, where we revise the state of the art in electronic noses; Section II.3, where we propose a design for a chemical sensing system based on an array of MOX sensors, and inspired by the architecture of the olfactory epithelium; Section II.4, where we explain in detail the different datasets acquired using our e-nose prototype; and finally, Section II.5 where we summarize the previous sections and conclude this chapter.

II.1. THE OLFACTORY SYSTEM

The sense of smell detects chemical information from odorants present in the environment. This capacity is shared by a vast number of species regardless its phylogenetic level, from simple bacteria to complex animals, being the most ancient of the senses of life. Among its many functions, the sense of smell assists life organisms in feeding, mating and warning against external dangers such as predators, toxics, food poisoning. The set of brain regions involved in smell perception are known as olfactory system. Throughout the history of life, evolution developed the olfactory system as a general tool responsible for the detection of the larger possible number of substances without any prior knowledge about the properties of those substances, preserving its fundamental organization (Hildebrand and Shepherd, 1997). As a result, the olfactory system is featured with large arrays of partially specific sensors in its sensory stage, followed by an extremely converging second layer architecture dedicated to integrate and

coding odorant information. In mammals, odour perception starts when airborne molecules enter through the nostrils and reach a small region of epithelial tissue on the roof of the nasal cavity covered with mucus, called the Olfactory Epithelium (OE). That tissue is populated by millions of Olfactory Receptor Neurons (ORNs), a type of cell endowed with Olfactory Receptor (ORs) proteins where odorants can bind to, which transduces the chemical information into electrical signals. ORNs expressing the same OR project their axons towards the olfactory bulb (OB) and merge in pseudo-spherical 50-100 μm structures (in diameter) known as glomeruli (Shepherd, 1998), in one the most severe cases of synapse convergence in nervous system (several thousands of ORNs per glomerulus). Axons leaving the OB glomeruli synapse to specialized regions of the brain such as the anterior olfactory nucleus, pyriform cortex, the medial amygdala and the entorhinal cortex, where odour olfactory patterns are intensively processed (Morris and Schaeffer, 1953)

Odour quality (identity) and quantity (concentration) encoding is achieved in the olfactory epithelium through the high ORN variety and their outstanding number of replicates. The kind of variety responsible for odour quality encoding is provided by the large amount of ORNs types (Buck and Axel, 1991): There are as many as 1000 genes for expressing ORs in mammals, being one of the largest gene families of their genome. These ORs have a broad sensitivity to odorants, displaying overlapping selectivities with different affinities for the different compounds. Since one particular OR protein characterizes the ORN type and this determines, through chemotropic convergence, its

corresponding glomerulus, odour quality is encoded as a spatiotemporal patterns of glomerular activity in the OB. Regarding odour quantity, the variety responsible of its encoding is the diversity within ORN types: Cells expressing identical ORs present significant discrepancies in parameters that play a key role in concentration-conductance transduction, such as shape, size and number of receptors (Vermeulen et al., 1997). Consequently, ORNs belonging to the same type exhibit a variety of dose-response curves. As each cell replicate is tuned for a given range of odour intensities, odour quantity encoding is performed by the entire population of neurons showing olfactory thresholds usually lower than those obtained from single cell measurements (Grosmaitre et al., 2006).

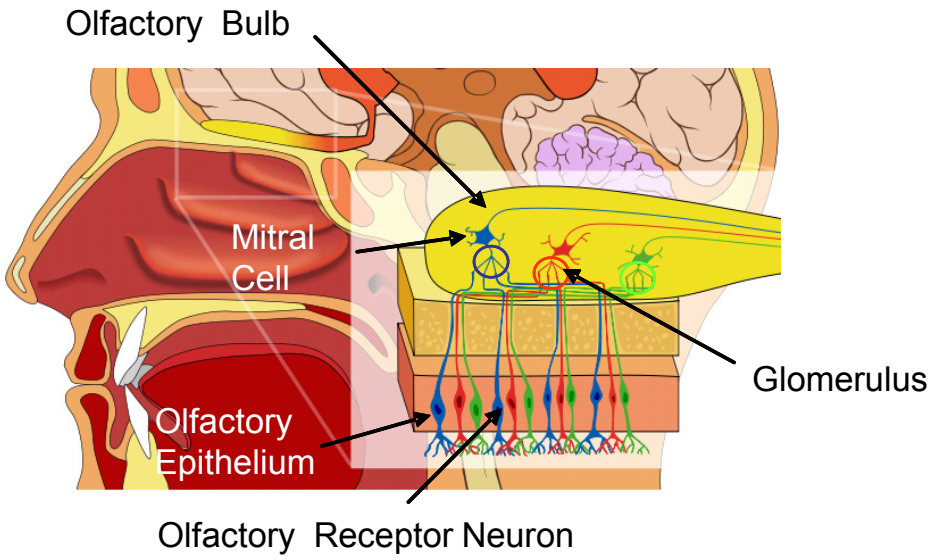

Fig. 1. Brain human sagittal section. The enlarged region on the picture corresponds to the Olfactory Epithelium and the Olfactory Bulb (adapted from 'Head lateral mouth anatomy.jpg' by Patrick J. Lynch, medical illustrator).

II.2. STATE OF THE ART IN ELECTRONIC NOSES

In this section, we review the state of the art of the electronic nose technology. We present the architecture of the classic e-nose instrument (including the most employed sensor technologies, odour delivery systems and pattern recognition techniques), in Section II.2.1. Next, we show the most advanced prototypes of e-nose found in the literature, in Section II.2.2.

II.2.1. Sensor technologies

Different sensor technologies, such as Metal Oxide Sensors (MOX), Metal Oxide Field Effect Transistors (MOSFET), Conducting Polymers (CP), Quartz Microbalance Sensors (QCM) and Surface Acoustic Wave Sensors (SAW), Optical sensors are broadly used is in gas detection (Arshak et al., 2004). We review these technologies, emphasizing their strengths and weaknesses.

II.2.1.1. Metal Oxide Sensors (MOX)

The principle of operation of the MOX sensor is based on their change of conductivity in response to a gas. There exist two types of MOX sensors: the n-type and p-type sensors, which are sensitive respectively, to reducing and oxidizing gases. N-type MOS sensors work as follows: The oxygen present in the atmosphere reacts with the semiconductor trapping free electrons present in the surface, or between the grain boundaries of the oxide. Due to the lack of carriers, the potential barrier between grains increases. As a result, the resistance of the semiconductor is increased in these areas (Barsan et al.,

2007). When a n-type MOS sensor is exposed to a reducing gas (H_2, CH_4, CO, H_2S or C_2H_4) in presence of oxygen, the gas reacts with the chemically adsorbed oxygen species and releases an electron to the material. This reduces the potential barrier between grains, allowing the electrons to circulate and decreasing the resistance of the material. On the other hand, p-type sensors respond to oxidizing gases (O_2, NO_2, and Cl_2), which extract electrons of the semiconductor, also reducing the resistance of the semiconductor (Albert and Lewis, 2000).

The main advantages of MOX sensors are their fast responses and recovery times, and their high sensitivities (Pearce et al., 2003). However, they exhibit poor selectivities, tend to have high power consumption and suffer from irreversible poisoning when exposed to volatile sulphur compounds (Dickinson et al., 1998).

MOX sensor's selectivity is markedly affected by its operating temperature since this parameter governs the kinetics of the oxido-reduction reactions that take place on the semiconductor surface (Clifford and Tuma, 1983a; Clifford and Tuma, 1983b). As a result, different oxido-reduction reactions tend to occur at different temperatures so the selectivity of the sensor also varies with temperature. In other words, that is to tune the individual gas influence to the total response. This temperature-selectivity dependence can be exploited to increase the discriminatory information provided by the sensor (Benkstein et al., 2009; Rogers et al., 2011; Rogers et al., 2012). Using this technique, the

sensor's operating temperature is modulated by applying a variable heater voltage during the gas exposure. The resulting sensor reading is a waveform characteristic of the given gas mixture (Lee and Reedy, 1999).

There are two approaches to perform temperature modulation with MOX sensors: thermal transients and temperature cycling (Gutierrez-Osuna et al., 2003). In thermal transients, sensor temperature is changed abruptly by means of step or pulsed heater voltage functions, and the discriminatory information is contained in the induced thermochemical transient. Conversely, in temperature cycling, sensor temperature is modified by the use of periodic, slowly varying heater voltage functions (sinusoidal, ramp profile, etc.), and the discriminatory information is found in the collection of *pseudo-sensors* corresponding to the set sensitivities obtained at different temperature.

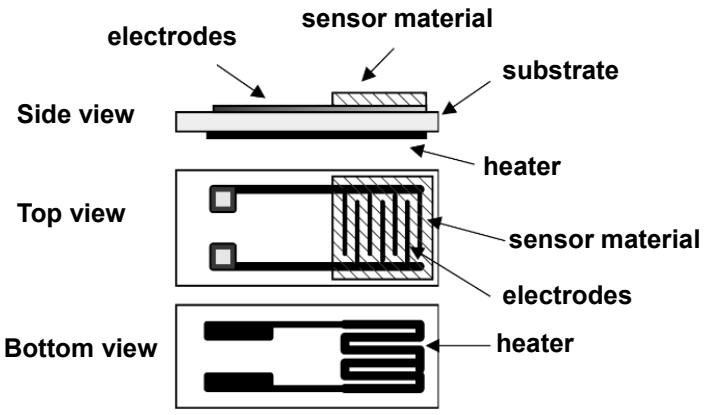

Fig. 2. Structure of a MOX gas sensor. A MOX sensor comprises a metal oxide and a resistive heater (adapted from Arshak et al., 2004).

II.2.1.2. Metal Oxide Field Effect Transistors (MOSFET)

MOSFET gas sensors working principle relies on the variation of the electrical conductivity experienced by a MOSFET transistor when exposed to a volatile compound. This type of sensors consists of a catalytic metal gate (iridium, palladium or platinum) on top of an oxide layer (typically SiO_2), and a p-type silicon with n-doped regions under the source and drain terminals, working in common source configuration (Gardner and Barlett, 1999; Pearce et al., 2003). Under such conditions, the voltage applied at the metal gate determines the current through the sensor. Above a threshold value of the gate voltage, an inversion layer (a channel) is created at the semiconductor-insulator boundary, allowing a current flow from source to drain terminals. The products of reaction between the catalytic metal of the gate and the gas species molecules through the gate create a dipole layer at the metal-semiconductor interface. As a result, the I-V characteristic of transistor is modified (the current through the device is different for the same value of gate voltage). The sensor response is measured by the change of gate voltage needed to maintain the source to drain current constant, usually the sensor response to a reference gas.

MOSFETs gas sensors can be fabricated using standard microelectronic techniques, fact that increases their repeatability. In addition to this, they can be operated at room temperature, reducing the power consumption. On a negative note, they present poor response variability to different gases due to a lack of sensitive materials, suffer from

baseline drift and instability, and need of accurate control of their surrounding environment because temperature dramatically affects their selectivity and sensitivity characteristics.

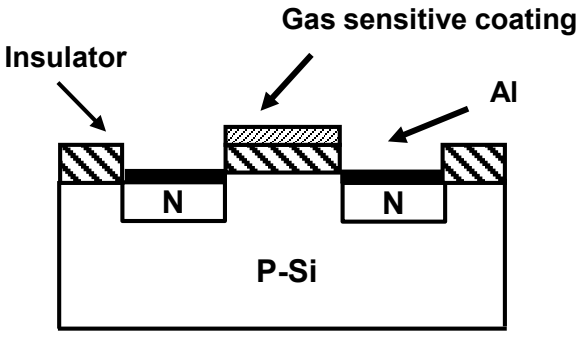

Fig. 3. Structure of a MOSFET gas sensor. The interaction between the gas molecules and the sensitive material on the gate allows the formation of the channel between gate and source terminals (adapted from Arshak et al., 2004).

II.2.1.3. Conducting Polymers (CP)

CP sensors measure the change of conductivity experienced by a polymer when interacting with organic vapours (Albert and Lewis, 2000). The polymer itself is composed by a chain of organic molecules (monomers) that generate orbital along the chain, allowing the circulation of charges through the material. The most commonly used polymers in CP sensors are polypyrrole, polyaniline, the politiofen and poyacetylene, which are formed respectively, by monomers of pyrrole, aniline and tiofen (Pearce et al., 2003). CP sensors can be doped so as to behave as semiconductors or conductors

(Heeger, 2001; Yasufuku 2001). When doped, CP sensors alter their band structure, inducing also an increase in the mobility of electrons (n doping) or holes (p doping). The conductive polymers are generally deposited on a substrate with interdigitate electrodes using electrochemical techniques or by chemical polymerization (Freund and Lewis, 1995; Yasufuku, 2001).

CP sensors have a number of advantages: First, a large variety of conducting polymers is commercially available (Albert and Lewis, 2000). Also, they operate at room temperature (Shurmer and Gardner, 1992), fact that simplifies the electronics of the measurement system and decreases their power consumption. Finally, CP sensors present fast responses and short recovery times for a wide range of analytes. Unfortunately, this type of sensors presents some drawbacks, such as a high sensitivity to moisture and temperature changes, and a tendency to drift over time. In addition to this, CP sensors manufacturing is complex and costly, with strong variations in sensor's characteristics between units of different batches (Nagle et al., 1998). Another drawback of CP sensors is its limited lifetime, typically from 9 to 18 months, due to the oxidation of the polymer sensing layer (Schaller el al., 1998).

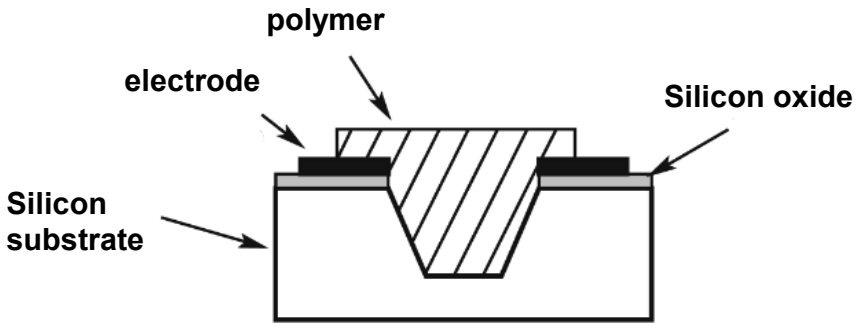

Fig. 4. Structure of a CP gas sensor. The polymer material deposited on the Silicon substrate allows electrical conduction between electrodes (adapted from Arshak et al., 2004).

II.2.1.4. Quartz Crystal Microbalances (QCM)

QMC gas sensors operate by virtue of the piezoelectric effect: When an AC voltage is applied to a piezoelectric quartz crystal; it begins to oscillate at its resonant frequency (Schaller et al., 1998). QMC sensors consist of a quartz disc coated with a polymeric coating layer and two gold electrodes deposited on either side of the disc. The electrodes apply an excitation voltage to the disc, while the sensitive membrane adsorbs gas molecules when exposed to an odour microbalance. As a result of this process, the membrane increases its mass, altering the resonant frequency of the quartz crystal (Albert and Lewis, 2000).

The sensors are typically micro machined QCM, which helps its miniaturization. Moreover, the sensitive coatings can be deposited them using techniques as diverse as: spin coating, airbrushing, inject printing or dip coating (Schaller et al., 1998). The strength of QCM sensors lies in their high selectivity (Pearce et al., 2003) and speed of

response (Haug et al., 1993). Regarding their disadvantages, QCM sensors typically show low sensitivity values, suffer from a lack of reproducibility (Dickinson et al., 1998) and are prone to drift. Besides, the manufacture process of the quartz resonators is costly and complex, so is its measurement circuity (Nagle et al., 1998).

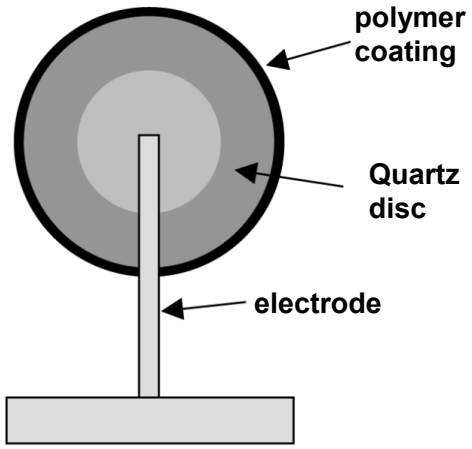

Fig. 5. Structure of a QCM gas sensor. The polymer material deposited on the Quartz disc acts as a sensing element in this sensor technology (adapted from Arshak et al., 2004).

II.2.1.5. Surface Acoustic Wave Sensors (SAW)

Similarly to QCM sensors, SAW sensors are also based on piezoelectric materials, although they work with a different principle of transduction. SAW sensors consists of a piezoelectric substrate with two interdigitated electrodes (transmitter and receiver), and a sensitive membrane placed between them (Khlebarov et al., 1992). To operate the sensors, an AC signal is applied to the transmitter electrode, generating a two-dimensional acoustic wave that propagates along the surface. When the signal reaches the

receiver electrode is transformed into an electrical output signal. The sensitive coating of the SAW sensor modifies its mass when loaded with molecules of analyte, fact that also modifies the frequency of the mechanic wave (Pearce et al., 2003; Nagle et al., 1998; Albert and Lewis, 2000). The piezoelectric substrates for SAW sensors are usually made with ZnO and quartz, while the sensitive coatings with liquid crystal or polymer.

SAW sensors can detect a variety of odours due to the wide range of sensitive coatings available (Carey et al., 1987a; Carey et al., 1987b; Grate and Abraham, 1991). In addition to this, they offer high sensitivities and fast response times (Nagle et al., 1998). Nevertheless, SAW sensors experience low signal noise ratios and require a complex circuitry to operate (Pearce et al., 2003). Finally, their main disadvantage lies in their low reproducibilities (Schaller et al., 1998).

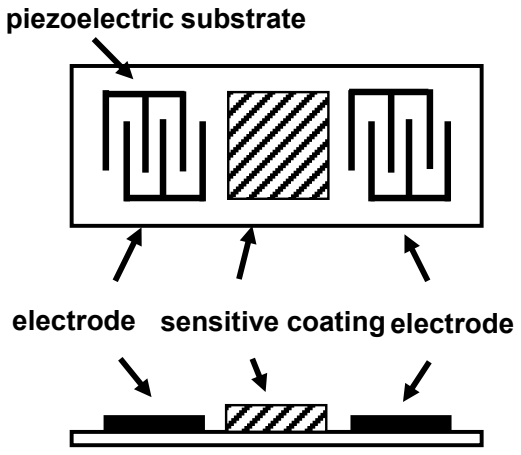

Fig. 6. Structure of a SAW gas sensor. A SAW sensor comprises a piezoelectric substrate, two transducer electrodes, and a sensitive material coating (adapted from Arshak et al., 2004).

II.2.1.6. Optical Sensors

Optical sensors utilize chemical indicators for detecting different gas species. Optical sensing allows identifying analytes through a variety of transduction mechanisms, including fluorescence intensity, lifetime spectral shape, polarization, absorbance, reflectance, refractive index, wavelength, colorimetry, etc. Typically, an Optical gas sensor is an optical fibre with an indicator immobilized on its distal tip. The sensitive end is illuminated through the optical fibre while exposed to the gas, and the resultant light is conveyed to a detection system (usually comprised of a CCD camera, a source of light and mirror) attached to the proximal end of the fibre. By immobilization of different polymers, the sensors can be tuned to detect different analytes.

Optical gas sensors can be combined very easily to create and array of sensors sensitive to a variety of compounds (multiple fibres of different indicators) and present very fast response times, around 10 seconds. However, there are several disadvantages associated to this sensor technology. On the one hand, the electronics required to conduct a measurement is complex, and thus, the process is costly. On the other, the indicators placed on the fibre tips have a quite short lifetime due photo-bleaching.

Fig. 7. Structure of an optical gas sensor. This sensor comprises a glass fibre coated with a sensitive dye (adapted from Arshak et al., 2004).

II.2.2. Generators of volatile compounds

We present a variety of odour generation techniques, including headspace sweeping, permeation tubes, bubblers, static systems, and dilution of volatiles into a carrier gas stream (Pearce et.al, 2003). Also, we discuss their virtues and limitations.

II.2.2.1. Headspace Sweeping

The head space is the space above a liquid sample in a bottle or vial. In the technique of headspace sweeping, a carrier gas (eg. dry air) pushes the molecules evaporated on the free surface of a liquid odorant conveys them to a measurement chamber (Nakamoto et al., 1991; Ide et al., 1993). This type of system is generally endowed with a pressurized source of carrier gas, which is connected to the sample vial through a Mass Flow Controller (MFC). The MFC is used to control the flow of carrier gas that sweeps the headspace (Gardner et al., 1994b). The vials are kept in sand or water baths at a controlled temperature so as to avoid variations in the odorant's vapour pressure.

The headspace sweeping is a simple method for odour sample generation. However, the method suffers from a drawback that limits its use in situations where odorant concentration is an important parameter of the experimental design: the concentration in the head space varies during the sweeping.

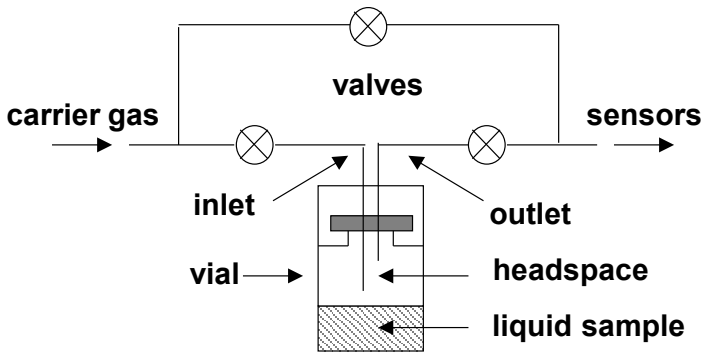

Fig. 8. VOC generator system based on the headspace sweeping (adapted from Pearce et al., 2003).

II.2.2.2. Permeation Tubes

Permeation tubes are cylinders of polymer (typically PTFE) sealed at the ends that contain a liquid volatile. That volatile diffuses through the walls of tube at a constant speed. The diffusion process is due to a gradient of analyte concentration experienced between the inner and outer surface of the tube. This gradient is proportional to the tube length and varies logarithmically with the inverse of temperature, so that this parameter must remain constant throughout the experiment. The odorant concentration can be controlled using a carrier gas flow to dilute the original concentration generated by the

permeation tube (Nakamoto et al., 1991). A volatile generation system based on this method comprises then: a source of pressurized carrier gas, permeation tubes, and a control system for temperature and flow of the carrier gas. Permeation tubes are commercially available for a variety of chemicals. Besides, the method allows generating concentrations below the ppb level. On a negative side, they present a limited lifetime and must be calibrated before used.

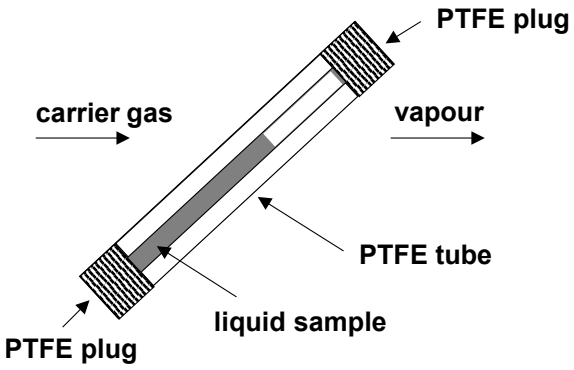

Fig. 9. Scheme of a PTFE permeation tube (adapted from Pearce et al., 2003).

II.2.2.3. Bubblers

A bubbler is a bottle partially filled with a liquid odorant, which is volatilized by means of a carrier gas flow forming bubbles. Consequently, a VOC generator based on this method only needs a source of pressurized carrier gas, a mass flow controller and, of course, a bubbler (Ohnishi et al., 1992).

Although the use of bubblers for generating VOCs is widespread in the e-nose community, the method is subjected to a severe limitation: As the bubbler's headspace may not be saturated with the analyte's vapour, it is not possible to know accurately its concentration. Moreover, the use of bubblers is not recommended for high carrier gas flows, since beads of analyte in liquid phase can be conveyed to the sensor chamber.

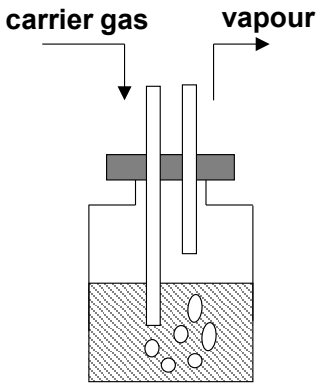

Fig. 10. Scheme of a bubbler (adapted from Pearce et al., 2003).

II.2.2.4. Static Systems

The aim of a static system is to generate a stable odorant concentration at constant temperature. The system usually consists of an insulated evaporation chamber (typically made with Teflon) surrounded by a temperature-controlled bath. An odorant sample generated with such type of systems is measured as follows: A certain amount of liquid odorant is injected into the evaporation chamber, where the sensors are placed.

Eventually, the liquid sample evaporates. Once the equilibrium is reached within the chamber, the response of the sensors is acquired (Grate and Abraham, 1987; Hatfield et al., 1994).

This method ensures stable concentrations as long as the temperature remains constant throughout the process. Unfortunately, the time required to achieve the steady state of concentration in the chamber substantially slows down the measurement process.

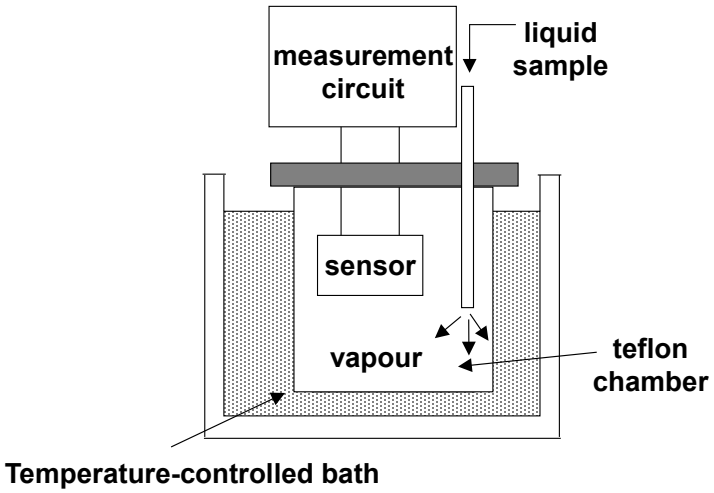

Fig. 11. Principle of static measurement circuit (adapted from Pearce et al., 2003).

II.2.2.5. Dilution of Volatiles into a carrier gas stream

This technique consists in diluting an odorant flow of known concentration into a carrier gas stream. The system comprises at least to gas cylinders, corresponding to the carrier gas and odorant and a pair of mass flow controllers. Once the fluidic steady state is

reached within the measurement chamber, the odorant concentration equals to the reason between the odorant flow and the total flow of the stream (Mandayo et al., 2003).

This method provides stable concentrations, but requires a conscious design of the fluidic circuit to avoid excessive transient times until reaching the steady state of concentration. It is recommended to include 2 additional mass flow meters (one per fluidic branch) so as to ensure an adequate estimation of the odorant concentration.

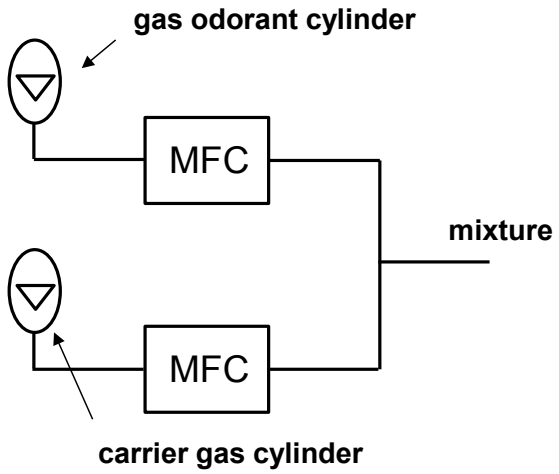

Fig.12. VOC generator system based on diluting gases into a carrier gas stream.

II.2.3. Signal processing

Pattern recognition techniques allow characterizing the multivariate response of an array of sensors so as to detect, identify or quantify odours. Data processing of the raw array response is mandatory to achieve reliable odour descriptors and predictions. Classically,

data processing follows a number of ordered steps (Gutierrez-Osuna, 2002): signal preprocessing, dimensionality reduction, prediction and validation (see Fig. 13). Signal preprocessing prepares the sensor signals for later analyses minimizing the spurious sources of variance (e.g. noise, drift, etc.) of the array response. Dimensionality reduction reduces the number of dimensions of the feature vector, preventing problems associated with high-dimensional data, the so-called 'curse of dimensionality'. The subsequent array response after dimensionality deflation is utilized in the prediction stage as an input feature vector to solve problems of diverse kind (class membership, odour concentration, related odour samples, etc.). The validation step, at last, aims to select which model and parameter settings are the most suitable to solve the given prediction problem. To do it, an optimization of a certain criterion function must be performed (e.g. classification rate, Fisher score, mean-squared error, etc.).

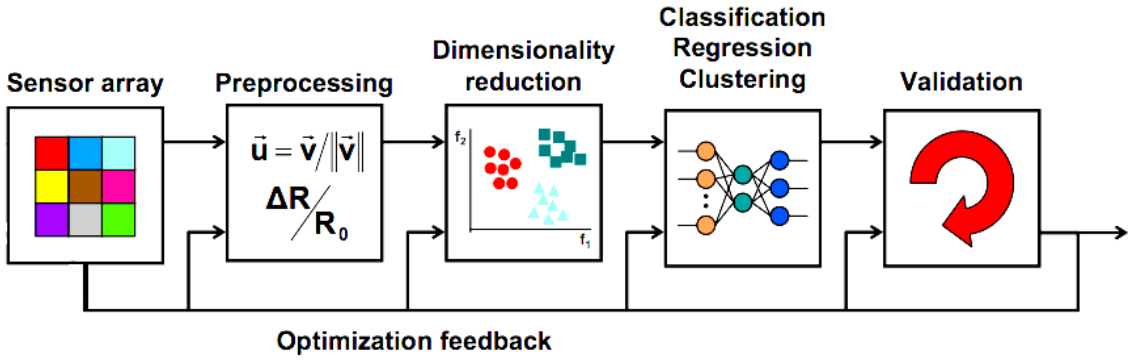

Fig. 13. Signal processing steps for pattern analysis in a gas sensor array (adapted from Gutierrez-Osuna, 2002).

II.2.3.1. Preprocessing

Sensor arrays of different technologies suffer from their own problems related to signal quality (Gardner et al, 1998). Although these problems need to be corrected through specific preprocessing stages, some general tasks involved in signal correction are identified (Gutierrez-Osuna and Nagle, 1999b; Gutierrez-Osuna et al., 2002). The most usual are: digital smoothing, decimation (or binning), baseline manipulation, compression, and normalization. Digital smoothing refers to the use of digital filters for supressing some unwanted aspect of the signal (e.g. background and impulsive noise. Examples of digital filters widely used by the electronic nose community are moving average and moving median filters (Pan et al., 2009) and Savitzky-Golay filters (Perera et al., 2002; Cheng et al., 2009). Decimation consist in averaging of consecutive signal features, which is a very effective manner to both reduce noise and the number of features of highly correlated high dimensionality data (Gutierrez-Osuna and Nagle, 1999b). Baseline manipulation aims to standardize the sensor's baseline in order to counteract the effect of drift. Baseline manipulation can be differential (Hielermann et al. 1995), relative (Ikohura and Watson, 1994) and fractional (Gardner, 1991). Data compression seeks to extract descriptive information of the sensor's transient response, reducing the acquisition time and decreasing the dimensionality of the input feature vector. Usual strategies of compression comprise parameter extraction (Eklov et al., 1997) and model fitting (Gutierrez-Osuna and Nagle, 1999a). Finally, normalization is used to down weight the contribution of factors that influence the sensor responses but

are not relevant (or even detrimental) for the given pattern recognition problem (Gutierrez-Osuna and Nagle, 1999b; Pearce and Gardner, 1998). There are several ways to perform a normalization of the feature vector. The most popular are, normalization to unit area, unit module and unit variance.

II.2.3.2. Dimensionality Reduction

There are two ways to perform dimensionality reduction: Feature extraction and feature selection (Marco and Gutierrez-Galvez, 2012).

Feature extraction consists in finding data projections to lower dimensionality subspaces preserving most of its information content (Fukunaga, 1991). The choice for a particular projection depends on which facet of the data information needs to be stressed. Signal representation techniques are focused on the structure of data, while signal classification techniques on data categorization (Gutierrez-Osuna, 1998).The most archetypal technique employed in signal representation is Principal Component Analysis (PCA), which projects the data along their directions of maximum variance. Regarding to signal classification, the most representative used technique is Fisher's Linear Discriminant Analysis (LDA). That technique optimizes the separability among classes, finding the projection that maximizes the distance among the different class clusters and minimizes spread within groups.

On the other hand, feature selection aims to create subsets of features that are relevant in terms of their informative content or predictive power (Fukunaga, 1991). Most of the methods that explore the feature space are based on the following search strategies: exponential (Narendra and Fukunaga, 1977), sequential (Pudil et al., 1994) and randomized techniques (Kirkpatrick et al. 1983; Michalewicz, 1996). Exponential algorithms, such as Exhaustive Search (ES), Branch and Bound (BB), and Beam Search (BS), built subsets of features whose search complexity increases exponentially with the number of features. Sequential search algorithms create the subsets of features adding or removing features sequentially, although they tend to become trapped in local minima. The most popular in e-nose literature are Sequential Forward Selection (SFS), Sequential Backward Selection (SBS), Plus-l Minus-r Selection (PMS), Bidirectional Search (BiS) and Sequential Floating (SF). Lastly, randomized algorithms attempt to overcome the complexity of exponential methods and the overfitting problems of sequential algorithms. Among others, the most widely used are Genetic Algorithms (GA) and Simulated Annealing (SA).

II.2.3.3. Prediction

Depending on the nature of the prediction problem, a pattern recognition system must perform classification, regression or clustering tasks (Gutierrez-Osuna, 2003).

Classification tasks aim to associate labels to unknown odorant samples from a set of discrete and previously learned examples. To do it, the classifier partitions the feature

space (usually after dimensionality reduction stage) into a number of decision regions according to the learned odorant classes (Duda, 2000). The boundaries between classes are defined by the intersection of equiprobable likehood contours (a sample with such feature vector has the same probability of belonging to more than one class). Consequently, different methods for mapping the feature space give rise to different types of classifiers (Friedman, 1989; Bishop, 1985; Rumelhart et al., 1986), namely: Quadratic (QUAD), Radial Basis Function (RBF), K- Nearest Neighbour (KNN), and Multilayer Perceptron (MLP) classifiers. In QUAD classifiers, the distribution of probability for each example class is assumed to be unimodal and the corresponding decision boundaries become quadratic surfaces. RBF classifiers allow modelling the different example distributions as a Gaussian mixture so the decision regions may be multimodal (with unconnected regions belonging to the same class). The K-NN classifier creates highly nonlinear decision boundaries around the example samples, known as Voronoi tessellation. Finally, the boundaries for the MLP classifiers consist of hyperplanes in the feature space.

The goal of regression is to build models of prediction that relate a set of independent continuous variables (the array features) to another set of dependent variables, which can be either discrete or continuous (Bishop, 1995; Duda, 2000). In first case, the regression model is equivalent to a classifier. Examples of regression based classifiers are Support Vector Machines (SVM), Logistic Regression (LG) and Partial Least Squares

Discriminant Analysis (PLSDA). For the case of continuous dependent variables, the prediction model must extrapolate to some extent the properties of unknown samples from a finite set of examples (i.e. extrapolate the concentration of the elements of a mixture from the array response to its pure compounds). Traditionally, a number of linear regression techniques based on the Ordinary Least Squares (OLS) regression models have been used in artificial olfaction (Geladi and Kowalski, 1986; Friedman, 1989; Frank and Friedman, 1993): Ridge Regression (RR), Principal Components Regression (PCR) and Partial Least Squares (PLS). These techniques overcome the OLS problems associated to collinearity in different manner. While RR is a regularization method designed to stabilize the OLS solution, PCR and PLS create new sets of decorrelated regressors (Principal Components and Latent Variables). Other non-linear techniques employed in regression problems are Artificial Neural Networks (ANN) and Support Vector Regression (SVR).

Finally, the purpose of clustering is to study the degree of similarity of set of objects (odour samples, features), arranging them in different groups or clusters (Duda, 2000). To perform a clustering task, three basic steps must be followed: First, to define a measure of dissimilarity between objects. Second, to define some clustering criterion to be optimized. And third, to define a search algorithm to assign example samples to clusters. However, since clustering is an unsupervised process and given that the notion of a ‘cluster’ cannot be precisely defined, a unique set of objects can generate multitude of

cluster arrangements. The basic clustering techniques employed in artificial olfaction are (Kohonen, 1982; Therrien, 1989; Ripley, 1996): Hierarchical Clustering, C-Means and Self-Organizing Maps (SOM). Hierarchical Clustering creates multi-level structures (dendograms) to group objects in a agglomerative or divisive fashion. C-means clustering generates a single-level partition of the examples into C independent clusters. To finish, SOM produce low-dimensionality discretized representations of the feature space of the examples (a map) that preserves the topology of the clusters.

II.2.3.4. Validation

Validation is necessary step in pattern analysis because warrants reliable predictions to unseen samples. The basic use of validation is to limit the complexity of the prediction model (i.e. number of latent variables in a PLS regression), preventing over-fitting to the example samples. To avoid over-fitting, the example data is divided in two sets: training and validation sets. The training set is used to create a collection of models of increasing complexity. That model that exhibits the best performance when applied to the validation set is selected due its ability to generalize predictions to new data. There are several ways to partition the data to perform validation (Ripley, 1996; Efron and Tibshirani, 1993). The most commonly used in machine olfaction are: the holdout method, K-fold and its variations leave-one-out (LOO) and leave-one-block-out (LOBO), and bootstrap methods. The holdout method consists in splitting the example data into a single train-and-validate trial. Although simple, the holdout method the can easily led to overfitting in case of limited data available. This problem can be partially overcome by partition the

dataset multiple times and averaging the performance of the models across the partitions. K-fold creates K partitions of a set of N examples, leaving N(K-1)/K subsets for training and N/K for validation. If the number of folds equals the number of examples the method is known as LOO, while if the number of folds equals to the number of blocks of repeated examples it is called LOBO. Regarding bootstrap, the method generates multiple training-validation partitions, with the particularity that sample repetition is allowed for the different training sets.

II.2.2.4. Large sensor arrays

Biological and artificial olfaction systems acquire information from odours generic chemosensory arrays. Despite this similarity, biological olfaction outperforms machine olfaction in terms of sensitivity, robustness to noise and tolerance to sensor damage (Pearce, 1996). This is because **(i)** biological olfactory systems are endowed with millions of sensory units, whereas 'traditional' e-nose instruments only present a few sensor units (thus e-nose arrays are less redundant); and **(ii)** olfactory receptors exhibit a narrower molecular receptive range than any of sensor technologies employed in e-nose instruments. Consequently sensor array responses to odours in e-noses are much more correlated than biological olfactory systems (or in other words, they present a lower degree of sensor diversity).

Two basic approaches have been proposed to increase the variability of the array response to odours in gas sensor arrays with a limited number of sensor units

(Hierlemann, Gutierrez-Osuna, 2008). First approach consists in modifying some intrinsic or operational parameters of the sensor units present in the array (presence of catalysts, thickness of the sensing layer, working temperature). This strategy is usually employed in homogeneous sensor arrays. The second approach is based on building heterogeneous sensor arrays combining a number of sensors technologies. The rationale behind this strategy for sensor diversity enhancement is that different sensing principles provide additional sources of chemical information to differentiate odours. On the other hand, the redundancy of a sensor array can be simply incremented replicating in large numbers the different sensor type units that constitute the sensor array (Hierlemann, Gutierrez-Osuna, 2008). However, it has not been until recently that large sensor arrays have become technologically available.

To the best of our knowledge, the first of these large arrays was presented in 1999 (Dickinson et al, 1999). The authors built a sensing system based on a high-density optical array, with thousands of bead sensors of three discrete classes (Nile Red/poly, Nile Red/silica and Sensidye) dispersed across the face of an etched optical fibre. To characterize their system, they exposed the sensors to a saturated pulse of methanol while collecting the sensor readings with a CCD camera. Then they assigned each bead to one of the discrete sensor classes by means of an imaging-software program. Sensors readings belonging to the same type of sensor beads were averaged. A signal to noise improvement of $n^{1/2}$ (where n was the number of beads) was achieved using this method.

Another large array of optical gas sensor is found on the work (Di Natale et al., 2009). The authors created a sensor array from a continuous sensitive layer of colour indicators (ZnTTP, MnTTP,CoTPP and PtTTP) dissolved into a PVC matrix. The system was exposed to vapours of ethanol, triethylamine, toluene and butyamine. During the odour exposition, the sensing material was illuminated with a three pure colour RGB sequence (red-green-blue) and their response was captured by the three channels (RGB) of a web camera. The authors focused this study on a 7845-pixel region where the illumination was uniform, considering each of these pixels as a sensory element. Pixels with similar odorant fingerprints were clustered (and added) into 8 artificial glomeruli by performing a k-means classification on the feature space.

Polymeric sensors have also been used for developing large arrays of gas sensors (Gardner et al., 2009). The investigators designed an artificial olfaction system that combined 3 replicated arrays of 300 composite conducting polymer sensors (24 polymer types) with two retentive columns coated with polar and non-polar compounds. The first array provided spatial information representing different essential oils presented to the system (Cinnamon, Lemon Grass, Lavender and Ylang Ylang). The second and third array replicates were connected to the first one through the retentive columns, obtaining each array the spatial and temporal information from its own separation profile. The joint response of the three arrays was obtained performing a convolution between

corresponding sensor pairs in each array. The area of the convolution integral was computed and used as a sensor feature.

In a different work (Bernabei et al., 2012); the authors also built a sensing system composed of a large-scale array of 16384 conducting polymers of 24 different classes. The array was tested with six concentration expositions to ethanol, seven of 2-butanone and three mixtures of the pure compounds (75% ethanol-25% 2-butanone, 50% ethanol-50% 2-butanone and 25% ethanol-75% 2-butanone, being 100% the maximum concentration presented for each substance). The relative resistance ratio obtained from the sensors in the steady state was used as a feature for the subsequent data analysis. Results for classical multivariate techniques applied to the data demonstrated that, the system was able to predict the concentration of the pure vapours (realizing Partial Least Squares regression), but also segmenting their binary mixtures depending on their pure substance ratio (performing Principal Component Analysis). In all these systems, the pooled response of the individual sensor elements was obtained through a dimensionality reduction stage that was analogous to the sensory convergence exhibited by the olfactory system.

II.3. OUR SENSOR ARRAY

The objective of this section is to design a large array of MOX sensors that mimics the high degree of sensor diversity and redundancy exhibited by the olfactory system. Section II.3.1 describes the architecture of our sensing system, which consists in a

measuring platform plus an odour delivery system. Special care is put in the description of the odour delivery system and the generator of volatile compounds, which is based on the direct evaporation method. To the best of our knowledge, this is the first time that the direct evaporation method is used to generate mixtures of volatile compounds.

II.3.1. Block diagram

Our chemical sensing system comprises two blocks: the measurement block, the odour delivery system. Fig. 14 shows a scheme of the system.

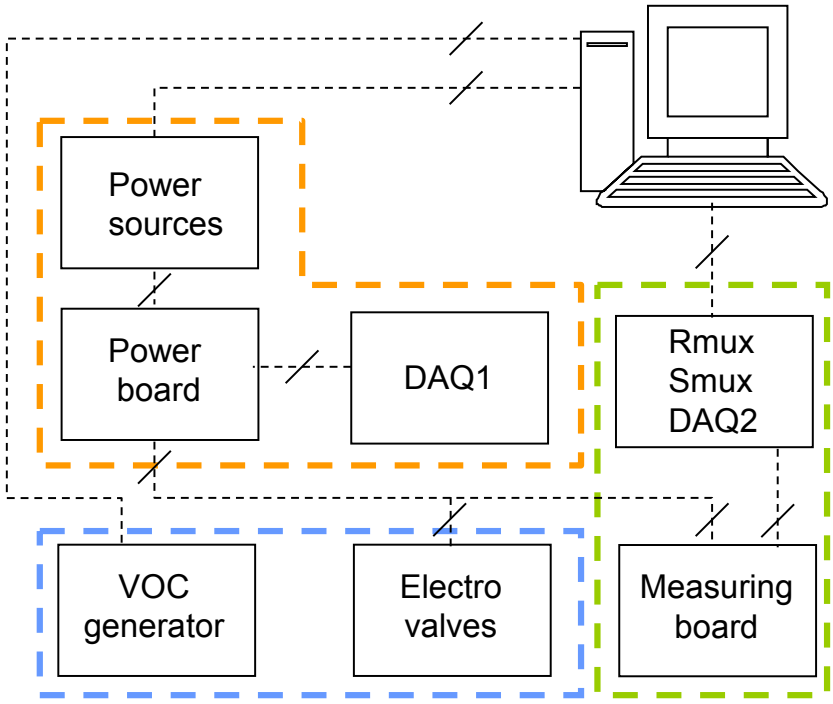

Fig. 14. Building blocks of our e-nose prototype. The components corresponding to the data acquisition platform, the power and control block, and the odour delivery system are enclosed, respectively, in green, orange and blue dashed lines.

The measurement block is presented in Section II.3.1.1. That includes the selection of the commercial MOX sensor types and their distribution on the sensor array, the multiplexing system to generate the variety of measuring circuits and the basic circuit for power distribution. Section II.3.1.2 is devoted to describe the odour delivery system. There, the generator of volatile compounds based on the 'direct evaporation' method and the fluidic circuit to convey the odour mixtures to the sensor chamber are presented. The 'direct evaporation' method is explained and an estimation of the obtained odorant concentration using this method is calculated.

II.3.1.1. Measuring system

This block is responsible for acquiring and storing the chemical information of the volatile compounds obtained from MOX sensors. The block includes the sensor array, and the electronics to control the sensor's power supply and to polarize the measuring circuits (voltage dividers). The sensor array diversity array is boosted by combining different sensor types units along with a modulation of the sensor's temperatures; and its redundancy, by using a number of replicates per sensor type, and modifying sensor's measuring circuit by means of a collection of load resistors.

The data acquisition system is formed by the gas sensors, a handmade measurement board, two multiplexors and a data acquisition board. We use 8 different types of MOX sensors provided by FIGARO (TGS-2600, TGS-2602, TGS-2610, TGS-2620) and FIS (SB-11B-00, SB-1500, SB-41-00, SB-AQ1-04) commercial houses with 12 replicates for

each type. These 96 sensors are placed on measurement board of 8 columns and 12 rows. Each column is independent from the others and corresponds to the powering of one sensor type. So, the 12 replicates sensors per sensor type are placed on the same column. A picture of the sensor array can be seen in Fig. 15.

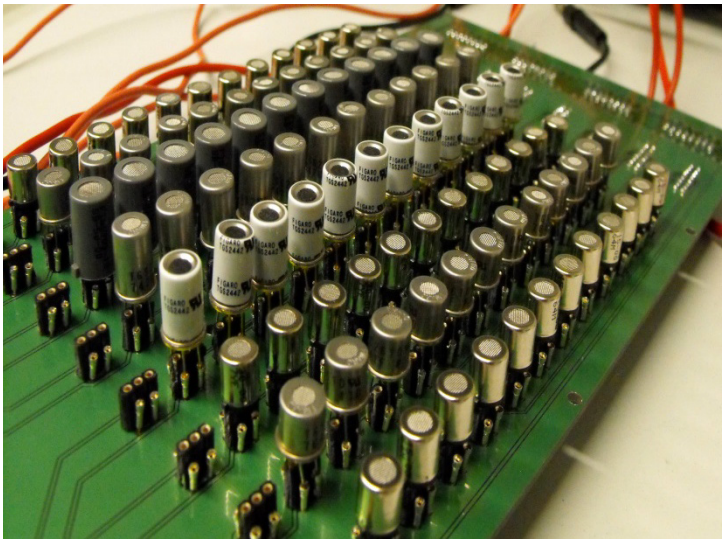

Fig. 15. Close-up view of the sensor array. Each of the 8 array columns corresponds to a different MOX sensor type (TGS-2600, TGS-2602, TGS-2610, TGS-2620, SB-11B-00, SB-1500, SB-41-00, SB-AQ1-04), with 12 sensor replicates per column.

The sensors are measured by a collection voltage dividers, so a battery of 16 load resistors (0.10K, 0.25K, 0.40K, 0.87K, 1.30K, 3.01K, 6.19K, 9.09K, 21.00K, 30.01K, 40.20K, 51.10K, 68.10K, 82.5K, 90.90K, 105.K) is included in the measurement board. The voltage dividers are built by means of a module with two high-speed multiplexors (PXI 2530, National Instruments). These multiplexors allow switching the connection of

the sensors to the load resistors. The connection point between multiplexors is taken to measure the sensor output, using a data acquisition board (PXI 4461, National Instruments). A sketch for this type of connection is found in Fig. 16.

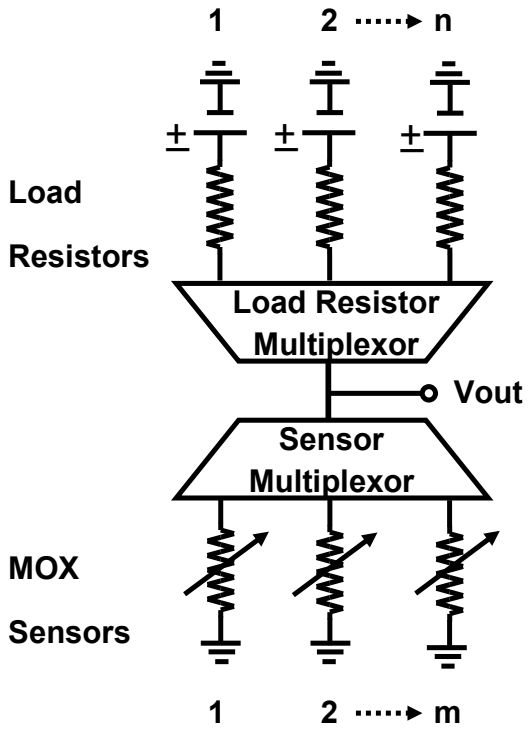

Fig. 16. Scheme of the large scale mutiplexing system. This aproach allows connecting each of the m sensors to a collection of n load resistors (m=96, n=16). The sensor readings (Vout) are taken in the connection point between multiplexors.

The power and control block comprises two independent power sources and a handmade control board. The basic circuit for power distribution of the control board consists of an operational amplifier (AD648, Analog Devices) connected to the gate terminal of a

PMOS power transistor (SUP900P06-09L, Vishay). The control is performed by comparing the digital signal provided by a DAQ (USB 3103, Measurement Computing) in the negative input terminal of the O.A. with a constant reference signal of 2.5V in the positive one. When the digital signal is at high level, the output of the operational is negative and the PMOS drives current. Otherwise the transistor is in cut-off. This circuit is presented in Fig. 17. We place 16 of these power basic circuits on the power board in order to select the sensor channels, both electrical and fluidic. MOX sensor are modulated in temperature following a 100 step ramp profile over a period of 90 seconds (from 0 to 5 V for Figaro sensors and from 0 to 0.9V for FIS) using a programmable a DC source (N6705A DC Power Analyzer, National Instruments), whereas the different voltage dividers are biased to 10 V using another DC power supply (PXI 4410, National Instruments).

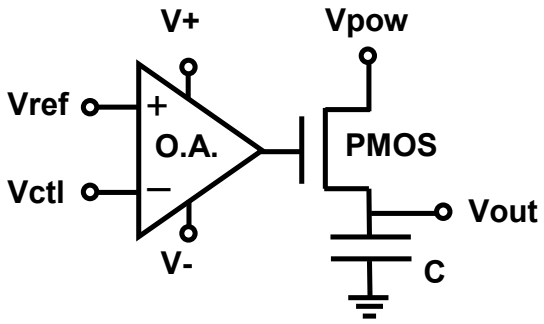

Fig. 17. Basic circuit for power distribution. V+=12,V-=-12, Vref=2.5 and C=100pF. The operational amplifier used is a AD648; and the MOSFET transistor is a SUP900P06-09L.

II.3.1.2 Odour delivery system

The function of this block is to generate odour mixtures at different concentrations and convey them to the sensor chamber. In this section, the layout of the odour delivery system is shown. In addition to this, the main characteristics of the generator of volatile mixtures and the calculus of the estimated analyte concentration are included.

The odour delivery system includes a generator of volatile compounds, a couple of handmade gas manifolds, a battery of 8 electro-valves, and a handmade measurement chamber. The generator of volatile compounds is based on the controlled evaporation of liquid compounds on a carrier gas flow (Fonollosa et al., 2013b) and presents two fluidic lines: On the one hand, the line for carrier gas delivery, constituted by a cylinder of synthetic dry air (CarburosMetalicos, Air Products Group) connected in series to a Mass Flow Controller (EL-FLOW F-201CV, Bronkhorst High-Tech B.V.), set to provide a constant flow of 1 l/min. And, on the other hand, the line for odorant supply, which consists of a programmable infusion pump (KDS200, KDScientific) and a precision syringe (1702 TLLX 25µl, Hamilton) that pushes the odorant in liquid form into a 150 µm fused silica capillary tubing (FS-115, Upchurch Scientific) though a Luer-to-Microtight Adapter (UP-P-662, Upchurch Scientific) until reaching a septum in the injection port, where both fluidic lines meet and odorant evaporation is performed. After the generator of volatile compounds, 1 to 8 manifold splits up the mixture in 8 streams symmetrically to introduce them to the 8 independent channels of the sensor chamber (28 cm3/channel). Different operating configurations can be achieved by means of 8 electro-

valves (E210C, Clippard) that control the pass of flow through the chamber channels. At the output of the chamber the 8 streams are brought together with an 8 to 1 manifold, recovering the original flow. An scheme of the odour delivery system is included in Fig. 18.

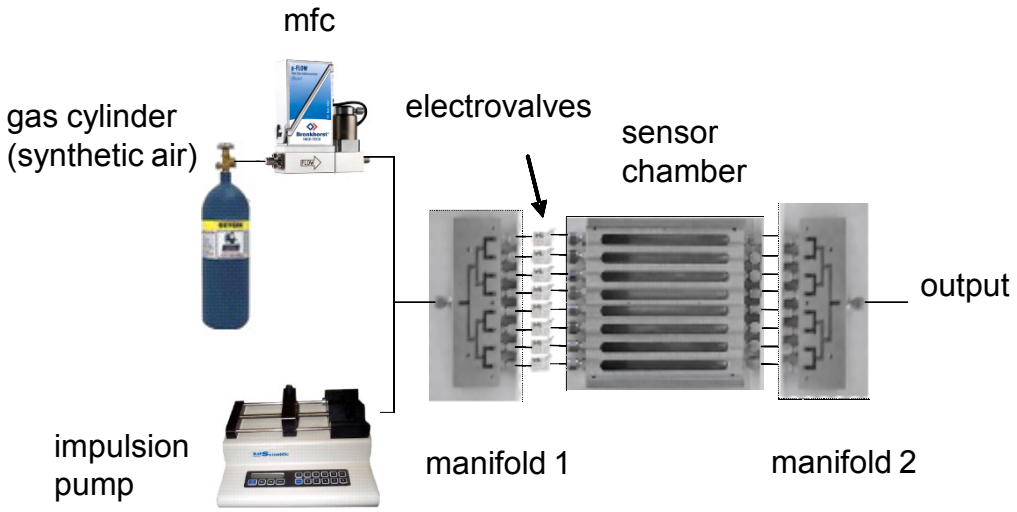

Fig. 18. Scheme of the odour delivery system.

The volatile generator subsystem is based on the 'direct evaporation', in which the liquid odorant is diluted into a stream of solvent gas. Basically, the volatile generator consists of two fluidic branches. On the one hand the solvent branch to which the air cylinder is connected. This branch includes a Mass Flow Controller (EL-FLOW F-201 C, Bronkhorst High-Tech B.V) to keep the flow constant throughout the experiments. On the other hand, the solute branch comprises two programmable infusion pumps (KDS200, KDScientific). Each of these pumps is equipped with high precision syringes containing

the solute in liquid form (1702 TTLX 25 µl, Hamilton). By means of a Luer-to-Microtight Adapter (UP-P-662, Upchurch Scientific) the solute is pushed into a 150 µm inner diameter fused silica capillary tubing at a controlled flow rate. Both branches meet at the injection port, a fluidic Tee connector where the inlets reserved for the solute lines are sealed with a septum to assure tight conditions. The injection port is presented in Fig. 19. The solute is evaporated at the injection port, and the resulting mixture is sent to the sensor chamber by the fluidic circuit.

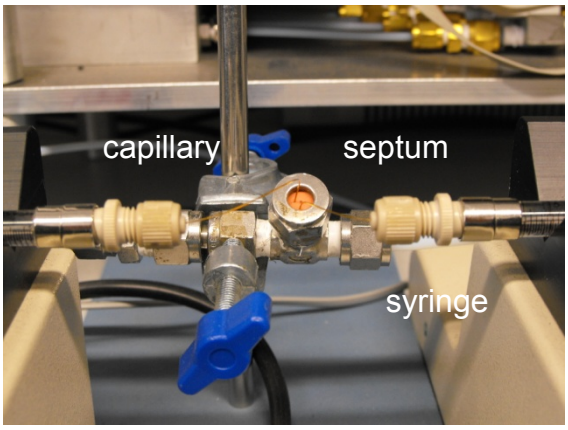

Fig. 19. Picture of the injection port. The odorant in liquid phase is conveyed by a capillary and introduced through a septum in the tee connector.

II.3.1.2.1. Computation of the analyte concentration

The odorant concentration is calculated from the odorant mole fraction in the mixture. Assuming a mass balance between the liquid flow supplied by the syringe and the gas flow evaporated at the end of the capillary, and that the resulting volatile is approximated as an ideal gas, the odorant concentration in the chamber can be estimated (2.1):

$$C = \frac{\Phi_{odorant}|_{gas}}{\Phi_{carrier}|_{gas} + \Phi_{odorant}|_{gas}} = \frac{\frac{\left(\Phi_{odorant}|_{liquid} \cdot \rho_d \cdot R \cdot T\right)}{M_d}}{\Phi_{carrier}|_{gas} + \frac{\left(\Phi_{odorant}|_{liquid} \cdot \rho_d \cdot R \cdot T\right)}{M_d}} \quad (2.1)$$

where C is the gas concentration of the sample diluted in synthetic air, Φ is the flow, M_d the molar mass of the odorant, ρ_d its density in liquid phase and T and P, the temperature and pressure at the injection port, respectively. Further details about the selected evaporation method can be found in next section.

II.4. DATASETS

To fulfil the objectives of this dissertation, three datasets were collected using this system: **(i)** the large concentration range dataset; **(ii)** the pure substance dataset; and **(iii)** the odour mixture dataset. In the following section, we present a brief description of these datasets.

II.4.1 Description of the datasets

The large concentration range dataset **(i)** contains the sensor array responses to 7 different concentrations of acetone distributed along 3 decades of concentration (10, 50 100,500, 1000, 5000 and 10000 ppm). For its part, the pure substance dataset **(ii)** comprises the sensor array readings to 6 different concentrations (0, 20, 40, 60, 80, 100 and 120 ppm) of 3 pure substances (Ethanol, Acetone and Butanone.). Finally, the odour mixture

dataset **(iii)** consists in the set of sensor response to the binary mixtures of ethanol, acetone and butanone. The experiments were designed to have a transition from a first analyte to second analyte in six steps, for each of 3 binary combinations of the 3 analytes.

In all these the datasets, additional measurements of synthetic dry air were acquired as a reference values before each of the experiments. The complete set of experiments was repeated 10 times, where the order of odour exposition was randomized. Figures Fig. 20, Fig. 21 and Fig. 22 show respectively, the sensor response to the three different datasets for a sensor taken as a representative of the array (TGS-2602, R_L=21KΩ). To show the repeatability of the sensor measurements, the sensor response is computed as the mean measure obtained from 10 repetitions, and includes error bars corresponding to its standard deviation.

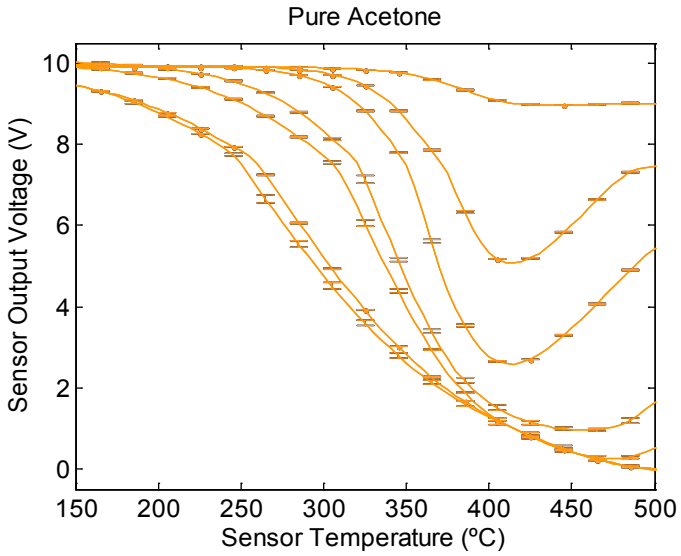

Fig. 20. Readings of a TGS-2602 sensor responding to dataset I. We show the sensor waveforms corresponding to different acetone samples for a large concetration range (R_L=21 KΩ).

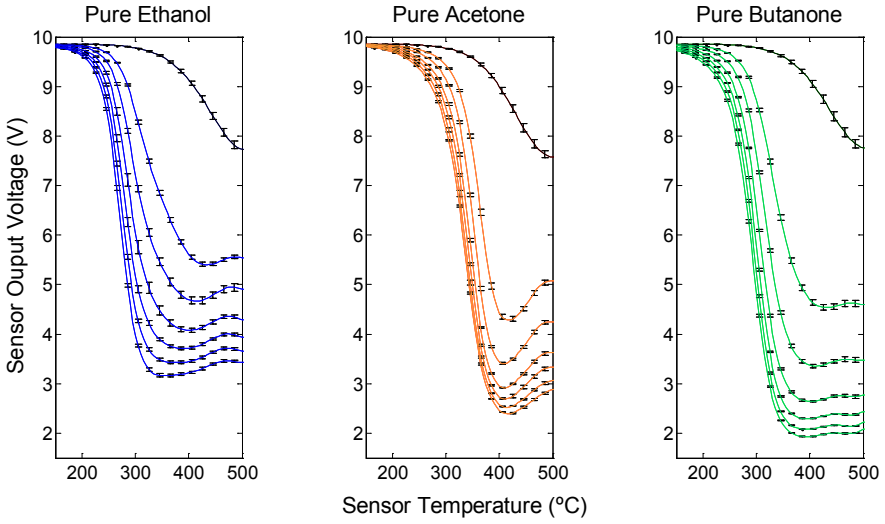

Fig. 21 Readings of a TGS-2602 sensor responding to dataset II. Blue, orange and green waveforms represent, respectively, ethanol, acetone and butanone samples (R_L=21 KΩ) .

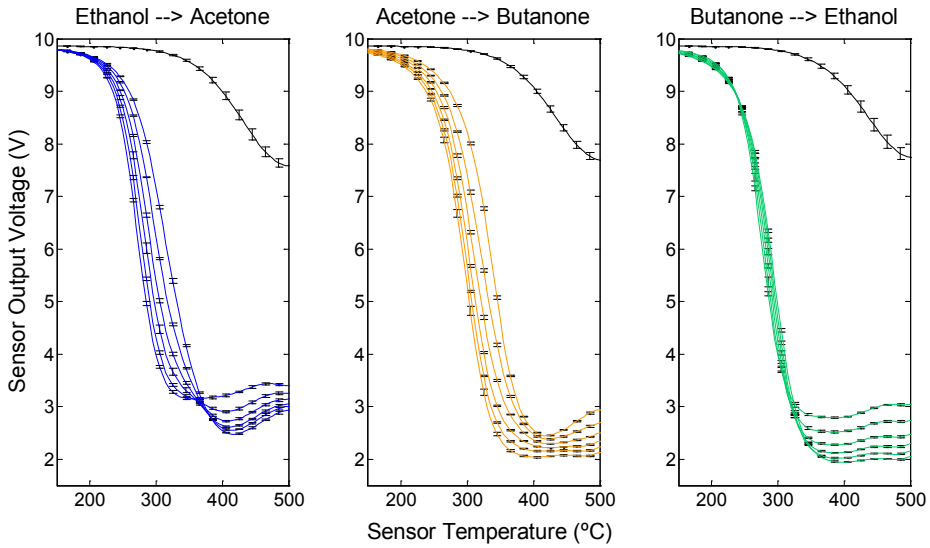

Figure. 22 Readings of a TGS-2602 sensor responding to dataset III. Blye , orange and green waveforms represent, respectively, the transition from ethanol to acetone, acetone to butanone, and butanone to ethanol (R_L=21 KΩ) .

II.5. CONCLUSIONS

In the first part of this chapter, we presented the electronic nose as a general purpose instrument for chemical sensing. We started showing the architecture of the natural olfactory system, which is the inspiration for such a kind of instrument. We reviewed the most commonly employed sensor technologies, sample generation methods, and signal processing techniques in machine olfaction. We detected two important differences between natural and artificial olfaction systems. **(i)** First difference was related to the number of sensors on the array (sensory redundancy); whereas **(ii)** to the degree of correlation of the array response to a set of odours (sensory diversity). In both cases, natural olfactory systems outperformed 'traditional' e-nose arrays. We revised different

methods to boost the levels of sensory diversity and redundancy of artificial sensor arrays. Novel e-nose prototypes that take advantage of these methods were also revised.

In the second part of this chapter, we designed and built a new prototype of bio-inspired e-nose instrument based on the MOX sensor technology. We endowed our system with large levels of *structural* sensory diversity and redundancy, in the sense that they were considered intrinsic properties of our sensor array. In our approach, sensory diversity was achieved through the use of 8 different types of MOX sensor modulated in temperature (100 temperature conditions); and sensory redundancy including 12 MOX sensor replicates for each type along with a multiplexing system to read the response of the sensor through a collection of voltage dividers (16 load resistors). The grand total of readouts per sample obtained with this sensor array was 153600 (8 sensor types x 100 temperatures x 12 sensor replicates x 16 load resistors= 153600 readouts). Finally, we used this system to acquire three different datasets.

CHAPTER III

SENSOR DIVERSITY AND REDUNDANCY

The olfactory system is the archetypal example of a sensory array that encodes the information of chemical stimuli using a vast population of sensory inputs, the ORNs (Friedrich and Stopfer, 2001; Korsching, 2002; Miura et al., 2012; Buck and Axel, 1991). Population coding is also present in the other sensory systems: gustatory (Schiffman et al., 1971) somatosensory (Johansson and Birznieks, 2004), auditory (Covey, 2000), and visual (Vinje and Gallant, 2000). The reason why evolution has selected population coding to acquire real-world information is linked to the robust noise-resistant properties that this strategy exhibits. The combination of large arrays of receptors with a highly convergent sensing architecture gives rise to the emergent phenomenon of sensory hyper-acuity (Bialek, 1987). Basically, the concept of hyper-acuity stands for that the sensory performance of a population of receptors is finer than any of the performances showed by the individual receptors. Two forms of hyper-acuity are present within the olfactory receptors (Pearce et al., 2001). First of these is related to the variability on the responses of a population receptors and it is responsible for the enhancement on odour quality estimation. Combining the signal of the different ORN types, complex mixtures not achievable by any single receptor type can be distinguished. In mammals, between 300-1000 of ORNs expressing different receptor proteins are responsible for odour quality encoding (Buck and Axel, 1991). The inherent cross-sensitivity of ORNs broadens the

detection range and increases the tolerance to interferences of the olfactory system. Although intuition suggests that arrays of specific odour receptors should provide more accurate odour discriminations, several theoretical works in neuroscience indicate that arrays of cross-sensitive sensors outperform selective arrays (Sánchez-Montañés, and Pearce, 2002; Wilke and Eurich, 2002; Brown and Bäcker, 2006). The second type of hyper-acuity is related to the replication in large numbers of different receptor types, and causes the enhancement on odour quantity estimation in natural olfactory systems. Giving some numbers, the olfactory epithelium in humans is endowed with 12 million of ORNs, while for bloodhound this quantity increases until 4 billion of receptors (Shier, 2004). In particular, the limit of concentration detection for an array of ORNs is substantially lower than the one corresponding to any of their single receptors. This fact has been observed in such different species as frogs (Duchamp-Viret et al., 1989; Drongelen, 1978), and cockroaches (Boeckh and Ernst, 1987).

We can find a number studies in the literature concerning these two types of sensor hyper-acuity in machine olfaction (hitherto, sensor diversity and redundancy respectively). Regarding sensor diversity, the researchers were mainly interested in quantifying the discriminative power of non-selective sensor arrays and describing the mathematical relations between the space of odour representation and sensor array space. One of the investigations that dealt with the problem of discriminating mixtures with an array of non-specific sensors was performed by (Zaromb and Stetter, 1984). In their

work, the authors performed a theoretical study to estimate the minimum size of an array of noiseless binary sensors to discriminate a mixture of A components. (Niebling and Mu, 1995) proposed the inverse feature space to design sensor arrays. This inverse sensor space corresponded to a subspace of the odour space. Projecting the sensor features in the odour space, the investigators showed which of the array features were more suitable to solve potential discrimination problems. The concept of sensor space was revised in a paper of (Gardner and Barlett, 1996). An upper limit for odour resolution (the maximum number of analytes distinguishable by a sensory array) was calculated for non-specific noisy sensors. That limit consisted in the ratio between the volume of the sensor space and the volume of the sensor errors. Pearce studied the problems of collinearity on the sensor space for an array of cross-reactive sensors (Pearce, 2000). He defined the concept of hyper-volume of accessible sensor space (V_S) as the volume on the sensor space containing the array responses to a set of odours. They found that very much correlated sensor responses caused low V_S values, and hence, a poor odour discriminability. This time, the upper bound of odour mixtures to be discriminated by the array was limited by the ratio between V_S and V_N, the hyper-volume spanned by the sensors' noise. Other estimations of the discriminative power of sensor arrays were based on Information Theory measurements. (Alkasab et al., 2002) calculated the Mutual Information (MI) for several synthetic arrays of noiseless binary sensors that coded a set of odour mixtures. Each of the populations was endowed with a different number of sensors featured with the same receptive range (the same percentage detectable odours of the odour space). The

authors found that MI increased with number of sensors of the population, obtaining the highest MI values for sensors with receptive ranges between 25%-35% of target compounds. In a more recent paper, (Fonollosa et al., 2013b) also employed the MI to evaluate the discriminatory power of an array of 4 MOX sensors modulated in temperature as a method of feature selection). They computed the MI between the presented stimuli (ethanol, acetic acid, 2-butanone and acetone) in the range of 0.1-1000 ppm and the response of the four-sensor array operating at different temperatures. The highest values of MI corresponded to the most discriminative features on the array. Sensor redundancy has also been studied by the e-nose community. To the best of our knowledge, the theoretical work presented by (Di Natale et al., 1993) was the first paper addressing the role of sensor redundancy in gas sensor arrays. They tried to reduce sensor noise of a simulated sensor array, for different types of noise. They showed that sensor redundancy was a key factor for signal denoising only in case of independent sensor noise. The effect of sensor aggregation in noise reduction was addressed in two works by (Wilson et al., 2000; Wilson, 2002). The authors calculated the theoretical computation for variance of the aggregate of sensors in case of identical independent and sensors. They found that for independent sensor noise, the variance of the sensor aggregate decreased a factor n^{-1} (where n was the number of sensors of the array). They compared the theoretical estimate of the variance with its measured value for an array of 40 nominally identical Tin-oxide gas sensors. Both computations of the variance were in agreement. Another approach to reduce sensor noise taking advantage of sensor

redundancy consists in selecting the subset of sensor units that contribute to noise in a population (Sánchez-Montañés and Pearce, 2001). In their work, the researchers performed this selection optimizing the Fisher Information of simulated arrays according to some parameter typical of the sensor's response characteristics. They presented two cases of study: Linear sensors subjected to independent Gaussian noise and sigmoidal sensors subjected to Poisson noise.

This chapter is focused on the study of sensor diversity and redundancy in our gas sensor array, and it is structured as follows. First, we show sources of structural sensor diversity and redundancy present in our array, in Section III.1. Section III.2 is devoted to illustrate that sensor diversity and redundancy support odour information encoding in sensor arrays. Taking into account the results of Section III.1 and Section III.2, we propose a more general definition of sensor diversity and redundancy for arrays of gas sensors, in Section III.3. Finally, in Section III.4 we discuss the different issues showed on this chapter and we present its main conclusions.

III.1. SENSOR DIVERSITY AND REDUNDANCY IN OUR SENSOR ARRAY

In Chapter II, we presented our bio-inspired prototype of electronic nose. We followed the strategy of combining sensor diversity and redundancy to build a chemical sensor array based on MOX sensors. On the one hand, sensor diversity was achieved using 8 different types of MOX sensors and modulating their temperature, which provided additional pseudo-sensors for different temperatures. On the other hand, sensor

redundancy was obtained by two means: first, including 12 sensors for each type for a total 96 and; second, using 16 different load resistors with a high-speed multiplexing system to read the response of the sensors through a voltage divider.

In the following subsections, we show a variety of examples of how sensor diversity and redundancy enhance to some extent the quality of the predictions obtained from an array of gas sensors. In particular, we check this issue for the different sources of structural sensor diversity and redundancy of our sensor array. This way, sensor diversity provided with different sensor types is studied in Section III.1.1, whereas sensor diversity obtained from different sensor temperatures is shown in Section III.1.2. In regard to sensor redundancy, Section III.1.3 presents sensor redundancy attained from a collection of sensor copies, and Section III.1.4 sensor redundancy acquired from the assortment of load resistors.

III.1.1. Diversity with different sensors

The combination of sensor readings belonging to different sensor units usually outperforms the predictive performance of the individual sensors in odour discrimination tasks. To exemplify this situation we present the following toy problem where we employ the readouts of two sensor types (SB-11 and SB-Q1) by separate and their combined response to odour samples with quadratic classifiers. Each of the sensors was set to operate at the same temperature (T=350 ºC). The experimental data consist of a subset 30 samples extracted from Dataset II. We expose the sensors to three pure odours (ethanol,

acetone and butanone) dosed at 20 ppm, for 10 times. This data is pre-processed converting the sensor's voltage readings into resistance values and posteriorly, performing the decimal logarithm of the result. We split up this dataset into training (60% of the samples) and test (the remaining 40% of the samples) subsets. To perform the odour identification, we build 3 quadratic classifiers. Two of them correspond to the individual sensor readings, whereas the third one is created from the combined response of the two sensor units. The predictive performance of the classifiers is checked using the test set samples.

Some data visualization is required for a better understanding of the problem that the classifiers are facing. Fig. 23(a) shows the combined response of the sensors to the 3 different odours, where blue, red and green markers represent respectively ethanol, acetone and butanone samples, and training and test samples are depicted using white-faced and solid triangles. From the figure, it is evident that the pooled response of the two sensors provides enough information to differentiate each of the odour classes from the others. However, none of the sensors can separately distinguish the three odours (note that the projection of the combined response on the X and Y axes corresponds, respectively, to the response of the sensors SB-11 and SB-Q1). We can see how sensor SB-11 differentiates acetone from ethanol and butanone, while sensor SB-Q1 discriminates butanone from the other two substances. The confusion matrices obtained using the different classifiers are found in figures Fig. 23(b) (sensor SB-11), Fig. 23(b)

(sensor SB-Q1), and, Fig. 23(d) (the combined response). As expected, Sensor SB-11 tends to confuse ethanol with acetone, whereas sensor SB-Q1 ethanol with acetone. Also in agreement with the data visualization, the classifier built employing the combined sensor response exhibits a perfect performance identifying the odour quality of the test set samples.

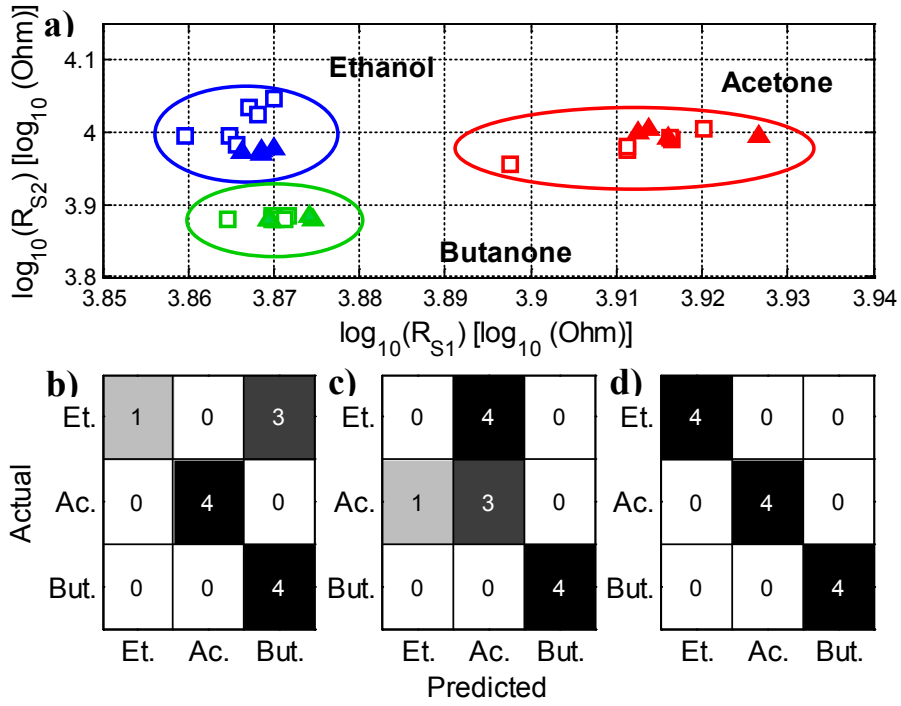

Fig. 23. Diversity with different sensors. (a) Scatter plot of the combined sensor response of an array of 2 sensors working at 350 ºC to 20 ppm of ethanol, acetone and butanone. On the figure R_{S1} refers to SB-11 sensor unit, whereas R_{S2} to the sensor SB-Q1; Confusion matrices of a quadratic classifier obtained from (b) the sensor SB-Q1, (c) the sensor SB-11, and (d) from combined response of both sensors.

III.1.2. Diversity with different temperatures

Temperature modulation increases the diversity of response of MOX sensors because modifies sensor sensitivity to odours. Thus, different odours cause a variety of response waveforms when exposed to the same sensor unit. We propose a binary classification task to show the advantages of temperature modulation for odour discrimination. The problem to solve is the following: we want to identify if a gas mixture contains more ethanol than acetone extrapolating from the sensor response to the pure components. That is to train a classifier (i.e. a linear classifier) from the sensor response to ethanol (Class A) and acetone (Class B) and check its performance when applied to samples were both compounds are present. We approach this task from two different points of view. First approach consists in a feature extraction problem, where we perform a dimensionality reduction of the set of sensor waveforms corresponding to different odour samples (Section III.1.2.1). This dimensionality reduction stage is realized by means of PCA decomposition. After that, we train and test the classifier with the projection of the samples on the PCA model (sample scores). PCA scores and loadings are analysed in order to obtain deeper comprehension about the role of sensory diversity in odour discrimination. The second approach is a feature selection problem, where only the pairwise combinations of sensor temperatures are considered input variables for the classifier (Section III.1.2.2). The figure of merit that allows us to select the best combinations of sensor temperatures is the area under the curve (AUC) of the Receiver Operating Characteristic (ROC) obtained from the classifier. Comparing the results of

sections III.1.3.1 and III.1.3.2 an intuitive inverse relationship between sensor feature correlation and sensory diversity is found. This toy problem is very interesting since illustrates that for an array of cross-sensitive sensory diversity depends on the complexity of the odour dataset.

We perform this binary classification problem using the readings of a TGS-2610 sensor unit (R_L=9.1 KΩ). We modulate the sensor temperature with a ramp profile with 90 temperature steps, from 25 to 475 ºC (ΔT_{STEP} =5ºC). Data samples from the training set are extracted from Dataset II and correspond to the sensor responses to pure ethanol and acetone at 20, 40, 60, 80, 100 and 120 ppm. On the other hand, test set samples belong to Dataset III and consist of the binary mixtures of ethanol and acetone with the following concentrations (in ppm): 100-20, 80-40, 40-80, and finally, 20-100. Each of data samples is acquired 10 times giving rise to a total of 120 samples on the train set (6 concentrations x 2 substances x 10 repetitions) and 40 samples on the test set (4 mixtures x 10 repetitions).

III.1.2.1. Feature extraction approach

We project the collection sensor waveforms corresponding to the set of odour samples onto a lower dimensionality space (2 dimensions) performing a PCA decomposition. By doing this, we can explore structure of the data and obtain some information about the effect of temperature modulation on the sensor's features. The scores plot of the data after dimensionality reduction can be seen in Fig. 24(a), where the white-faced black-

edged squares and the white-faced red-edged triangles represent respectively, samples from the training and test set. On the figure, we can see how the first Principal Component provides information related to sample concentration (concentration increases from positive to negative values on the PC 1 axis); whereas the second Component seems to be related to its chemical composition (positive values of PC 2 axis denote mixing proportions biased towards pure ethanol and vice-versa). Using this projected data, the linear classifier obtains a perfect performance. It is possible to find out which sensor features cause the chemical separability on the second Principal Component analysing the second loading vector, as can be seen on Fig. 24 (b). There, we observe that sensor temperatures with negative values on this loading tend to be sensitive to acetone, whereas positive ones to ethanol. Thus, we can roughly cluster the sensor features in two groups according to their ability to discriminate ethanol from acetone. The cluster temperature centres correspond to most extreme values of the loading vector. That is around 295 ºC, for the first cluster, and 390 ºC, for the second one.

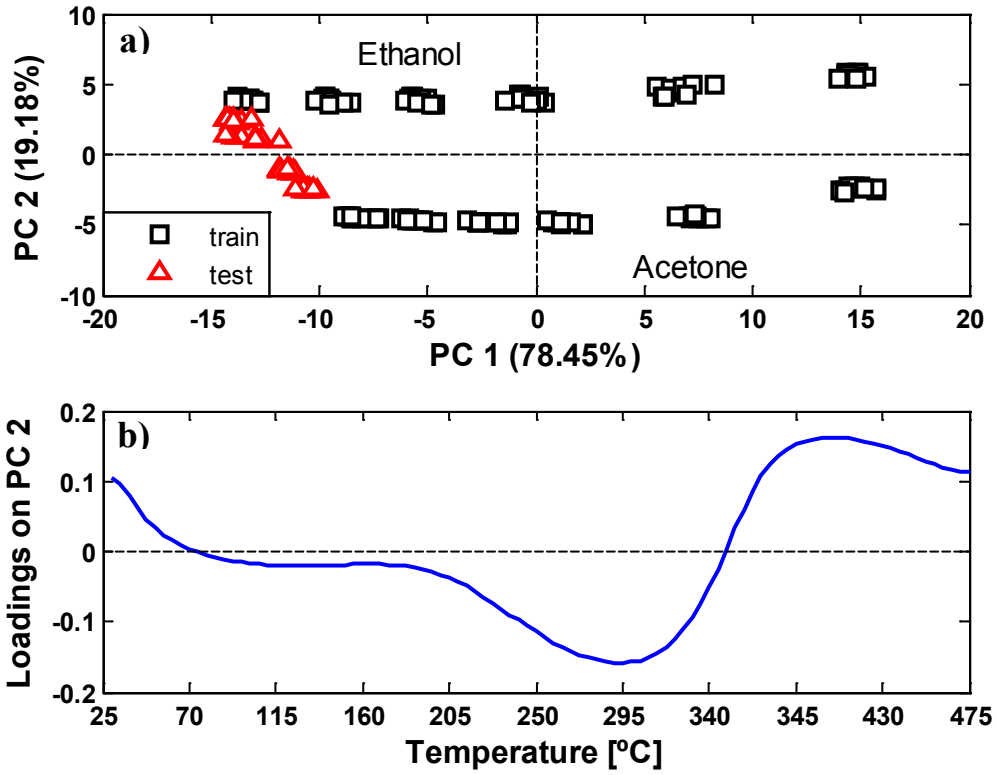

Fig. 24. Diversity with different temperatures plus feature extraction. (a) Scores plot of the PCA decomposition (2 Principal Components) obtained from the mean-centered waveform output voltage of the sensor TGS-2610 (RL=9.1 KΩ). The training set (pure odour samples) was represented by white-faced black-edged squares, and the test set (odour mixture samples) using white-faced red-edged triangles. We observe that the second Principal Component discriminates test set samples according to the pure major component on the mixture, (b) plot of the loading vector corresponding to the second Principal Component. We identify on this loading two clusters of sensor temperatures related to odour separation.

III.1.2.2 Feature selection approach

In order to identify the major pure compound present at the different samples belonging to the test set, we realize a feature selection problem consisting in optimizing the sensor response at two different temperature conditions. To do so, we evaluate the performance of the binary classifier for each pairwise combination of non-repeated sensor waveform features (9900 non-repeated temperature combinations = 100 x 100 temperature combinations -100 repeated temperature combinations). Since our classification problem is binary this can be done using the Receiver Operating Characteristic (ROC) curve. Basically, a ROC curve is a plot of the fraction of false positives (FPR) against the fraction the true positives (TPR), obtained from a classifier at a various threshold settings. For balanced class datasets (those that have a similar number of samples for the two sample classes), the area under the ROC curve (AUC) ranges from 0.5 to 1. An AUC equal to 1 indicates a perfect performance of the classifier, whereas if its value is close to 0.5 denotes a random classification.

So for each of the pairwise combination of sensor response features a ROC curve is generated. The process consists in calculating the FPR and the TPR for the collection of thresholds values from 0 to 1 in steps of 0.1. The FPR and the TPR are obtained as follows: First, the threshold to assign the class to new samples is selected. Then, the classifier is applied to the unlabelled samples. As a result, the classifier provides a posterior probability value of belonging to class A or B, for each sample. If the posterior

probability of a sample is greater than the threshold value, the sample is labelled as ‘Class A’, otherwise as ‘Class B’. Finally, a confusion matrix is created and the FPR and the TPR are calculated. For each of the ROC curves, the AUC is computed using the trapeze method of integration. The results of these calculations are shown in Fig. 25 where each binary combination of sensor temperatures is coloured in different warm tonalities according to their AUC value: lighter towards 1 and in dark tones towards 0.5. Besides this, we include contour lines on the figure to separate regions with different AUC level. Since the AUC value obtained from two features is the same independently of their sorting, the plot presents symmetry. The blue line that connects the lower left and the upper right corners of the colour map is its axis of symmetry.

These results are in agreement with those showed in Fig. 24(b). That means that feature combinations that perform a perfect classification (AUC=1) are found loading in opposite directions on the loading vector of the second Principal Component. On the contrary, the performance of the classifier tends to be lower when they are found on the same direction of the loading vector. The reason for that behaviour is that sensor sensitivity to odours varies gracefully with temperature. Consequently, sensor readings acquired at different enough temperatures tend to increase the variety of the sensor response **(i)**. On the other hand, similar temperatures tend to provide very much correlated sensor responses **(ii)**. From this point of view, we can consider the sensor features in **(i)** belonging to a different type of sensory unit, whereas in **(ii)** to the same type. Interestingly, the degree of

similitude between sensor features depends on the complexity of the set of odour stimuli. This is because we are estimating feature similitude using a limited set of odour conditions (both, quality and quantity). If a new analyte (i.e. butanone) was included to the current dataset, sensor features that exhibited similar responses to ethanol and acetone might show very different readings to the latter. Thus, sensory diversity of the response would increase. This effect would also be reflected in the loadings of a PCA decomposition performed on the new expanded dataset.

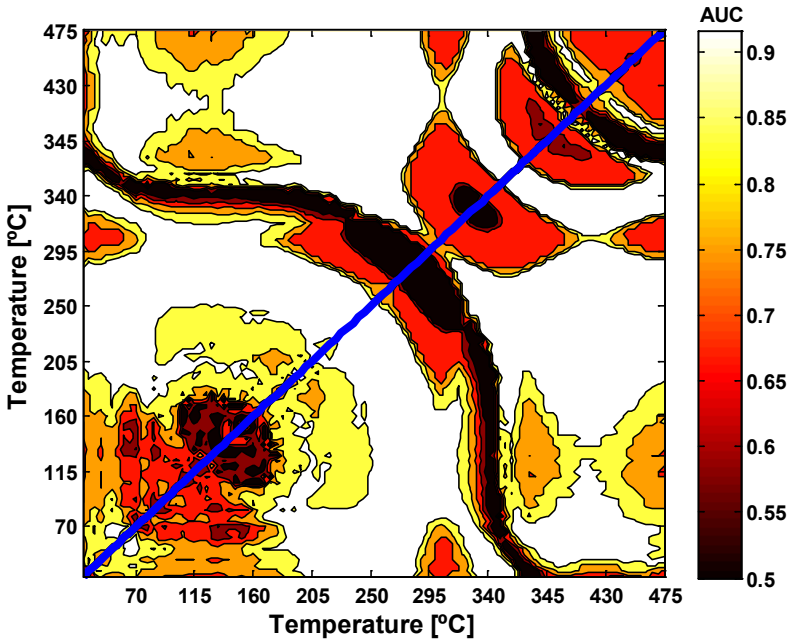

Fig. 25. Diversity with different temperatures plus feature selection. Contour map of the area under the ROC curve for the collection of linear classifiers built from the pairwise combinations of sensor output voltages (TGS-2610, R_L=9.1 KΩ) at different sensor temperatures. The performance of the classifier is coded by colour. Dark tones indicate poor odour discriminability, whereas light ones a good performance in odour separation. The blue line on the figure is drawn to point out the symmetry of the plot.

III.1.3. Redundancy with different sensor copies

The aggregation of different sensor copies in an array of sensors enhances its tolerance to independent sensor noise. The reason for that is that, under such a condition, each sensor reading can be considered the sum of two addends: first addend is the sensor response due odorant detection, whereas second one the independent sensor noise. Sensor aggregation of nominally equal sensors tends to reinforce the first addend (which is common to all the sensors), while reduces the contribution of the second (different for each of the sensors). Consequently, we expect to obtain a better predictive performance from the aggregate of sensors than from any of the sensor copies.

To illustrate this idea, we propose an odour quantification task where we compare the error of prediction achieved by an aggregate of 12 sensors (TGS-2610, T= 350ºC, R_L=9.1 KΩ) with the one obtained in average from the individual copies. These sensors were exposed to 7 different concentration of acetone (10, 50, 100, 500, 1000, 5000 and 10000 ppm) plus an additional measurement of synthetic dry air (dataset I). The complete set of experiments was repeated 10 times, where the order of concentration exposition was randomized. We divided this dataset into training (all the samples belonging to 10, 100, 1000 and 10000 ppm classes) and test subsets (the samples corresponding to the interleaved concentrations), to whom the Gaussian noise is added (μ=0, σ^2 increasing from 10^{-8} V^2 to 10^{-2} V^2, in steps of 10^{-8} V^2).

We used the training set to build the different sensor models based on the Clifford-Tuma dose-response curve, whereas the test set was employed to check their predictive performance. For each noise condition, 13 models were created: one per each of the individual sensor copies (12 models) plus one for aggregate of the sensors (1 model). Therefore, the number of models generated and tested amounts to 13000 (13 models x 1000 noise conditions).

The results of this study are shown in Fig. 26, where the mean RMSEP obtained from the individual errors of the sensor copies (left-sided boxplot) is compared with the RMSEP of the aggregate of sensors (right-sided boxplot). As can be seen, the individual sensors, *in average*, exhibit a worse tolerance against noise than the aggregate, since their RMSEP values are more spread and tend to higher values. Although some of the individual sensor copies may outperform the aggregate on quantifying acetone concentration for each noise condition, this information is not available *a priori* (before the calibration stage). So the most general option to enhance the concentration estimation while keeping robust predictions still is the aggregation sensor responses (for independent sensor noise and homogeneous arrays).

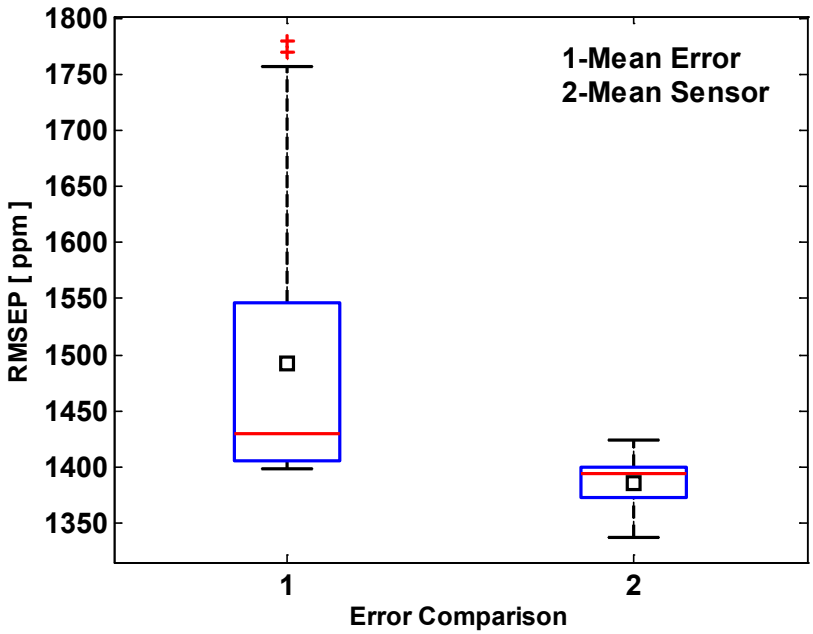

Fig. 26. Redundancy with different sensor copies. Boxplot corresponding to (1) the mean RMSEP of the individual sensor replicates and, (2) the RMSEP of the mean individual of the population, for a variety of Gaussian noise conditions. The sensor array was exposed to 10, 50, 100, 500, 1000, 5000 and 10000 ppm. We trained a Clifford-Tuma model employing the sensor readings at 10, 100, 1000 and 10000 ppm. The RMEP was calculated from the model predictions at 50, 500 and 5000 ppm.

III.1.4. Redundancy with different load resistors

Often, sensor copies are not perfect in the sense that they present a certain degree of variability in their dose-response characteristics to odour stimulus. In such a case, sensor optimization is another possible approach to reduce sensor noise in homogeneous arrays. This strategy consists in selecting the suitable subset of sensors that optimizes a given condition.

We propose an odour quantitation task where we use sensor array optimization to down-weight the contribution of independent sensor noise, and thus, to enhance the predictive performance of a sensor array. To this end, we built a homogeneous sensor array from combining a single sensor unit with collection of load resistors (our sensor array comprises a set of voltage dividers). We propose to find out the set of voltage dividers that optimizes data collection for a set of odour concentrations. Moreover, we propose to compare the predictive performance in concentration estimation achieved by this feature selection approach to the one obtained from the individual voltage dividers. Intuition suggests that the best sensing condition for encoding a particular odour concentration occurs when a sensor unit exhibits the maximum sensitivity to that concentration. The condition for maximum sensitivity in our measuring circuit is achieved when the resistance of the MOX sensor equals the resistance of the load resistor (R_L=R_S). When this condition is fulfilled, the response of the voltage divider is V_O=V_{DD}/2, where V_{DD} is the bias voltage (V_{DD}=10 V in our sensor array).

Our sensor array is composed of 16 sensor units corresponding to voltage readings from connecting one TGS-2610 gas sensor (T=350ºC) to a set of 16 load resistors (0.10K, 0.25K, 0.40K, 0.87K, 1.30K, 3.01K, 6.19K, 9.09K, 21.00K, 30.01K, 40.20K, 51.10K, 68.10K, 82.5K, 90.90K, 105.K). We exposed this sensor array to 7 different concentrations of acetone, according to dataset I (10, 50, 100, 500, 1000, 5000, and 1000 pmm). We splited up this dataset into training and test subsets, as in Section III.1.3. And

we added independent Gaussian noise to these subsets (μ=0, σ^2 increasing from $0.33 \cdot 10^{-5}$ V^2 to $3.0 \cdot 10^{-5}$ $V^{2,}$ in steps of $0.33 \cdot 10^{-5}$ V^2). Then, we transformed the sensor readings from voltage (V_S) to resistance (R_S) values. We performed this transformation in two different manners: First manner consisted in using the value of load resistor corresponding to the current voltage divider to convert voltage to resistance, for each voltage divider. Therefore, we obtained an array of 16 sensor units. The second way consisted in calculating the value of the sensor resistance for each concentration, using the load resistor that was closer to satisfy the condition of maximum sensitivity of the voltage divider. Note that following this strategy of sensor array optimization we only obtain a single sensor unit. Employing these set of sensor readings expressed in resistance, we created 17 Clifford-Tuma models from the training set samples (16 from the individual sensor readings plus one 1 the feature selection approach), for each noise condition. Next, we calculated the error of calibration (RMSEP) for all these models using the test set samples. In order to perform a statistical analysis of the results, this process was repeated 1000 times for different noise initializations. Thus, the total number of prediction models generated for this task was 15300 (17 sensor units x 9 values of the noise variance x 1000 initializations).

Fig. 27 shows the RMSEP along the noise variance for the voltage divider that minimizes the RMSEC (R_L=6.19KΩ), and for the set of sensor resistances acquired in conditions of maximum sensitivity. We can observe that the mean RMSEP of the two sensors keeps

constant around a similar value for increasing levels of noise variance. This is a direct consequence of our selection of the sensor noise, since it was Gaussian with zero mean. The main difference between sensor lied is their ability to reject the variance of the sensor noise. Clearly, our sensor array optimization approach is the most robust since we obtain a narrower range of RMSEP values (at least 3 orders of magnitude for the worst case of noise variance).

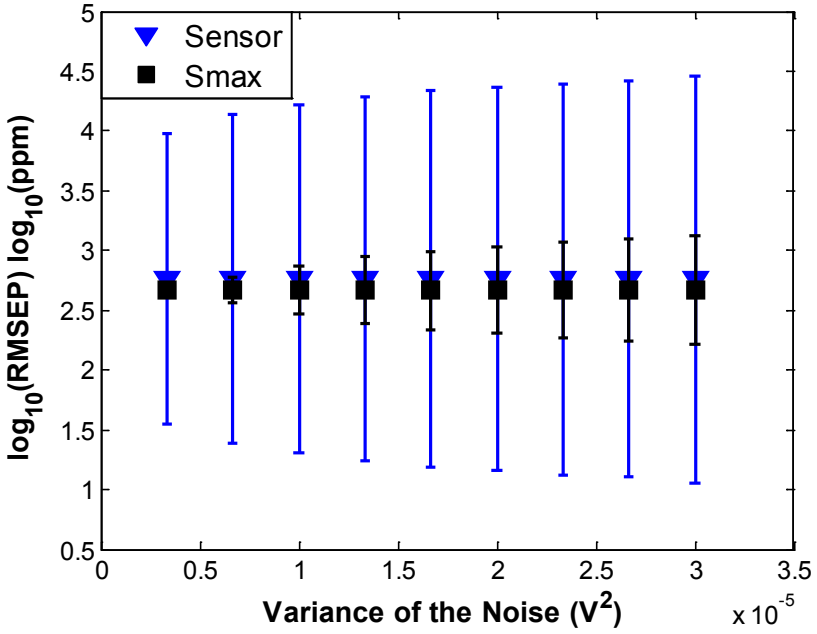

Fig. 27. Redundancy with different load resistors. Root Mean Square Error along noise variance (Gaussian noise, μ=0) for the test set. Black squares represent the error values obtained at the best sensitivity conditions for data acquisition, whereas blue triangles those ones acquired for the combination of sensor and load resistor that minimizes the error of the training set.

III.2. ENCODING ODORANT INFORMATION

Along Section III.1, we have seen in an intuitive manner how sensor diversity and redundancy support the coding of the odorant information in our sensor array. Now, we present a more formal approach to address this issue based on statistics and Information Theory measures. This section is divided in two parts: Section III.2.1, where we evaluate the coding capacity for arrays of virtual sensors endowed with different degrees of sensor diversity; and Section III.2.2, where we study in deep the role of sensor redundancy in noise reduction.

III.2.1. Sensor diversity and coding capacity

The performance of a sensor array in encoding odour stimuli can be estimated from an Information Theory (IT) point of view. This task can be done by using two different measures of information content: Entropy and Mutual Information.

Entropy measures the uncertainty of guessing by chance the state of the random variable X from the probability of occurrence of each of the possible states of X, $p(x_i)$:

$$H(X) = -\sum_i p(x_i)\, log_2 p(x_i) \tag{3.1}$$

According to the previous equation, the greater is the entropy of a set of states (message) the more complex is to guess the current state of X.

Similarly, Mutual Information (MI) is a measure of the information that two random variables X,Y share. Mutual Information is calculated from the marginal probability distributions p_x (i) and p_y (j), and the joint probability distribution function p_{xy}(i,j):

$$MI(X,Y) = -\sum_{i,j} p_{xy}(x_i)\, log_2 \frac{p_{xy}(i,j)}{p_x(i)p_y(j)} \tag{3.2}$$

Note that for independent random variables $p_{xy}=p_x\, p_y$ and MI=0. We can employ mutual information to measure how much information from a set of odour stimuli can be explained from a set of sensor responses.

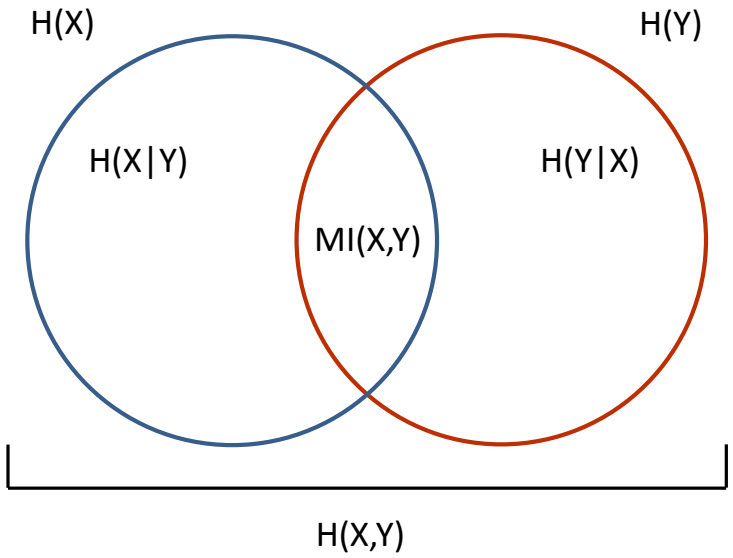

Fig. 28. Venn diagram for various information measures: Individual entropies (H(X), H(Y); Conditional entropies (H(X|Y), H(Y|X)); Joint entropy (H (X,Y); and Mutual Information (MI(X,Y)). Note that X and Y are correlated variables.

III.2.1.1. Measure of the quality of the odour encoding

We conducted a synthetic experiment to compare the quality of the odour encoding achieved by arrays of sensors endowed with different levels of sensor diversity. To this purpose, we measured a set of odours (L=1024) consisting of mixtures of pure substances (M=10) dosed at different concentrations using two arrays of virtual sensors. In first of these arrays, the sensors worked as partial selective detectors with zero concentration thresholds. That means that a sensor unit responded with a logical '1'only to the pure components to which was sensitive (its molecular receptive range, RR) and '0' otherwise (see Fig. 29). In the second array, the sensors were identical to the above-mentioned, but included an additional source of sensor diversity. This sensor population was endowed with a variety of dose-response characteristics. In particular, each of the sensors responded only to a subset of pure compounds beyond a limit of detection (different for each pure compound). In both arrays, the number of sensors (N) and their molecular receptive range (RR) were tuneable parameters. We computed H for the given set of odours, and MI for a number of sensor arrays with different size (N=1, 2, 4, 8, 16, 32, and 64 sensors) and receptive range (RR= 5, 10, 15, 25, 30 35, 40, 45, 50, 55, 60, 65, 70, 75, 80, 85, 90 and 95%). This process was repeated 100 times. As a result, the values for the average MI and its standard deviation were computed, for each N-RR combination. Section III.2.2.1, explains in detail explain how to build the sets of odours and sensor responses, and how to obtain the MI between both groups.

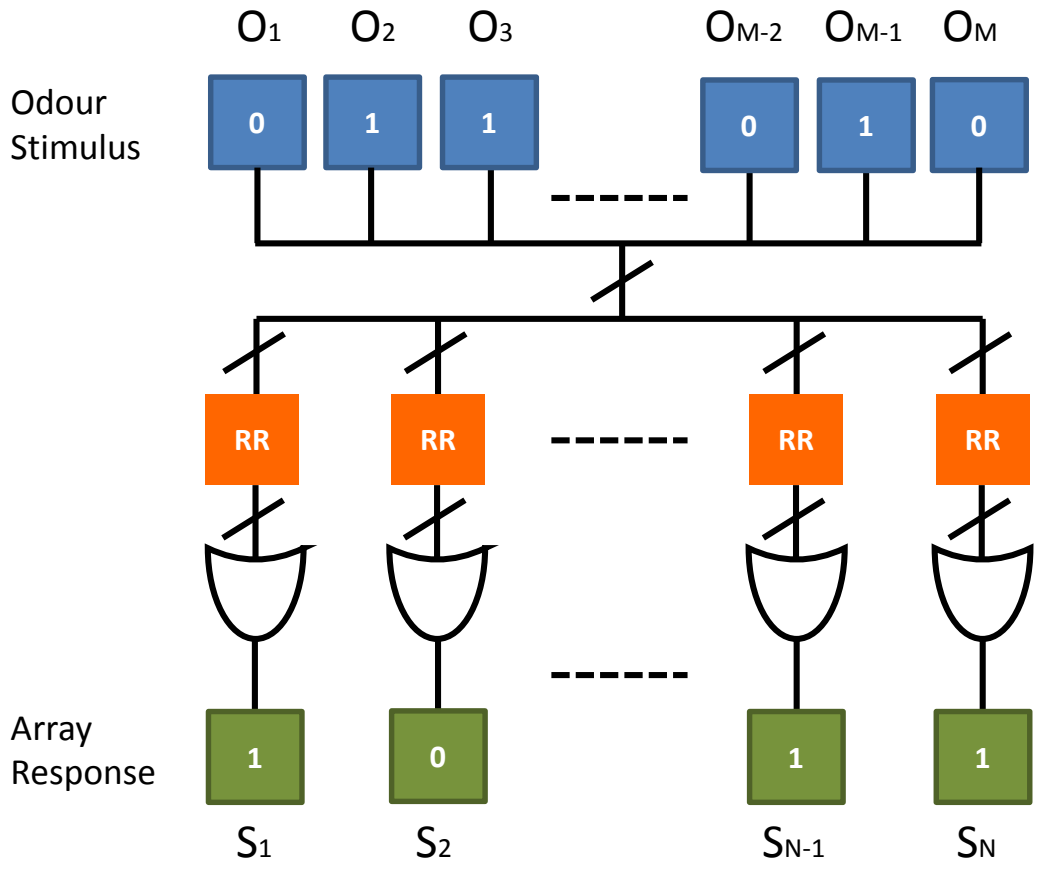

Fig. 29. Scheme of the generation of the array response. We obtain a set of virtual binary sensors (S_1 to S_N) from a mixture of pure compounds (O_1 to O_M). Note that this scheme is simplified since no information about odour concentration is provided.

III.2.1.2. Methods

To conduct this experiment we had to realize three different subtasks. First task was the creation of the set of odour samples. Second tasks consisted in building the set of sensor responses. Finally, the first tasks the computation of the MI information between the odour and sensor sets.

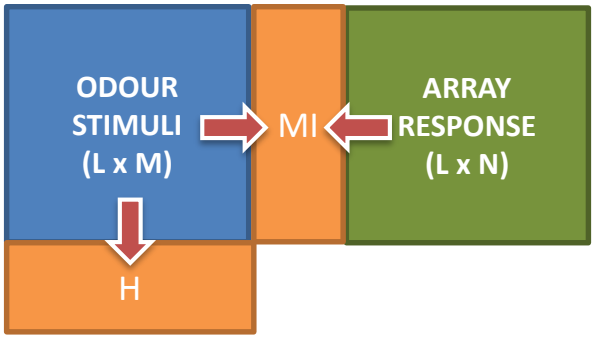

Fig. 30 Block diagram of the computation of the H and MI. These measures are computed, respectively, from the odour stimuli set and odour stimuli and the array response sets.

We generated a synthetic combination of pure odours by concatenation of the M bits that represented the pure compounds. A logical '1' stood for the presence of the pure odour on the mixture and, '0' its absence. Each of the 2^M possible combinations had an equal probability of occurring. We assigned a concentration value to the pure odours of the mixture from a uniform distribution of values ranging from C_1 to C_2 arbitrary units of concentration. The final dimension of the set of odour mixtures (L x M) was achieved repeating the previous process L times. The entropy of the set was then obtained through the calculus of the frequency of occurrence of each mixture, according to equation (3.1). Regarding the set of set of sensor responses, we created an array of N sensors sensitive to some of the pure odour compounds and blind to the rest in a process of three stages. In first stage, we built a correspondence map (CM) between pure odours and sensors. The map was generated comparing the elements of an N x M matrix of uniformly distributed numbers ranging 0 to 1 with a threshold value. If the element matrix was higher than the

threshold, then the sensor is sensitive to this pure compound (‘1’). If not, the sensor was not able to detect it (‘0’). The value for threshold was set to 1-RR, where RR was the receptive range of the sensor. Note that, at this point, the CM did not provide any information about concentration. In the second stage, we set the thresholds of detection of each sensor to its respective detectable pure compounds. To do it, we took two different approaches: a) the thresholds of detection were always placed at a zero concentration level and b) the thresholds of detection followed the same uniform distribution that generates the concentration of the pure odours. Thus, if a sensor was sensitive to a pure compound its response was ‘1’: a) regardless of their concentration and b) only if the concentration is higher than the threshold of detection. At the end of this stage, the original CM was kept in a), but a new CM’ providing information about the mixing proportion of the odour combination was obtained from b). We calculated the combined response of the set of sensors to an odour mixture on the third stage. The individual sensor response to a combination of pure odours was computed as the logical OR of the different sensor responses to the pure compounds. Therefore, if a sensor was sensitive at least to one of the pure components of the mixture, its response is ‘1’. Finally, the individual sensor outcomes to the mixture were linked and the pattern of response was obtained. As the set of odour mixtures was composed of L samples, the set of sensor responses has a dimensionality L x N. Once we generated the set of odour mixtures and their corresponding array responses, we calculated its mutual information following equation (3.2). The marginal distributions of probability of the set of mixtures and the set

of responses were obtained computing the frequency of occurrence of each odour mixture and array responses in their respective sets. To obtain the joint probability distribution, a mapping between the odour mixtures and the different non-repeated array responses was created. Then, the probability of having a certain odour stimulus knowing the state of the response was calculated, for each of the responses.

III.2.1.3. Results

The outcomes of this experiment are shown in Fig. 31 (for the first array) and Fig. 32 (for the second one). On both figures, each curve represents the MI of a different-sized (N) array of sensors along the sensor's RR. Also, the value for the entropy (H) of the odour stimuli set is included on the plots using an orange dashed line. We note that this value corresponds to the maximum value of MI that can be obtained from a sensor array that encodes the set of odour stimuli (basically, the complexity of the odour set can be totally explained by the set of array responses). In our simulated odour datasets, entropy takes the value of 10 bits.

Regarding MI, we first comment on the results of the first sensor array. Noteworthy, MI is more affected from changes on the sensor's RRs than from the particular pure odour subset to which the sensors are sensitive, since it is different for each MI calculation. As a general result (that is with independence of the size of population, N), MI is an non-symmetric unimodal curve, whose maximum value is found around the 15-25% of the RR, and that decreases to zero when the RR tends to 100%. This behaviour can be

explained considering the variability on the array response according to the sensor's RR: For lower RRs the sensors tend to respond only to one pure odour, so many of the array responses to the set of stimuli may be identical. When the sensor RR increases, the number of different array responses also does, and a lesser number of odour stimuli are confounded. The maximum variability on the array response corresponds to the maximum MI. Beyond this point, an increase on the sensor's RR decreases the MI because the sensors can detect enough pure compounds such that different combinations of them cause the same array response. On the other hand, an increment on the array size enhances the performance of the MI. Concerning the evolution of the MI maxima; it can be observed that beyond an array size the contribution to MI of new added sensors is lesser. This occurs when the set of array responses is complex enough to explain most of the variability of the odour stimuli, so adding new sensors mostly provides redundant information. If we turn our attention to the results of second array, we can observe a manifest improvement on the odour information encoding. First, the maximum MI value (which is placed near the 25% of the RR) is always higher for population size of sensors in this array. And, second, the MI is more robust to the deterioration of sensor selectivity occurred at high RR values. This is because each sensor on the array contributes both in decreasing the state uncertainty of odour quantity and quality of the set of stimuli.

These results are quite interesting; in the sense that they provide some intuition to how different olfaction systems (natural or artificial) encode for odour information. In natural

olfaction systems, the olfactory receptors have been tuned by evolution to optimally extract the information from the set of odours that maximize the probability of survival. This set of odour stimuli may be considerably different for each animal species (i.e. in size and complexity). Consequently, large differences in terms of receptor characteristics are expected between very distinct species. This optimization process performed by nature on the olfactory receptor is analogous to our problem of maximizing the MI in our sensor arrays. Comparing the set of maxima values of MI of the two arrays, we realize the major contribution to odour encoding depends on the ability of the population of receptors to estimate the identity of an odour stimulus, not its intensity.

On the contrary, in artificial olfaction systems, no optimization of the population of sensor elements is performed a priori. Moreover, typical gas sensor technologies (MOX, CP, QCM, etc.) employed in artificial olfaction are poor selective to odours (they present large RR values). Again, if we contrast the results of MI of both arrays, we observe that set of odour stimuli can be efficiently encoded by a (large) population of poor selective receptors only if they provide differential information odour intensity. So, we may say that in artificial olfaction systems odour encoding is mainly concentration-based.

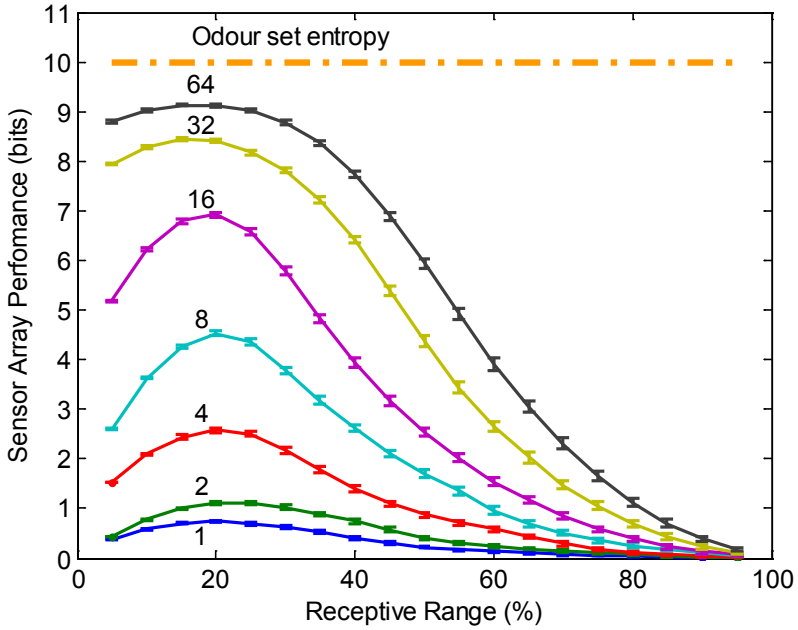

Fig. 31. Computation of the coding power for the first array of sensors. Mutual Information (MI) along the molecular receptive range of the population of receptors (RR). These sensors exhibit a binary response to odours (‘1’ when a sensor is sensitive to a pure compound, and ‘0’ if not), independently of the pure compound concentration. The corves on the figure correspond to different sizes of the population of receptors (N). The orange dashed line is the value for the entropy of the odour stimuli set.

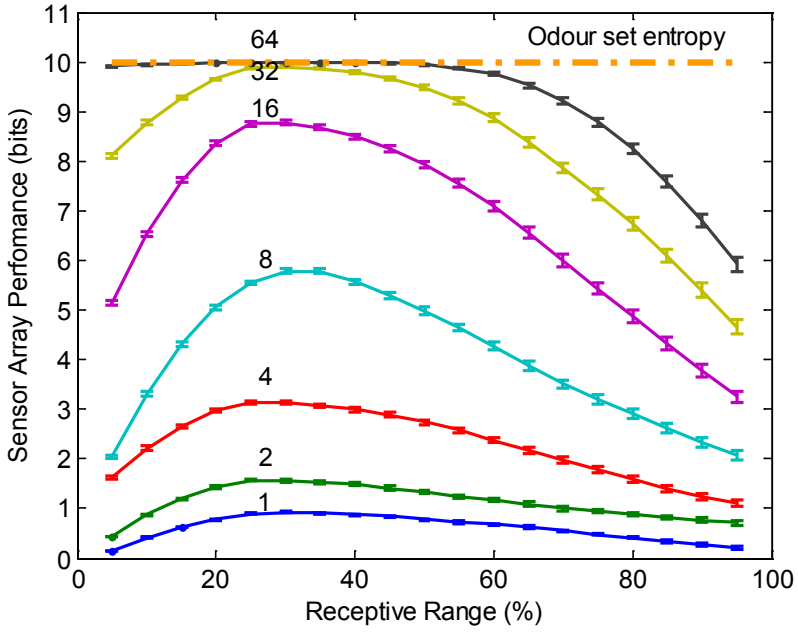

Fig. 32. Computation of the coding power for the second array of sensors. Mutual Information (MI) along the molecular receptive range of the population of receptors (RR). These sensors exhibit a binary response to odours (‘1’ when a sensor is sensitive to a pure compound, and ‘0’ if not), beyond a threshold level of concentration. The corves on the figure correspond to different sizes of the population of receptors (N). The orange dashed line is the value for the entropy of the odour stimuli set.

III.2.2. Sensor redundancy and noise reduction

This section explores formally the role of sensor redundancy for noise reduction in gas sensor arrays. We perform this study following two types of noise reduction strategies: sensor aggregation (Section III.2.2.1) and sensor array optimization (Section III.2.2.2).

III.2.2.1. Noise reduction by sensor averaging

In order to compact the redundant information of an array of homogenous MOX sensors, we can average their response performing the mean of their output voltage:

$$\bar{V}_O = \sum_{i=1}^{i=N} \frac{V_{Oi}}{N} \tag{3.3}$$

where N is the number of sensors of the array, V_{oi} is the individual sensor output and $\overline{V}_O$ their mean value. Assuming that the output voltage of each sensor is independent from the others, the variance of the aggregate of sensors becomes:

$$\sigma_{\bar{V}_O}^2 = \sum_{i=1}^{i=N} \sigma_{\bar{V}_{Oi}}^2 \left(\frac{\partial \bar{V}_O}{\partial \bar{V}_{Oi}} \right)^2 \tag{3.4}$$

But the variance of $\sigma_{V_{oi}}^2$ the individual sensor is equal to the variance of the population of sensors:

$$\sigma_{V_{Oi}}^2 = \sigma_{V_O}^2 \tag{3.5}$$

Performing the derivative respect V_{oi} in equation (3.3), we find that:

$$\frac{\partial \bar{V}_O}{\partial \bar{V}_{Oi}} = \frac{1}{N} \tag{3.6}$$

And therefore, the variance of the output voltage for the aggregate of sensors is:

$$\sigma^2_{\bar{V}_O} = \frac{\sigma^2_{V_O}}{N} \tag{3.7}$$

That means that increasing the number of sensors of the array the independent contributions to sensor noise are down-weighted. So the dispersion on the output voltage values (for a given stimulus) decreases as 1/N. However this is not the general case of sensor noise in chemical sensing. There are common mode contributions to sensor noise due to the inherent sensing architecture of the instrument. For instance, in our array, the sensors are heated up simultaneously through the same heater waveform V_H, and all the measuring circuits are polarized using a unique voltage V_{DD}. Similarly, the errors due to instabilities on the odorant concentration are also common to all the sensors of the array since the measurements are performed approximately at the same time. In this case, the variance of the aggregate of sensors is:

$$\sigma_{\bar{V}_O}^2 = \sum_{i=1}^{i=N} \sigma_{\bar{V}_{Oi}}^2 \left(\frac{\partial \bar{V}_O}{\partial \bar{V}_{Oi}}\right)^2 + 2 \sum_{j=1}^{j=N} \sum_{i<j} cov(V_{Oi}, V_{Oj}) \left(\frac{\partial \bar{V}_O}{\partial \bar{V}_{Oi}}\right)\left(\frac{\partial \bar{V}_O}{\partial \bar{V}_{Oj}}\right) \tag{3.8}$$

where $\mathrm{cov}\ (V_{oi}, V_{oj})$ is the covariance between the output voltage of the sensors *i* and *j*. Substituting (3.7) in (3.8), we find that:

$$\sigma_{\bar{V}_O}^2 = \frac{1}{N^2}\left(\sum_{i=1}^{i=N} \sigma_{V_{Oi}}^2 + 2 \sum_{j=1}^{j=N} \sum_{i<j} cov(V_{Oi}, V_{Oj})\right) \tag{3.9}$$

The two addends on the right side of (eq.3.9) can be rearranged in a unique term. Thus:

$$\sigma_{\bar{V}_O}^2 = \frac{1}{N^2}\left(\sum_{j=1}^{j=N} \sum_{i=1}^{i=N} cov(V_{Oi}, V_{Oj})\right) \tag{3.10}$$

Example:

To show the limitations of noise reduction using sensor aggregation due to the common mode sensor noise, we compute the output voltage variance of an aggregate of MOX sensor copies, for an increasing number of sensors. This result is compared with the theoretical value of variance that would be obtained from the aggregate, assuming that the sensor noise is independent. Our study is performed using 12 sensor copies of a TGS-

2610 sensor model, set to work at 350ºC and connected to load resistor of 9.1 KΩ. The sensors were exposed to 500 ppm of acetone. The concentration of acetone was generated independently for each of the 10 repetitions of the experiment (Dataset I).

We analyse the covariance matrix of the output voltage obtained from the 12 voltage dividers for a better understanding of the nature of noise (Fig. 33). The diagonal elements of the matrix are the variances corresponding to each of the individual sensor responses, so they are always greater than zero. For the non-diagonal elements, the covariance value can be either positive or negative. If noise tends to increase or decrease the value of both sensor responses, the relationship is positive, otherwise is negative. If only independent sensor noise is present in the array, the addition of the non-diagonals elements should approach to zero because the random errors in sensor's output voltages would tend to compensate. That summation for the current case is $3.9\ 10^{-3}\ V^2$, which is higher than the value for the addition of the diagonal elements of the covariance matrix, $1.8\ 10^{-3}\ V^2$, so sensor noise is dependent. From (3.10) the variance on the output voltage for the aggregate of N sensors, $\sigma^2_{\bar{V}_o}$, is the sum of the elements of the covariance matrix divided by N^2. For N=12, the result is $3.96\ 10^{-5}\ V^2$.

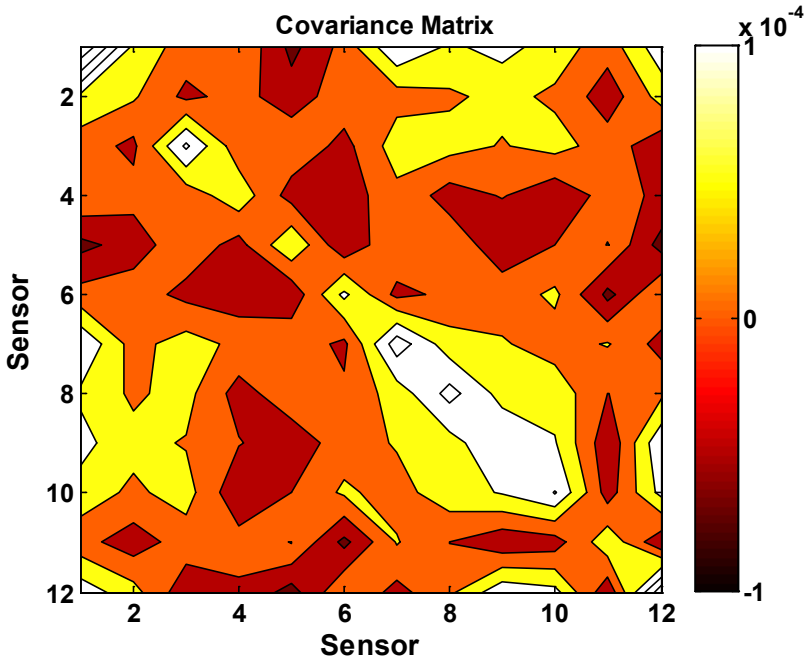

Fig. 33. Covariance matrix of a redundant sensor array. This array includes 12 sensor copies exposed to 500 ppm of acetone. Sensor readings were expressed in terms of the sensor output voltage.

Alternatively, the variance of the aggregate can be calculated directly from the value of the averaged output voltage of the N sensors. This result is shown in Fig. 34. There we can see the variance of the aggregate for an increasing number of sensors (from N=1 to N=12) in a black curve with red square markers. We note that the variance calculated from the aggregate of 12 sensors agrees with the value of variance obtained from (3.10). The plot also includes the expected value of value of the variance in case of uncorrelated noise (blue dashed line). It is verified that its value decreases faster with the number of for the ideal case than in the real measurement.

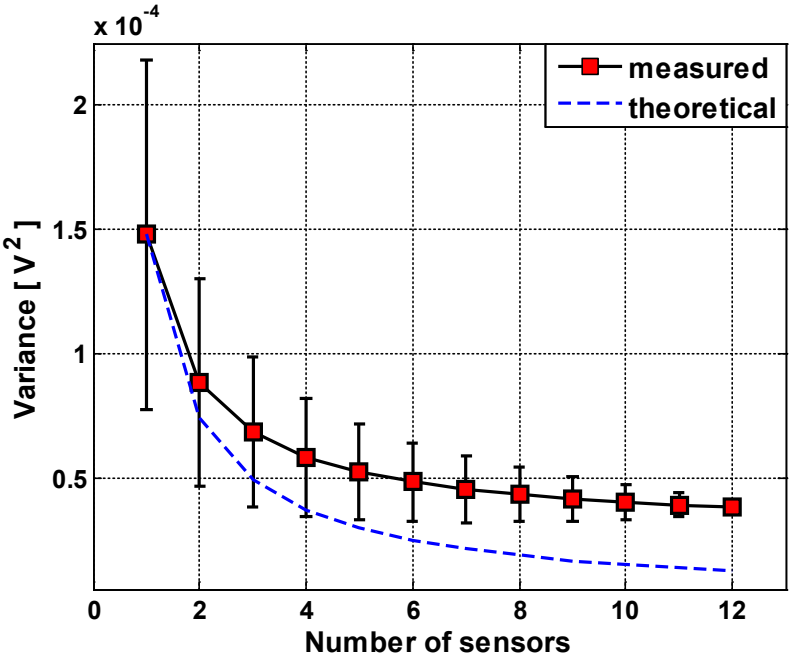

Fig. 34. Variance of the aggregate of sensors along the number of copies. This array was exposed to 500 ppm of acetone. The black curve with red squares markers corresponds to the measured value of the sensor array variance, whereas the blue dashed one to its theoretical value in case of uncorrelated noise. Sensor readings were expressed in terms of the sensor output voltage.

III.2.2.2. Noise reduction by sensor array optimization

Sensor noise can be decreased optimizing the set experimental data acquired by the sensor array. In section III.1.3, this optimization was performed for a collection of voltage dividers built from a single MOX sensor and a collection of 16 load resistors with different values. Our optimization criterion was to select those load resistors that maximized the sensitivity of the voltage divider, for each concentration condition. In this section we justify theoretically our choice. We propose to optimize a synthetic sensor

array of voltage dividers subjected to independent Gaussian noise, using the Fisher Information. In order to model the response to odorant concentration of the sensor, we employ a Clifford-Tuma dose-response curve. First we revise the formalism behind the computation of the Fisher Information, and after that we compute its value for our particular synthetic sensor array.

When we expose an array of sensor elements (k=1,..,N) to a quantity of stimulus *s*, it provides a collection noisy responses r_k according to some probability distributions $p(r_k|s)$. Then, the Fisher Information $J_k(s)$ for k-th element of the array comes given by:

$$J_k(s) = \int dr\, p(r_k|s) \left(\frac{d}{ds} ln \;\; p(r_k|s) \right)^2 \tag{3.11}$$

The Cramér-Rao bound estates that the inverse of the Fisher Information is the lower limit on the variance of any unbiased estimator $\hat{s}$ that uses r_k to estimate the intensity of stimulus *s*:

$$var(\hat{s}) = J_k^{-1}(s) \tag{3.12}$$

Additionally, it can be demonstrated that the expected error in quantifying *s* from r_k of any unbiased estimator $\hat{s}$ satisfies:

$$E[(\hat{s}-s)^2]|_k \geq \int ds \;\; p(s) \;\; J_k^{-1}(s) \tag{3.13}$$

where *p(s)* is the a priori density of probability of the intensity of stimulus. From the above equation, it can be seen that maximizing Fisher Information corresponds to minimizing the expected error.

Let's suppose that the k-th sensor of our array suffers from a Gaussian noise $p_G(r_k|s)$, whose variance σ_k is independent from the intensity of the stimulus:

$$P_G(r_k|s) = \frac{1}{\sigma_k\sqrt{2\pi}} exp\left(-\frac{\left(r_k(s)-\bar{r}_k(s)\right)^2}{2\sigma_k^2}\right) \tag{3.14}$$

where $\bar{r}_k(s)$ is the mean response of the k-th sensory element obtained from its stimulus-response curve. Replacing this probability density in equation (3.11) and arranging terms, it is found:

$$J_k(s) = \frac{1}{\sigma_k^4}\left(\frac{\partial\bar{r}_k}{\partial s}\right)^2 \int dr \;\; p_G(r_k|s) \;\; \left(r_k(s)-\bar{r}_k(s)\right)^2 \tag{3.15}$$

But the integral in equation (eq.3.15) is the calculation of the variance:

$$\int dr \;\; p_G(r_k|s) \;\; \left(r_k(s) - \bar{r}_k(s)\right)^2 = E[(\hat{s} - s)^2]|_k = \sigma_k^2(s) = \sigma_k^2 \tag{3.16}$$

Thus, the Fisher Information of the *k-th* sensory element can be written as:

$$J_k(s) = \frac{1}{\sigma_k^2}\left(\frac{\partial \bar{r}_k}{\partial s}\right)^2 \tag{3.17}$$

At this point, we only need to know $\bar{r}_k(s)$ to compute Fisher Information. The Clifford-Tuma approach is usually employed to model the stimulus-response curves of MOX gas sensors. This model relates the sensor resistance R_{sensor} to the concentration odorant c through the following almost power law:

$$R_{sensor}(c) = R_o\left(1 + k_{gas}c\right)^{-\beta_{gas}} \tag{3.18}$$

where β_{gas} , k_{gas} are gas dependent constants that correspond, respectively, to the sensitivity and threshold of detection to the given gas and R_0 is the initial sensor resistance value in synthetic air or any other carrier gas. As the measuring circuit used to acquire sensor resistance is a voltage divider, the sensor response (for the given the sensor model) is obtained substituting $R_{sensor}(c)$ from equation (3.18) into the formula of the voltage divided formed between $R_{sensor}(c)$ and R_L:

$$V(c) = \frac{V_{DD}}{1 + \frac{R_L}{R_0}\left(1 + k_{gas}c\right)^{\beta_{gas}}} \tag{3.19}$$

We can optimize the sensor response acquisition under Gaussian noise conditions through the selection of the best tuning curve $V(c,R_L)$, for a given range of concentrations. That is to select the best R_L from a load resistor in that range. Computing the Fisher Information according to (3.17), and assuming that the variance of the noise σ^2 is identical for each of the voltage dividers then:

$$J_{R_L}(c) = \frac{1}{\sigma^2}\left(\frac{\partial V(c,R_L)}{\partial c}\right)^2 \tag{3.20}$$

Therefore, the Cramér-Rao bound is:

$$var(\hat{c}) \geq \sigma^2\left(\frac{\partial V(c)}{\partial c}\right)^{-2} = \frac{\sigma^2}{V_{DD}^2\beta_{gas}^2k_{gas}^2}\frac{\left(1 + \frac{R_L}{R_0}\left(1 + k_{gas}c\right)^{\beta_{gas}}\right)^4}{\left(\frac{R_L}{R_0}\right)^2\left(1 + k_{gas}c\right)^{2(\beta_{gas}-1)}} \tag{3.21}$$

The right term of the inequality can be rewritten as a product of two factors replacing the explicit dependence of the sensor resistance to concentration in (3.18) by R_{sensor}:

$$var(\hat{c})_{R_L} \geq \frac{\sigma^2}{V_{DD}^2 \beta_{gas}^2 k_{gas}^2}\left(1 + k_{gas}c\right)^2 \left(\left(\frac{R_L}{R_{sensor}}\right)^{\frac{1}{2}} + \left(\frac{R_{sensor}}{R_L}\right)^{\frac{1}{2}} \right)^4 \tag{3.22}$$

The first factor depends on V_{DD}, the sensor (β_{gas} , k_{gas}) and noise (σ) characteristics, and concentration (c); whereas the second one only depends on the ratio of the resistances R_{sensor} and R_L. Note that the minimum value for the second factor is achieved for R_L=R_{sensor}, and that far beyond this point (R_L<<R_{sensor} or R_L>>R_{sensor}) its contribution to the variance of the unbiased estimator of *c* increases dramatically. Consequently, to optimize the response of the sensory element is equivalent to maximize the sensitivity of the voltage divider, for a given odour concentration. So, for the best noise rejection conditions, the Cramér-Rao bound becomes:

$$var(\hat{c})|_{S_{max}} \geq \frac{16 \ \ \sigma^2}{V_{DD}^2 \beta_{gas}^2 k_{gas}^2}\left(1 + k_{gas}c\right)^2 \tag{3.23}$$

Example:

We study the effect modifying the parameter R_L (R_L= 0.05, 0.2, 0.8, 3, 13, 52, 205 and 820 KΩ) on the quality of a signal acquired by a simulated MOX sensor exposed to a gas X ($\beta_{X=0.9}$, $k_X=10^{-3}$) with noisy conditions (Gaussian noise, $\mu=0$, $\sigma^2=10^{-4}$). Our figure of merit is to evaluate the tolerance to noise is the Fisher Information. Fig. 35 shows the tuning curves along concentration for the different voltage dividers, the optimum signal acquisition (R_{sensor} always equals R_L for any concentration) and the average response of the voltage dividers. As expected, each load resistor presents its own tuning curve with the $J_{R_L}^{-1}$ minimum located at a different concentration, so that the high resistive loads perform better in measuring the lower concentration range and vice versa. The optimum signal acquisition $J_{S\max}^{-1}$ tends to the envelope of the different $J_{R_L}^{-1}$ minima for $k_x c > 1$, and is not significantly lower below this concentration value. Therefore, we could approach $J_{S\max}^{-1}$ from the $J_{R_L}^{-1}$ minima, as long as that they were numerous enough and well distributed along the concentration axis. Given that the relationship between concentration and MOX sensor resistance power law for a wide range of concentrations, load resistor values should be distributed logarithmically, as in the present example. Obviously, the dynamic range obtained from reconstructing the optimum signal acquisition curve enhances any of the dynamic ranges obtained from the individuals. This is also true for the averaged response of the voltage dividers, although the degree of improvement on the dynamic range is lesser.

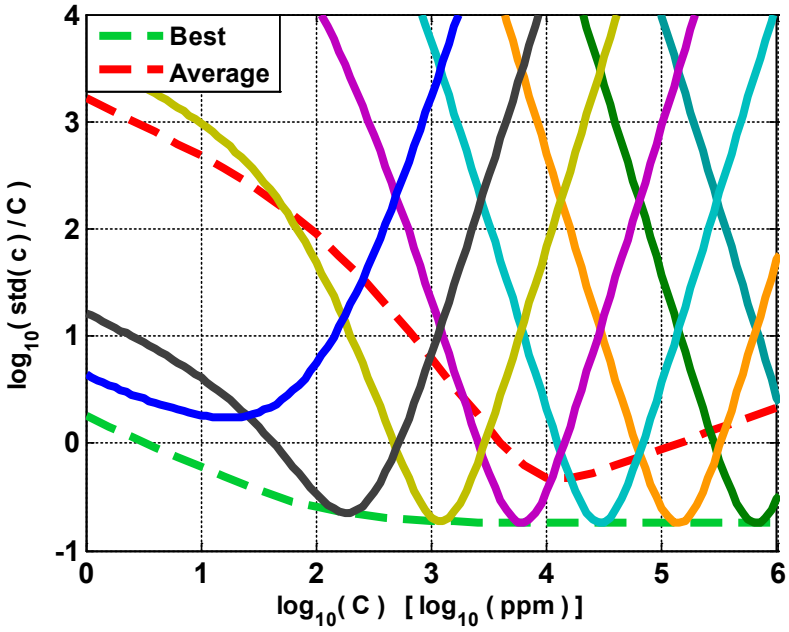

Fig. 35. Inverse of the sensor's FI to odour concentration. The plot shows a number of tuning curves corresponding to the different voltage dividers in solid coloured lines, the optimum signal acquisition condition in a dashed green line, and the average response of the voltage dividers in a dashed red line.

III.3. FUNCTIONAL DEFINITION OF SENSOR DIVERSITY AND REDUNDANCY

In Section I.1, we defined sensor diversity as the number of different receptor types responsible for supporting the array response variability to a collection of odours; and sensor redundancy, as the average number of receptor replicates on a population. We note that the previous definitions imply a clustering of the array receptors according to a criterion of similitude. This way, groups of similar receptors are considered of the same type. The number of sensors clusters corresponds then to the sensor diversity of the array, and the average number of receptors along clusters to its sensor redundancy.

A perfect example for sensor clustering can be found on early stages of the olfactory pathway. There, Olfactory Receptor Neurons (ORNs) expressing the same receptor protein converge to the same semi-spherical structure, called glomerulus. Thus, the sensor diversity of this array of ORNs equals the number of glomeruli. According to the results of Section III.2.1, the previous sensing architecture allows to optimally encode for odour information for the suitable tuned population of receptors. The discrimination of complex odour stimuli in such a case mostly depends on the codification of odour identity, but also on the quantification of its intensity. However, in arrays of poorly selective sensors, where sensor responses to different odours are much correlated, the discrimination of odours seems to be more related to the ability of the sensor array to encode for odour concentration. The strategy we propose for clustering sensor units of these poor selective arrays consist in grouping them according to how they co-vary. As we saw in Section III.1.2, sensor units exhibiting very much correlated sensor responses to a set of odours contribute similarly to the loadings of a PCA decomposition of this data. Different clusters of sensor units tend to present different sensitivities to the same set of odour stimuli, so effectively, they can be considered a source of sensor diversity. Again, sensor redundancy can be evaluated as the averaging number of sensors along the clusters. This sensor redundancy can be employed to reduce independent sensor noise by sensor averaging and sensor array optimization, as can be found in Sections III.1.3, III.1.4 and III.2.2. However, this noise removal stage can be performed after and with independence of the clustering of the sensor units.

In section III.3.1, we develop our method of sensor clustering to obtain the sensor diversity and redundancy of an array of cross-reactive sensors.

III.3.1 Characterization of diversity and redundancy

To characterize diversity and redundancy, we propose a method to estimate the degree of sensor diversity and redundancy of an array of sensors based on clustering of their sensory units. More specifically, we perform a clustering by angle on the loadings of a PCA of the sensor response data. Our rationale behind these definitions is the following. We take into account that a PCA model of the data is a projection of the original data onto a set of new axis corresponding to the eigenvectors of the covariance matrix of the data (the directions on the feature space where the data varies the most). This eigenvectors expressed on the original axis are usually referred to as the loadings of the PCA model. Array sensor units that explain the variance of the similar data contributes similarly to the loadings. Thus, those sensor features that are redundant tend to span the same solid angle on the loadings space and become grouped on the same cluster. Likewise, the number "effective" directions to cluster the array features account for their sensor diversity. In Section III.3.2, we present an experiment to evaluate the sensor diversity and redundancy for and array of synthetic sensors.

III.3.2 Sensor clustering experiment

We build a toy problem to illustrate our method for estimating the sensor diversity and redundancy of an array of sensors. Our basic idea consists in generating a population of

similar sensors and after that cluster them in order to now the sensor diversity and redundancy of the array.

We create an array of 3 virtual sensors. These sensors provide the following set of responses to 3 odours (A, B and C): x_A=(1,5,-2), x_B=(-2,3,1), and x_C=(1,-4,3). To simulate the process of data acquisition, we corrupt the array readings using independent Gaussian noise (μ=0, σ^2=1). This process is repeated 10 times. Thus, the original dataset X_O is a matrix with dimensions 10 rows x 3 columns. We can expand our original array using sensors that are similar to the original ones. We consider that a new sensor is similar to its corresponding homonymous in the original array when they respond proportionally to the set of odours. So to expand our sensor array, we propose to add copies of the 3 sensors multiplying the value of their responses by a factor *n*. This array expansion is performed from *n*=2 to *n*=20. Next, we simulate again the data acquisition process. Notice that sensor noise is added after the sensor scaling in order to warrant the same noise conditions along the expanded dataset, X_E. And the end of this stage, X_E is a matrix of dimensions 10 rows x 60 columns. To perform sensor clustering, we first reduce the dimensionality of X_E by means of PCA data decomposition (2 Principal Components), and after we analyse its loadings vectors.

We present the results of this section in Fig. 36 and Fig. 37. Fig. 37 shows the scores plots of the PCA decomposition for X_E, where the data is mean-centered. We can see that our virtual expanded array discriminates the 3 odours. Fig. 38 is the loadings plot of the PCA decomposition. Observe that the array sensors are distributed in 3 different directions on the PC-plane. Each of these directions corresponds to a sensor type, so sensor diversity for the given problem is 3. Since each of the sensor types contains 10 sensor units, sensor redundancy in our expanded array takes the value of 10.

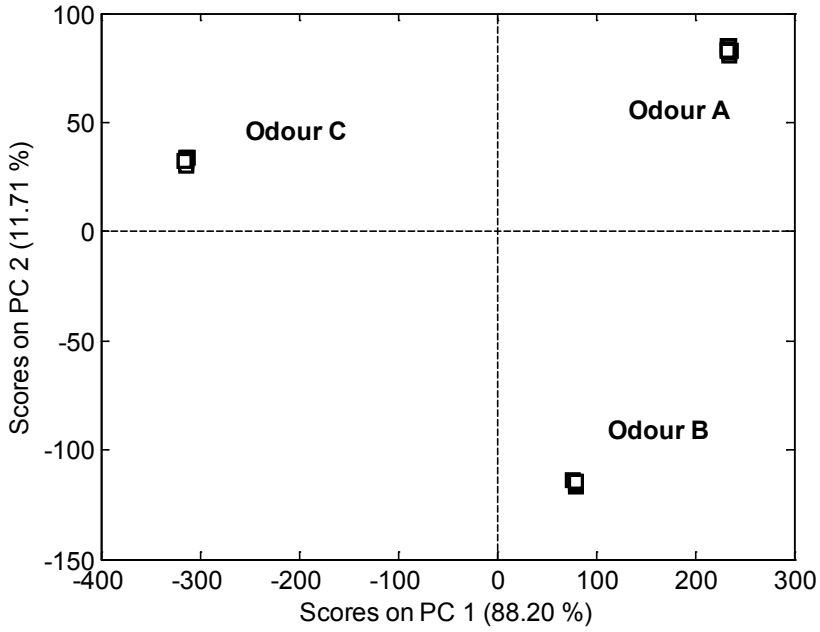

Fig. 36. Scores plot for our simulated data (2 PCs). The 3 odours (A, B, C) are perfectly discriminated by our expanded sensor array of virtual sensors.

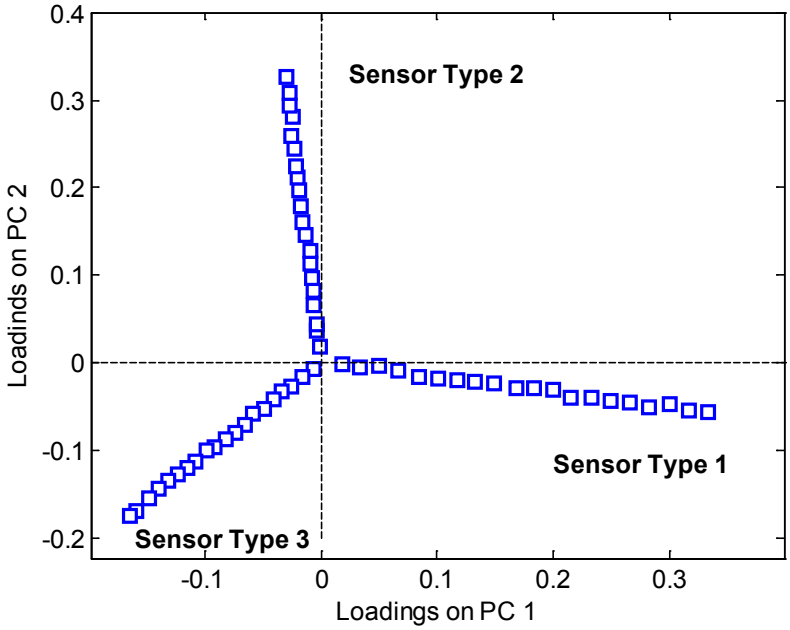

Fig. 37. Loadings plot for our simulated data (2 PCs). We can see how the sensors are clustered following 3 different directions on the plane defined by the loadings. Sensor diversity and redundancy of this sensor array and for this particular problem are, respectively, 3 sensor types and 10 sensors per sensor type.

Due to simplicity of this toy problem, we performed the clustering process by simple visual inspection. However, for more complex datasets it is needed an additional condition for defining the tolerance of the hyper-angle of each sensor cluster. This condition should be based on the optimization of the array performance when solving a given problem (i.e. finding the clustering that minimizes the prediction error of the model built using the cluster representatives). This issue will be revised in Chapter IV (Section IV.1.2.2).

III.4. CONCLUSIONS

In this chapter, we investigated the role of sensor diversity and redundancy in chemical sensing systems. In a first qualitative approach, we checked that our sensor array enhanced its ability to discriminate odours as long we incremented the variability of the sensor responses (with different sensor types and sensor temperatures). Also we found an intuitive inverse relationship between sensor correlation and sensor diversity. Regarding sensor redundancy, we showed that this property was a key factor to minimize independent sensor noise. This task was performed employing two different methodologies: sensor aggregation (with different sensor copies) and array optimization (using a collection of load resistors). The previous results suggested that sensor diversity and redundancy were intimately related to the ability of a sensor array to encode for odour information.

Next, we presented a more formal to odour information encoding supported by sensor diversity and redundancy. First, we studied quantitatively the relationship between sensor diversity and the coding power in sensor arrays. To do so, we evaluated the MI of an array of synthetic sensors exposed to a variety of simulated odour stimuli. We roughly detected two types of sensory diversity. **(i)** First type is responsible to encode for the identity of the odour stimuli. **(ii)** Second type accounts for the codification of the odour stimuli intensity. We used the results of this experiment as analogy to compare the manner how natural and artificial olfaction systems encode for odour information.

According to our analogy, the major source of response variability to odours in natural olfaction comes from **(i)**, whereas in artificial olfaction systems it is mainly due to **(ii)**. The principal difference between both scenarios of odour encoding was referred to degree of response overlapping of their sensor units (artificial olfaction systems are much less selective). Second, we studied why sensor redundancy reduced noise contributions to sensor array responses. Sensor aggregation was very useful to minimize independent sensor noise in homogeneous sensor arrays (with nominally identical sensor copies) because the variance of the sensor aggregate decreases as 1/N, where N is the number of sensor. However, we demonstrated that when a sensor array presented a common component of sensor noise the variance of the aggregate decreased more slowly. On the other hand, array optimization was very effective to decrease independent sensor noise in homogeneous arrays with sensor units exhibiting different sensitivities to odour concentration. We showed that the optimum condition to encode for a given odour concentration was to maximize the sensitivity of the measuring circuit to this concentration. This optimization was performed using the Fisher Information as a figure of merit.

Finally, in order to estimate quantitatively the level of sensor diversity and redundancy of an array of cross-selective sensors, we proposed a method based on sensor clustering of its sensory units. Our criterion for sensor similarity was to consider as same type of sensor units those array features that exhibited much correlated responses to a set of

odour stimuli. Thus, they contributed similarly to the loadings of PCA decomposition. The resulting number of clusters containing similar sensor units is the sensor diversity of the array, and the average number of sensor units along the clusters, its sensor redundancy. This clustering of array features depends on the particular dataset to which we performed the PCA decomposition. In other words, sensor diversity and redundancy are not absolute magnitudes.

CHAPTER IV

ROBUSTNESS TO SENSOR DAMAGE

Sensor ageing, poisoning and electrical failure, are the principal causes for sensor damage in an array of gas sensors. Sensor damage constitutes a handicap in chemical sensing because degrades the performance of the prediction models trained in absence of faults. To ensure reliable predictions damaged sensors must be replaced by fault-free sensors and the array has to be recalibrated, which is an expensive and time-consuming process. Several alternatives have been proposed to overcome the drawbacks of sensor replacement, including fault detection (Pardo et al., 2000), fault correction (Tomic et al., 2004; Padilla et al., 2007; Padilla et al., 2010) and algorithmic mitigation (Fonollosa et al., 2013a). A different approach to prevent the effect of sensor damage consists in exploiting the redundant information obtained from large arrays of sensors. This approach is inspired by the massive sensory redundancy at the early stages of the olfactory system: the olfactory epithelium and the olfactory bulb. The olfactory epithelium is endorsed with a large number (around 10000 in rodents) of olfactory receptor neurons of the same type providing a large amount of sensory redundancy (Firesten, 2001). Olfactory receptor neurons expressing the same type of receptors converge to the same pseudo-spherical structures (the glomeruli) on the olfactory bulb, where electrical signals are integrated obtaining a single response per receptor type

(Bozza and Kauer, 1998). This allows the olfactory system to generate stable odour representations despite the faulty readings of damaged olfactory receptor neurons.

The important role of redundancy in chemical sensor systems has been studied experimentally for arrays with a limited number of sensors (Di Natale, 1993). Several studies have proposed to aggregate the inputs of redundant sensors to decrease the variance of the aggregate output, increase the array sensitivity to chemical compounds and expand its dynamic range, for relatively small array sizes (Wilson et al., 2000; Pearce et al. 2001; Wilson et al. 2002). It has not been until recently that large sensor arrays have become technologically available (Dickinson et al, 1999; Di Natale et al., 2009; Gardner et al., 2009; Bernabei et al., 2012). In all these systems, the pooled response of the individual sensor elements was obtained through a dimensionality reduction stage that was analogous to the sensory convergence exhibited by the olfactory system.

Despite these common points, there is a significant difference between the large arrays of sensors and the olfactory system in terms of tolerance to sensor damage. Our hypothesis is that the distribution of damaged sensors across sensor types and not only the redundancy level is key to make the system robust to sensor failure. While different olfactory receptor neuron types are spread across the entire sensory epithelium, the sensory units of these large arrays that belong to the same sensor type tend to be clustered together. This results in a very different distribution of damaged sensors across sensor types, when the sensory area suffers any sort of damage that affects a number of

contiguous sensory units. In the olfactory epithelium damaged neurons will then be distributed among neuron types, whereas in the chemical sensor arrays, damaged units will belong to one or a few sensor types.

The goal of this work is to study the effect of the distribution of damaged sensors in the performance degradation of a sensor array system. To this end, we used experimental data from a highly redundant large sensor array of MOX sensors modulated in temperature with two redundancy levels: 1) 12 replicates of each sensor type for a total of 96 sensors, and 2) measurements using 16 load resistors per sensors for a total of 1536 redundant measures per second. To determine the performance degradation of the system we carried out two experiments where sensory units were forced to fail considering two different scenarios of sensor fault distribution. In the first experiment, we characterized the evolution of the system diversity and redundancy during the progressive failure of sensory units. To do so, we propose a functional definition of diversity and redundancy based on clustering of sensory units. A second experiment was designed to determine specifically the performance degradation. The system is trained to separate ethanol, acetone and butanone at different concentrations using a model that combines PCA and LDA. Test set samples were synthetically corrupted by means of three different simulated types of faults (electrical failure, poisoning and variation of the sensor sensitivity). To evaluate the tolerance of the array against sensor failure, we used a measure of the separation of the odour classes such as the Fisher score, since it provides a much more sensitive measure than classification.

IV.1. MATERIALS AND METHODS

We introduce first the highly redundant sensor array that we used in this study and then the sensor damage experiments that we performed with the data obtained from the array.

IV.1.1. Highly redundant MOX sensor array

We built a chemical sensing system based on an array of gas sensors composed of 8 different types of commercial MOX sensors (TGS-2600, TGS-2602, TGS-2610 and TGS-2620 from Figaro Inc. and SB-11B-00, SB-1500, SB-41-00, SB-AQ1-04 from FIS Inc.), where each sensor type is replicated 12 times and the sensors are modulated in temperature. The system consists of a data acquisition platform, a power control module, and an odour delivery system. The data acquisition platform is based on a PXI 4461 acquisition card (National Instruments), on a customized, eight-channel measuring board (one channel per sensor type), and on a high-speed multiplexing system (two PXI-2530/ TBS-2630 modules, from National Instruments) that connects sequentially each of the sensors to a set of 16 load resistors (RL= [0.1, 0.25, 0.4, 0.87, 1.30, 3.01, 6.19. 9.1, 21.0, 30.0, 40.20, 51.1, 68.1, 82.5, 105.0] KΩ) in a half bridge configuration (voltage divider). Thus, our sensor array is endowed with two redundancy levels due to: 1) sensor replication and 2) load resistor multiplexing. The power control module comprises two programmable DC sources (PXI-4110 from National Instruments, and N6705A DC Power Analyzer from Agilent Technologies) which are utilized, respectively, to polarize the voltage dividers at 10 V and to modulate the operating temperature of the sensors applying a periodic ramp profile on their heater resistance (from 0 to 5 V for Figaro

sensors and from 0 to 0.9 V for FIS sensors during 90 seconds, with 100 temperature conditions each). Therefore, the grand total of measurements per analyte is 153,600 (8 sensor types x 12 sensor replicates x 100 temperatures x 16 load resistors) shown in Fig. 38.

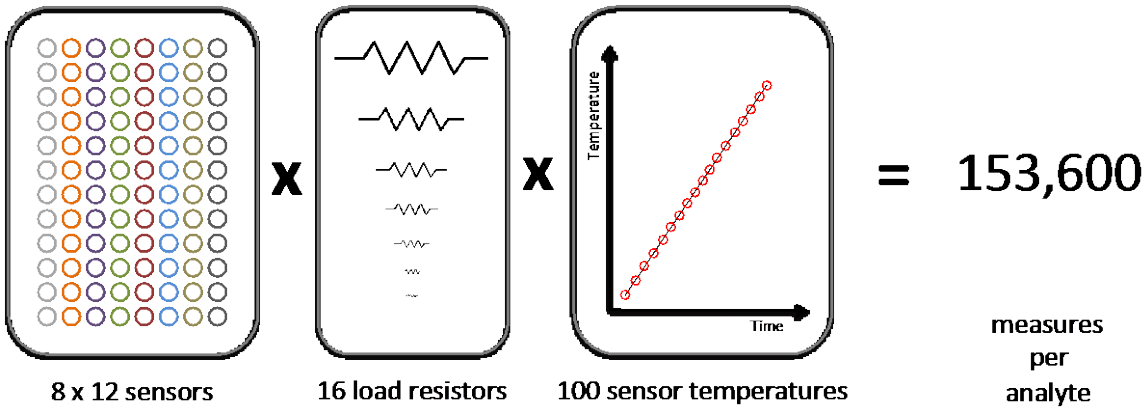

Fig. 38. Gas sensor array. Total amount of measurements that the sensor array acquires per analyte.

Hitherto, we will refer to every combination of physical sensor, temperature, and load resistor as a sensory unit. Finally, the odour delivery system consists of two fluidic branches: first, a high-pressure cylinder containing the carrier gas (synthetic air) connected to a mass flow controller (FLOW F-201CV, Bronkhorst) that keeps constant the carrier gas flow at 1 l/min; and second, a programmable two-syringe infusion pump (KDS200, KDScientific) containing the odorant in liquid form. Both branches meet at the injection port, where the odorant is vaporized and the resulting mixture is sent to the sensor chamber.

In our experiments, we acquired a dataset of 3 analytes (ethanol, acetone and butanone) dosed at a 6 different concentrations (20, 40, 60, 80, 100 and 120 ppm).This measurements corresponded to the dataset I. Fig. 39 summarizes the set of experiments used in this chapter. Sensor readings along a heater period were taken after 900 seconds of odorant exposition to ensure a steady state concentration level on the sensor chamber. After each measurement block, the sensor chamber was cleaned in synthetic air over a period of 1800 seconds. Each of these experiments was repeated 10 times, where the collection of experiments was randomized. After data acquisition, sensor voltage readings were converted to resistance values.

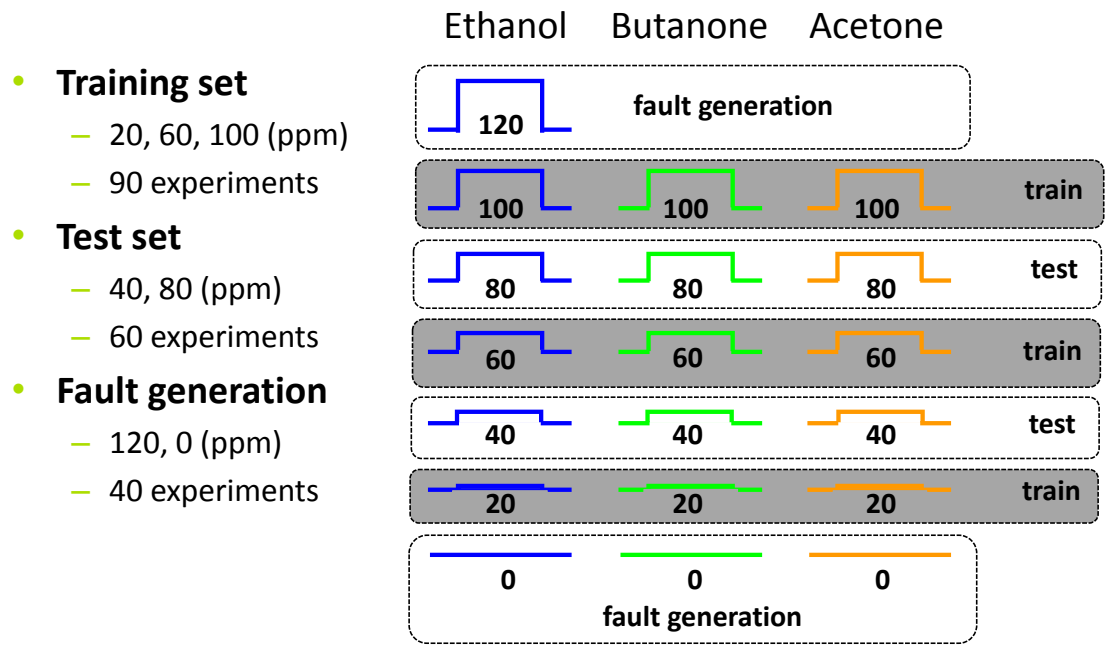

Fig. 39. Set of experiments used in Chapter IV.

IV.1.2. Sensor damage experiments

In this subsection, we present the experiments carried out to study the degradation of the array performance and to characterize the reduction of diversity and redundancy as sensory units are progressively damaged. The performance degradation experiment is presented first since part of the methodology will be used in the diversity redundancy measuring procedure.

IV.1.2.1. Performance degradation experiment

To evaluate the degradation of the array performance with increasing number of faulty sensors, we build a dimensionality reduction model based on two consecutive stages: PCA and LDA, where we measure the reduction of odour separation with the Fisher score (Duda et al; 2001). The study is performed using three different types of simulated sensor failures and taking into account two different scenarios for the distribution of damaged sensors. In the dimensionality reduction model, PCA is applied first to reduce in an unsupervised manner the high dimensionality of the sensory units from 153,600 to 9. To determine this optimum number of final principal components (PC), our criterion was to keep the minimum number of PCs to maintain the same odour separation (FS) after the PCA projection. This computation revealed that the FS for increasing number of PCs saturated at a value of 9 PC.

In a second dimensionality reduction stage, supervised this time, we applied LDA to obtain a better clustering of odours at different concentrations. This is obtained by

considering 3 LDA classes corresponding to the 3 different odours regardless of the concentration. The selection of training and test from the dataset was as follows. Samples corresponding to odorant concentrations of 40, 80 and 120 ppm were used as a training set (90 samples), while the experiments with concentrations of 60 and 100 ppm were used for testing (60 samples).

Fig. 40a shows the PCA and Fig. 40b the PCA-LDA model scores, where the ethanol, acetone and butanone samples are represented in blue, orange and green ellipses, respectively. Note that the projections of the test samples in the PCA model (red triangles) are interleaved with respect to the projection of the train samples (black squares). Comparing both figures, we can see that the LDA projection of the PCA scores achieves the desired clustering according to odour class and ignoring concentration. Noteworthy, the projected test samples on the LDA space fall on top of the training samples of the same class, denoting that the LDA stage does not over train. The separation of odours in this LDA-PCA space will be reduced as the number of sensory units becomes damaged. We consider this odour separability our figure of merit to determine the performance degradation of the array. To measure this separability, we use the Fisher Score (FS) that considers the distance between classes centroids taking into account also the different class spreads (see Appendix A). The FS increases with the separability of the classes.

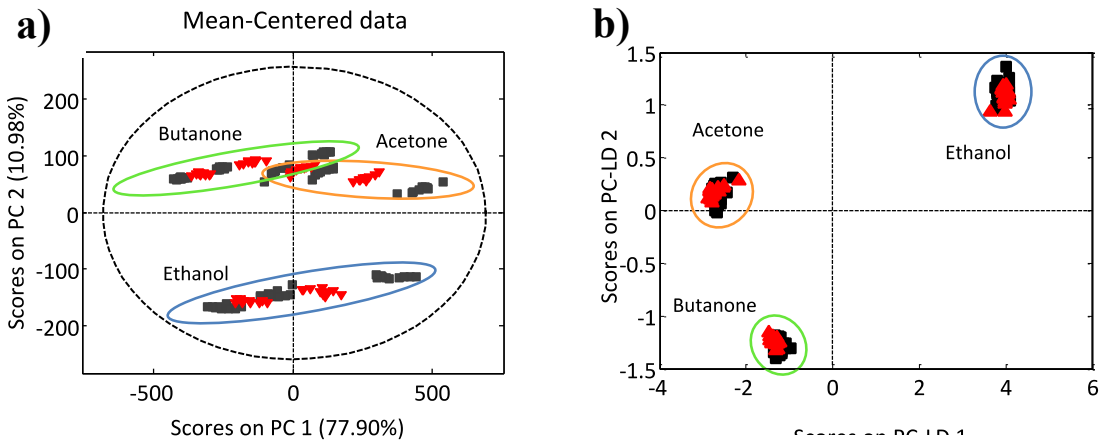

Fig.40. PCA and PCA-LDA models. This figure shows the projections of train (black squares) and test set samples (red triangles) on (a) a 2 component PCA model, and (b) the PCA-LDA. Samples corresponding to ethanol, acetone and butane are enclosed respectively in blue, green and orange ellipses. Notice that the LDA projection minimizes the variance of the data samples due to changes in concentration.

The performance of the array is tested introducing sensory unit faults in the test set samples. We have simulated three kinds of sensor faults. The first type is an electrical failure that emulates a faulty connection on the measurement circuit. This fault is implemented substituting the original response by zero on the damaged sensor unit. The second fault type mimics the behaviour of sensor unit that has been poisoned, so that its response becomes saturated to a fixed level. In this case, the fault is simulated by exchanging the sensor response to any analyte and concentration with its response to 20 ppm's of ethanol. Finally, the last fault type corresponds to a variation on the sensor's

sensitivity due to sensor ageing. This means that the damaged sensor provides two considerably different patterns in response to two identical and independent odorant expositions. In practice, this failure is simulated substituting the readings of the original sensor by the readings of another one. We show a scheme that explains the different nature of these sensor fault types and their corresponding effect on the sensor's response in Fig. 41.

To study the difference in performance of the array for different distributions of damaged sensors across sensor types, we studied two scenarios. In the first scenario, each of the combinations of physical sensor, temperature, and load resistor obtained from the array is considered as an independent sensory unit (153600 = 96 physical sensors x 100 temperature conditions x 16 load resistors), in the sense that the failure on a particular sensory unit does not affect any other one in the array. As opposed, the second scenario takes into account that one physical sensor propagates its fault along all its derived sensory units (1600 = 100 temperature conditions x 16 load resistors). Hitherto, we will refer to these scenarios as the dependent and the independent scenario respectively. Fig. 42 depicts in detail the dependent and the independent scenario in terms of sensor failure propagation across our sensor array. We corrupt the selected faulty units on the test set samples with three different sensor faults types. The Fisher Score is then computed as a figure of merit of the array tolerance against sensor failure.

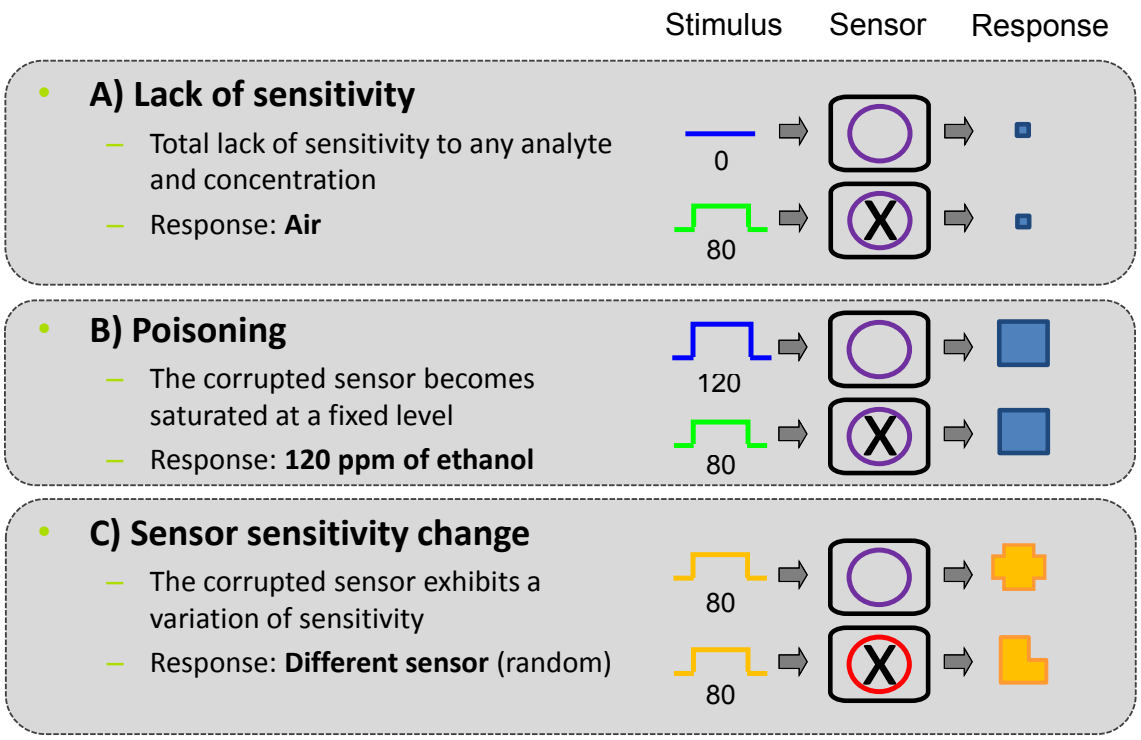

Fig. 41. Sketch of the three types of sensor failures.

IV.1.2.2. Characterization of diversity and redundancy

We used the methodology defined in Chapter III to characterize the level of sensor diversity and redundancy of our sensor array. Our method was based on the clustering of sensor array features according to the angle that they spanned on the loadings of PCA data decomposition (see Fig. 43). We used k-means as a clustering algorithm and the following strategy to determine a suitable number of clusters (k). Our criterion to determine k was to obtain a similar Fisher score on the clustered data (train and test) than that obtained on the complete data set. This criterion ensures that the clustering properly captures the class distributions since it does not change significantly their separability.

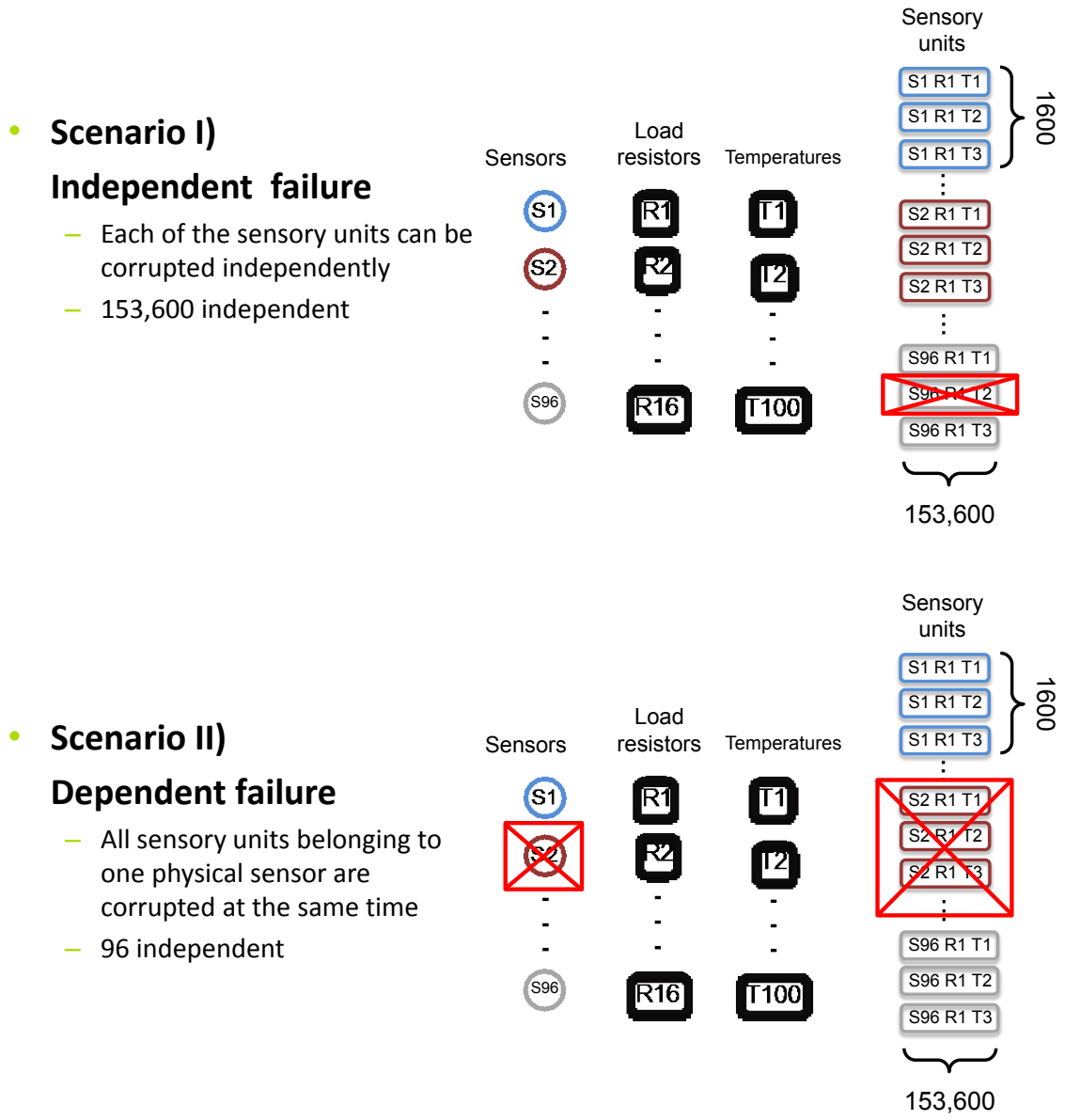

Fig. 42. Propagation of error faults across of our sensor array. Basically, in the independent scenario we corrupt sensor features distributing the faults across the different physical sensor units. On the contrary, in the dependent scenario the sensor faults occur in blocks, where each of these blocks corresponds to a physical sensor.

The Fisher score on the clustered data is computed using cluster representatives and repeated for increasing number of clusters logarithmically distributed in base 2 from 2 to 1024. To avoid spurious results due to unfortunate random initializations of the k-means algorithm, the process of clustering is repeated 100 times.

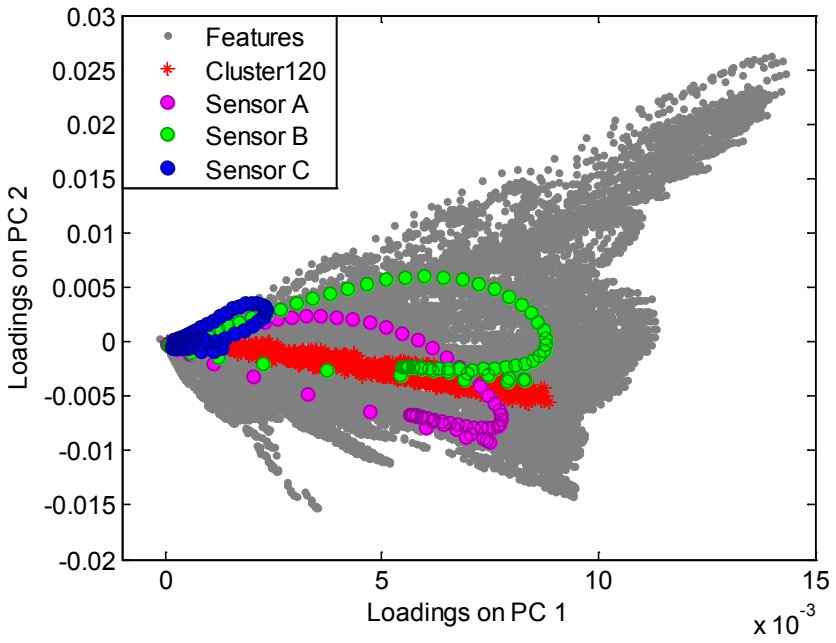

Fig. 43. Loadings for a PCA model built from our data set (2 PCs). The figure represent array features belonging to cluster number 120 as red asterisks along with three MOX sensor replicates corresponding to sensor families TGS-2600 (sensor A), TGS-2610 (Sensor B) and TGS-2620 (sensor C) as magenta, green, and blue circles respectively. Notice that each one of the sensors spans a range of directions on the PCA space due to the effect of temperature modulation. As a consequence each sensor overlaps cluster 120 in a number of contiguous features.

Fig. 44a and 44b show, the boxplots of the Fisher scores for the reduced PCA-LDA models in terms of the number of clusters (k) used in training and test, respectively. Both figures include a grey-dashed line corresponding to the Fisher score of the complete PCA-LDA model. The figures show that for 128 clusters the Fisher score for clustered data in training and test is the closest to that of the complete dataset. Once the sensory diversity of the complete dataset is known 128, its sensory redundancy can be computed as well. In this case, the average number of features per cluster (redundancy) is 1200.

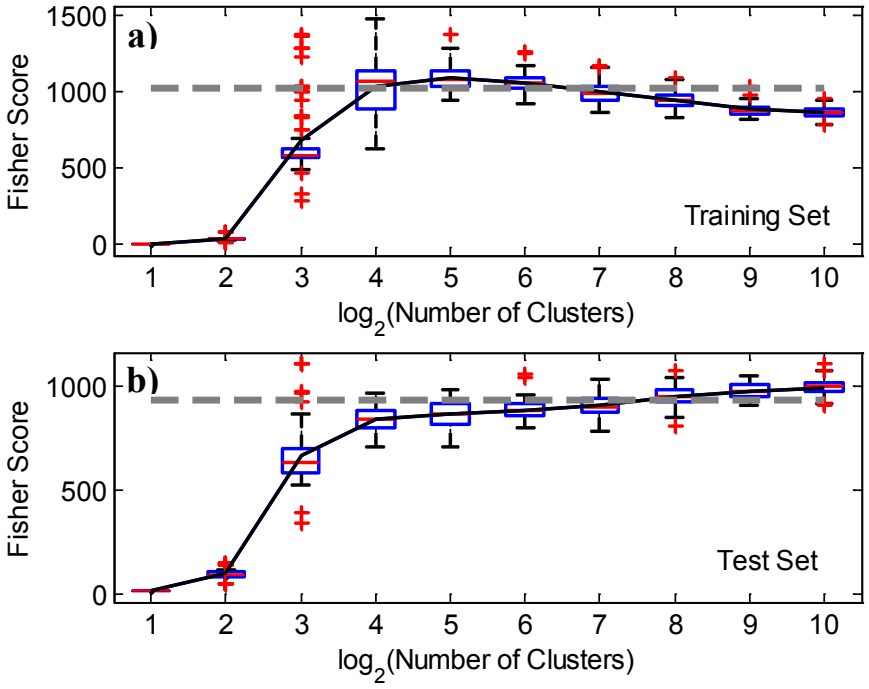

Fig. 44. Boxplots of the FS for the reduced PCA-LDA models. We compute this parameter in terms of the number of clusters used for (a) training and (b) test sets. The FS values of the complete PCA-LDA model for the training and test sets are included on the Figure in grey dashed lines.

IV.2. RESULTS

First we use the definitions in the materials and methods section to quantify the rate at which diversity and redundancy in our gas sensor array drops as the number of sensory units damaged increases. This characterization will help us understand the role played by diversity and redundancy in the performance degradation of the array. Second, we present the results of the performance degradation experiment.

IV.2.1.Characterization of diversity and redundancy

To characterize our sensor array in terms of diversity and redundancy, we performed an experiment where we randomly eliminate sensory units while monitoring the number of active clusters remaining (diversity) and the mean number of sensory units per active cluster (redundancy). We consider active clusters those that convey discriminatory information. Since clusters become depopulated as we eliminate sensory units, for a certain level of sensory decease the clusters will no longer contribute to discriminate odours. To determine which clusters are still active, a naive option would be to consider that a cluster is active as long as it has sensory units alive. However, since in this study we are considering that the response of faulty sensors is included in the global response of the system, we have to consider somehow its negative effect. This leads us to define a threshold in the percentage of sensory units alive within a cluster below which the cluster is no longer active. We have characterized redundancy and diversity in our system in terms of the value of this threshold.

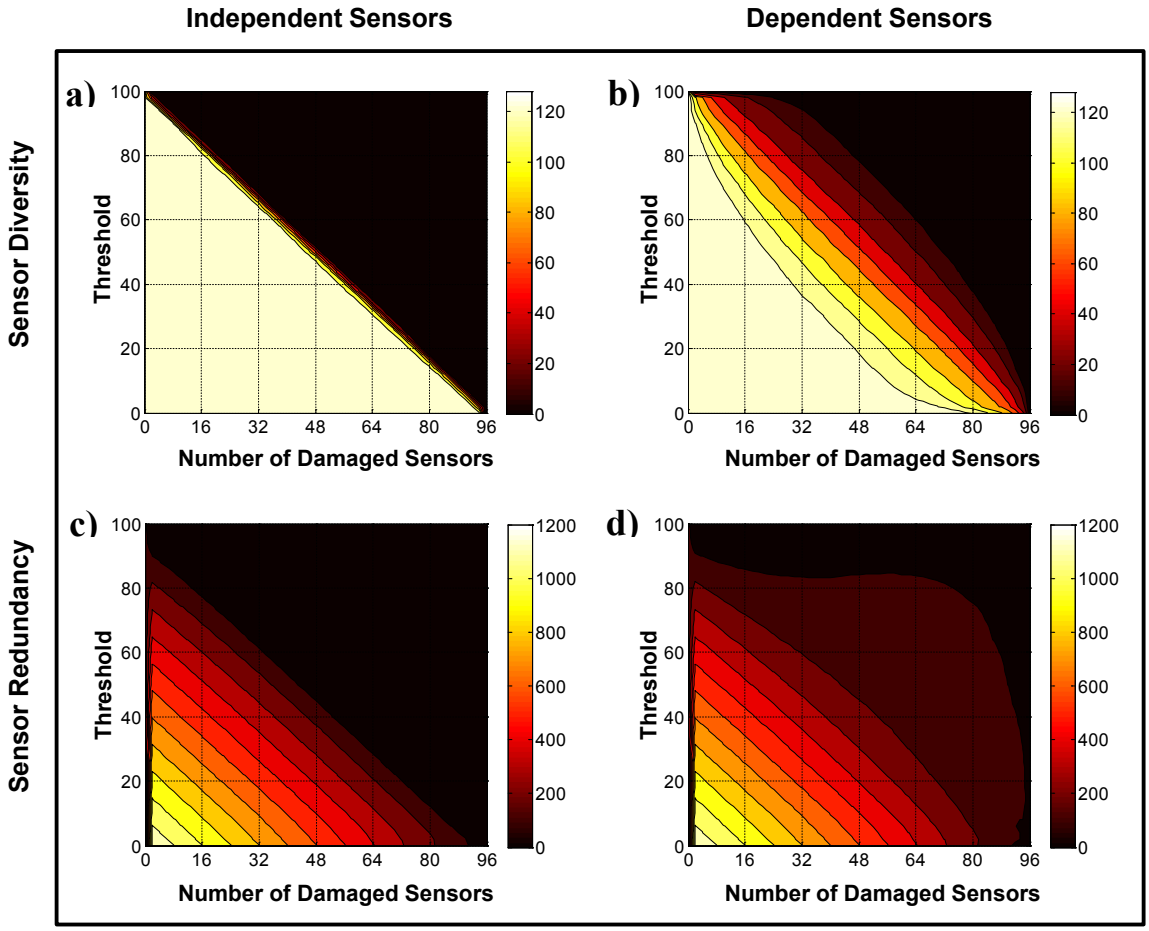

Fig. 45. Sensor diversity and redundancy obtained in both scenarios. Contour maps corresponding to the array mean sensory diversity for (a) independent and (b) dependent scenarios and, mean sensory redundancy for (c) independent and (d) dependent scenarios. The mean redundancy and diversity values are represented as a function of the number of damaged sensors and for increasing values of the threshold from 0% to 100% in steps of 2% of the sensory units damaged per cluster.

Fig. 45 shows the diversity and redundancy results for the scenario where removal of sensory units is done considering them independent. These results are represented as

contour plots of the mean of diversity and redundancy for increasing values of damaged sensors and all possible threshold values. Experiments are repeated 1000 times randomly changing the order of selection of removed sensory units. The clustering is done once and the clusters are kept fixed during all repetitions. Fig 45a show the mean value of the computed diversity, which has maximum value (128) for any threshold until the percentage of removed sensors reaches the threshold value (diagonal). Then diversity drops abruptly to 0. These results indicate that all clusters become inactive all together, making diversity (number of active clusters) go from 128 to 0. This is due to the random distribution of removed sensory units across clusters that make them, in average, keep the same percentage of sensory units during all the experiment. Thus, all clusters become inactive almost at the same time when they reach the threshold value.

As opposed to this behaviour, in the dependent scenario diversity is decreasing smoothly for a certain range (Fig. 45b). For instance, focusing on the threshold value of 60, we can see that diversity starts decreasing for 16 damaged sensors and it reaches 0 for 64 damaged sensors. This behaviour is consistent with the different way in which sensory units are removed when we consider them dependent. Each physical sensor corresponds to 1600 sensory units that are contiguous in the PCA space. In consequence, the decease of each physical sensor will remove sensory units of a reduce number of clusters instead of getting randomly distributed among all of them (independent scenario). This explains

the asymmetrical distribution of faulty sensory units among clusters and thus the progressive inactivation of clusters.

If we now turn our attention to the redundancy results of Fig. 45c and 45d, we can see that redundancy decreases progressively in both scenarios. For a threshold value of 0, the redundancy level decreases linearly with the number of damaged sensors in the independent scenario Fig 45c. Almost the same behaviour can be observed for the dependent scenario (Fig. 45d) except for a slight deviation from linearity for a high number of damaged sensors. This linear behaviour is maintained for higher values of the threshold in both scenarios, where the redundancy profile gets shifted to the left as much as the value of the threshold. The upper right part of the dependent scenario (Fig. 45d) differs to that of the dependent scenario. This area corresponds to low values of redundancy and the different distributions in this area seem to be due to the different termination of the clusters in the two different scenarios.

IV.2.2. Performance degradation

The results of the performance degradation experiment are shown in Fig. 46. This figure shows the evolution of the Fisher score in terms of the number of damaged sensors for the 3 fault types and the 2 damaged sensory unit scenarios. For visualization purposes, we represented the results of the independent scenario to match with the x-axis of the dependent scenario by grouping sensory units every 1600, which corresponds to the

number of sensory units in one physical sensor. The first thing we can observe from the result curves is that for any type of sensor failure, the performance is much more robust in the independent scenario that in the dependent. In the independent scenario curves, the FS is maintained without nearly any loss until a 60-80% of the sensors damaged and drops abruptly after that. This shows a high robust behaviour to this distribution of faults. The curves of the dependent scenario degrade more gracefully, however they do it from the very beginning and up until the end of the progressive failure of sensory units. This makes the system much less robust to the same amount of sensor failure.

In terms of fault types, the electrical failure is the mildest of the faults since the system is able to cope better with it than with the other two faults for both scenarios (Fig. 46). On the contrary, ageing is the more severe fault type for the sensor array. That is clearly shown in the results of the dependent scenario where the ageing curve is dropping faster than and remains below the rest. In the independent scenario ageing and poisoning have a comparable behaviour crossing at a level around 80 sensors damaged. This results show that a change of sensitivity of the sensors has a stronger negative impact on the ability of the system to differentiate odours than an insensitive sensor that always provides the same value.

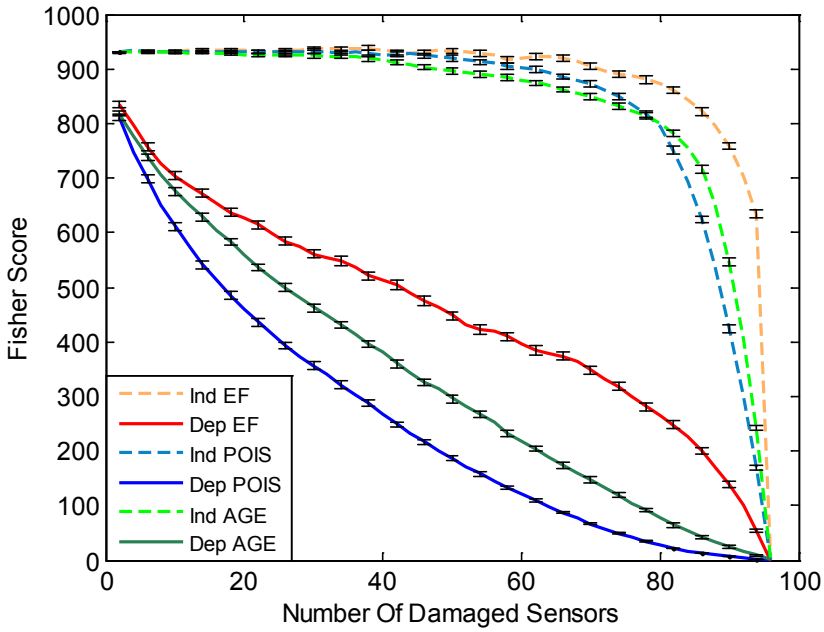

Fig. 46. Mean FS values in test along the number of faulty sensors. Curves corresponding to the independent sensor failure scenario were plotted in dashed lines (orange, light blue and light green line colours for, respectively, electrical, sensor poisoning and sensor ageing fault types), whereas those corresponding to the dependent sensor failure scenario is represented in solid lines (with red, dark blue, and dark green curves for the same sort of fault type cases as in the independent scenario). The standard deviation of the mean FS was included in all these curves as error bars. Notice that the FS performance for the independent sensor failure scenario is markedly better than that on the dependent scenario, regardless the type of sensor fault.

IV.3. DISCUSSION

In this chapter we have presented an experimental study on the impact of the distribution of faults across different sensor types on the odour separation performance of a highly redundant chemical sensor array. We carried out a first experiment where we characterized the diversity and redundancy of our sensor array for an increasing number

of damaged sensory units. To do this characterization, we proposed a definition of redundancy and diversity based on a clustering of sensory units where the number of active clusters represents diversity and the number of sensory units per cluster represents redundancy. In a second experiment, we computed the performance drop of the system in a 3 odours / 6 concentrations problem again as the number of damaged sensors were increased. The system performance was computed as the separability of the different odour patterns using the Fisher score. Both experiments were carried out considering two different scenarios of sensors faults distributions across the sensor array. Our results show that the performance is radically different depending on the distribution of the sensory faults. The best performance is obtained when the faulty sensory units are distributed uniformly across the different sensor types. And the array performance decreases when faulty sensory units concentrate in some sensor types.

This different degradation of the performance can be explained by looking at the results of the experiment on redundancy and diversity characterization. Fig. 45c and 45d show that the redundancy level of the array is practically equal for both scenarios at any level of the sensor damage process. We can disregard here the effect for small values of redundancy. This means that, surprisingly enough, the difference in performance in both scenarios is not directly due to the redundancy level of the array. On the other hand, Fig. 5a and 5b show a remarkable difference between the diversity level of the system in both scenarios. This clearly shows that the difference in performance of the system under both

scenarios is due to the level of diversity that the system is able to maintain at each level of the sensor damage process. For any fixed threshold value if we go along Fig. 45a as the number of damaged sensors increase, we can see that the diversity level is kept constant until it drops abruptly when it reaches the threshold value. This is the cause of the robust behaviour of the system performance Fig. 46 for the independent scenario, where the dashed curves keep the original FS value as long as the system has maximum diversity and falls abruptly when diversity is lost. If we do the same exercise in the dependent scenario (Fig. 45b), we observe that diversity is decreasing progressively, which causes the graceful decrease of the array performance in Fig. 46 for the dependent scenario, solid line curves.

The comparison of the results of both experiments allowed us also to realize that the effect of different fault types of the performance degradation experiment correspond somehow to different threshold values on the diversity and redundancy characterization experiment. The threshold can be interpreted as the number of free-fault sensors in a cluster needed to maintain the discriminatory information of that cluster. Therefore, different sensor fault types will have different effects on the cluster and correspond to different threshold values. The performance degradation curves of the independent scenario (Fig. 46) correspond to values of the threshold around 20 (Fig. 45a) since the falling starts around 80. In the case of the dependent scenario, it is more difficult to determine but seems to be in values around 50 since the sensor degradation curve is quiet

symmetric. In any case, the decrease of diversity does not exactly match the performance degradation. This is because in the characterization we are assuming that faulty sensory units affect only the cluster they belong to and this is not the case for the simulated sensor fault types.

Further insight on the differential effects of the three sensor-fault types on the array performance degradation can be gained in the PCA-LDA scores projection. As a general result, all fault types modified the triangle formed by three pure odour classes for an increasing number of damaged sensory units. However, the way in which this triangle was altered depended on the fault type. The lower degradation was produced by the electrical failure, followed by sensor poisoning and ageing. A common effect of this three fault types was a shift of the triangle along with a reduction of the triangle area. Noteworthy, the FS is not sensitive to pattern shifting. Alternative approaches to evaluate the robustness to sensor failure can be focused on this issue (i.e. using classifiers). The most similar fault types were electrical failure and poisoning, in the sense that they tended to bring the array response to a fixed level. Their main difference was that sensor poisoning also included random variations of response around that level. The fact of adding this random error increased the spread on the triangle vertices. As a consequence, poisoned sensory units showed lower performances on the FS. Sensor ageing produced the same effects than sensor poisoning and electrical failure along with new one: the distortion of triangle's aspect ratio. This is due to the accumulative effect of interchanging

sensory responses dramatically misled the PCA-LDA projection. Accordingly, sensor ageing was the worst-case fault in terms of FS degradation.

We believe that the results of this study are general and not confined to our particular chemical sensor array and neither confined to the limited number of odours of our experiments. The measure of diversity and redundancy proposed in this study uses clustering of sensory units to extract an intrinsic dimensionality of the array based on odour separability. This abstraction step makes our results array independent. With respect to the limited number of odours of the study, the results obtained can be considered more general since we use a sensitive measure such as the FS. Nonetheless, the FS as well as the FDR have the underlying assumptions of Gaussianity of the class distributions. Thus, our results are limited to problems with this type of class distributions.

In conclusion, this study shows that not only the level of sensor redundancy is important to have a robust system against sensor damage, but also the distribution of faults across sensor types plays a crucial role. Spreading faults among different sensor types is important to maintain as many different sensor types as possible, which is what at the end of the day provides the discrimination capacity of the system.

CHAPTER V

FEATURE SELECTION

Metal Oxide sensor (MOX) technology is widely employed in artificial olfaction because it provides low-cost, commercially available sensors endowed with high sensitivities to a broad variety of gas species (Arshak et al., 2004; Figaro, 2014). However, MOX sensors suffer from an inherent lack of selectivity that hinders its application in precise odour discrimination tasks. One possible strategy to increase the selectivity of MOX sensors consists in modifying their operational temperature. This parameter modifies the sensor sensitivity across odours, and thus, the degree of selectivity of a MOX gas sensor when exposed to an odour mixture (Clifford and Tuma, 1983a; Clifford and Tuma, 1983b). This temperature-selectivity dependence is usually exploited in temperature modulation techniques, where a voltage profile is applied on the sensor's heater (Lee and Reedy, 1999).

A number of works have been published focusing on the optimization of these temperature profiles according to some condition, for different odour discrimination tasks. Some researchers faced this optimization problem from a heuristic point of view. Ortega et al. modulated the temperature of a commercial tin-oxide sensor with a variety of cycling profiles (Ortega et al., 2001). The authors combined spectral and transient analysis of the sensor features to increase the separation between two odour patterns.

Temperature optimization was performed taken into account measures of intra-cluster distance, between cluster dispersion and cluster similarity. In a different work, Huang et al. studied qualitatively the effect of different periodic temperature profiles on the response of a thick film SnO_2 sensor (Huang et al., 1999). They concluded that frequency was the key factor to enhance odour discrimination, regardless the specific shape of the profile. Best results were obtained for lower frequencies. Raman et al. used a variation of the Fisher Score to optimize temperature modulated micro-hotplates aimed for detecting hazardous gases (Raman et al., 2009a; Raman et al., 2009b). Similarly, Muezzinoglu et al. selected the set of best operating temperatures of two commercial metal-oxide sensors employing the Mahalanobis distance (Muezzinoglu et al., 2010). Other authors preferred a more systematic approach to optimize temperature profiling. The standard procedure consists in acquiring the sensor readings at diverse temperature conditions in order to model the sensor dynamics. Thus, temperature optimization is performed using these models. Kunt et al. employed wavelet networks to optimize the operation of micro-hotplate gas sensors (Kunt et al, 1998). Vergara et al. used multilevel random sequences to select the optimal set of frequencies for multi-sinusoidal voltage profiles (Vergara et al., 2005 ; Vergara et al., 2007 ; Vergara et al., 2010). A more challenging tentative for temperature optimization was presented by Gosangi and Gutierrez-Osuna (Gosangi and Gutierrez-Osuna, 2010; Gosangi and Gutierrez-Osuna, 2013). They proposed an active sensing strategy based on Partial Observable Markov Decision Processes for real time temperature optimization. More recently, Vergara et al. utilized the Kullback-Leiber

divergence to find the individual sensor temperatures for maximizing multi-odour classification (Vergara et al., 2010). Finally, Fonollosa et al. presented a methodology for temperature selection in multi-sensor arrays based on maximizing the Mutual Information (Fonollosa, 2013b).

In this chapter, we present an offline approach to enhance odour discrimination in temperature modulated MOX arrays. Our method is based on the theoretical framework stablished by Pearce and Sanchez-Montañes (Pearce 2000, Pearce and Sanchez-Montanes, 2003) to optimize the detection performance of chemical sensing systems. Basically, the authors proposed to maximize the projection of the odour stimuli volume onto the set of sensor responses, considering noise effects to constrain feature selection. To do it, they defined the concept of Number of Discriminable Odour Features (N_O). This parameter accounted for the quantity of odour conditions that can be discerned by an array of noisy sensors. Through the years, their work has become very popular in the e-nose community since illustrates very kindly the problem of sensor collinearity (Snopok and Kruglenko, 2002; Hierlemann and Gutierrez-Osuna, 2008; Vergara and Llobet, 2012). Still, no practical applications of the method have been found in literature. We believe that this peculiar situation is caused mainly for two reasons: First, their method experiences a notable increment of complexity when is applied to arrays of non-linear sensors. Note that this is the usual scenario in artificial olfaction (Albert et al., 2000). Second, the application of the technique is limited to odour discrimination tasks where

the amount of sensor features equals, as much, the number pure odours on a dataset. This fact constitutes a severe drawback, since current sensor arrays tend to provide large amounts of data per odour sample (Dickinson et al, 1999; Di Natale et al., 2009; Gardner et al., 2009; Bernabei et al., 2012). The main contribution of our work consists in using an upgraded version of their method for dealing with large datasets of non-linear sensors by means of multivariate regression techniques. In particular, we propose the use of Partial Least Squares Regression (PLSR) to both linearize the odour to sensor space transformation and reduce the dimensionality of the sensor space.

To test the feasibility of our approach, we optimize the operational temperatures of an array of two commercial MOX gas sensors (TGS-2610 and TGS-2620, from Figaro Inc.) to discriminate ethanol, acetone and their linear mixtures in the range from 0 to 120 ppm. In our study, we employ the Number of Discriminable Odour Features (N_O) as a figure of merit for feature selection. A regularization of this parameter is also proposed so as to prevent the effect of sensor collinearity. In order to prevent the acquisition of new data samples for unseen odour conditions, we propose to model the sensor response across temperature to simulate sensor readings. Then, we optimize sensor temperature of a simulated array of three sensors (TGS-2602, TGS-2610 and TGS-2620 from Figaro Inc.) for mixtures around 60 ppm of ethanol and 60 ppm of acetone.

V.1. THEORY

V.1.1. Hyper-volume of accessible sensor space (V_S)

According to Pearce and Sanchez-Montanes, the *Odour Space* (Y^T) is defined by the set of pure compounds that generate an odour mixture. Analogously, the *Sensor Space* (X^T) comprises the set of sensor units of a sensor array. Both spaces are related by means of the sensor's sensitivity matrix (S). Note that this transformation is local due to the sensor's response-concentration profile. For the particular case of linear sensors, S is a matrix of constant coefficients and the transformation becomes global:

$$X^T = SY^T \tag{5.1}$$

The hyper-volume spanned by the samples of the Odour Space (V_O) can be projected onto the sensor space, giving rise to the *hyper-volume of accessible Sensor Space* (V_S). The computation of V_S is straightforward for linear sensors. If S is a square matrix, namely if the number of pure compounds equals the numbers of sensors, V_S is computed as:

$$V_S = V_O \cdot |det(S)| \tag{5.2}$$

For calculations of V_S involving non-square marices, please refer to (Pearce and Sanchez-Montanes, 2003).

V.1.2. Hyper-volume of noise in the sensor space (V_N)

The hyper-volume of noise on the sensor space (V_N) limits the odour resolution (both in quality and quantity) of the sensor array. In the original implementation of the method, sensor noise is considered Gaussian and independent of the odour stimulus. Thus, V_N is enclosed by a hyper-rectangle with sides σ_i (the standard deviation of noise for each sensor i). Instead, we propose to take into account noise correlation among different sensor units. To calculate V_N, first it is necessary to estimate the noise matrix (N). This can be done by subtracting the different odour class centres to its corresponding odour class samples on the sensor space. Then, V_N is obtained from the generalized variance (GV) of noise:

$$V_N = (2k)^m \sqrt{GV(N)} \tag{5.3}$$

where m is the number of sensors, and k the number of standard deviations from the mean. The correcting factor $(2k)^m$ comes from considering the Chebishev's inequality. To estimate the odour discriminability we use the ratio $N_O = V_S / V_N$, where No is termed the Number of Discriminable Odour Features. Fig.47 shows an example of Odour to sensor Space transformation that provides in order to help the reader in understanding the concepts of V_S, V_N, and N_O.

V.1.3. Linearized sensitivity matrix, $\hat{S}$

We can linearize the sensitivity matrix S to take advantage of the simplicity exhibited by linear transformations between Odour and Sensor Spaces. This task can be done by

means of multivariate regressions methods, and in particular using Partial Least Squares Regression (PLSR). Note that this stage involves a dimensionality deflation of S that depends on sensor correlation (Fig. 48). It can be demonstrated that the linearized sensitivity matrix ($\hat{S}$) and the regression matrix on the latent variable space (Q) are related through the following matrix relationship:

$$\hat{S} = (Q^T)^+ \tag{5.4}$$

This demonstration is found in Appendix B.

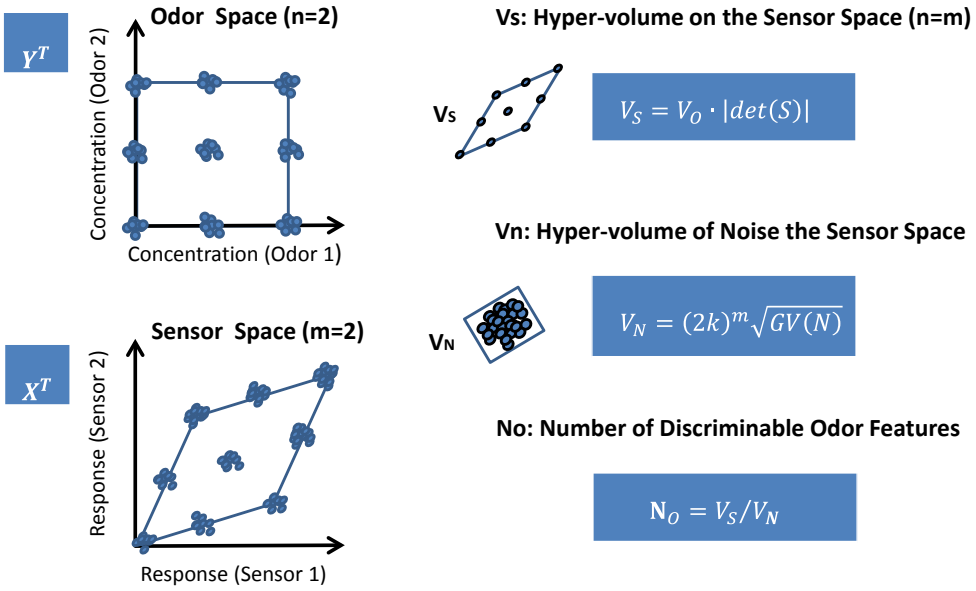

Fig. 47. Example of an Odour to Sensor space transformation (n=m=2). We include on this figure of the formulas for the computations of V_S, V_N, and N_O.

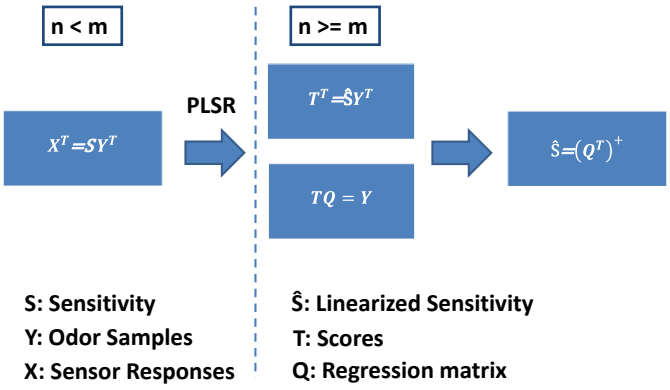

Fig. 48. Scheme of the dimensionality reduction stage. This stage allows compacting the redundant sensor information to obtain the linearized sensitivity matrix.

V.2. METHODS

V.2.1. Experimental

We built a chemical sensing system based on an array of two temperature modulated commercial MOX sensors (TGS-2602 and TGS-2610, y TGS-2620, from Figaro Inc.) The system consists of a data acquisition platform, a power control module, and an odour delivery system. The data acquisition platform is based on a PXI 4461 acquisition card (National Instruments), and on a 3 channel customized measuring board. The power control module comprises two programmable DC sources (PXI-4110 from National Instruments, and N6705A DC Power Analyzer from Agilent Technologies) which are utilized, respectively, to polarize the voltage dividers at 10 V and to modulate the operating temperature of the sensors applying a periodic ramp profile on their heater resistance (from 0 to 5 V during 90 seconds, with 100 temperature conditions each). Finally, the odour delivery system consists of two fluidic branches: first, a high-pressure cylinder containing the carrier gas (synthetic air) connected to a mass flow controller (FLOW F-201CV, Bronkhorst) that keeps constant the carrier gas flow at 1 l/min; and second, a programmable two-syringe infusion pump (KDS200, KDScientific) containing the odorant in liquid form. Both branches meet at the injection port, where the odorant is vaporized and the resulting mixture is sent to the sensor chamber.

We measured the output voltage of the two commercial sensors when exposed to 6 different concentrations of ethanol and acetone (0, 20, 40, 60, 80,100 and 120 ppm) and

their linear mixtures (20-100, 40-80, 60-60, 80-40, 100-20 ppm). To acquire sensor voltage we connected the sensors to a load resistor of 6.1 KΩ in a half bridge configuration (a voltage divider). Therefore, total of measurements per odour sample is 200 (2 sensor types x 100 temperatures). Sensor readings along a heater period were taken after 900 seconds of odorant exposition to ensure a steady state concentration level on the sensor chamber. After each measurement block, the sensor chamber was cleaned in synthetic air over a period of 1800 seconds. Each of these experiments was repeated 10 times, where the collection of experiments was randomized. This information is summarized in Fig. 49. The temperature of the sensors was calculated according to (Lee and Reedy, 2000).

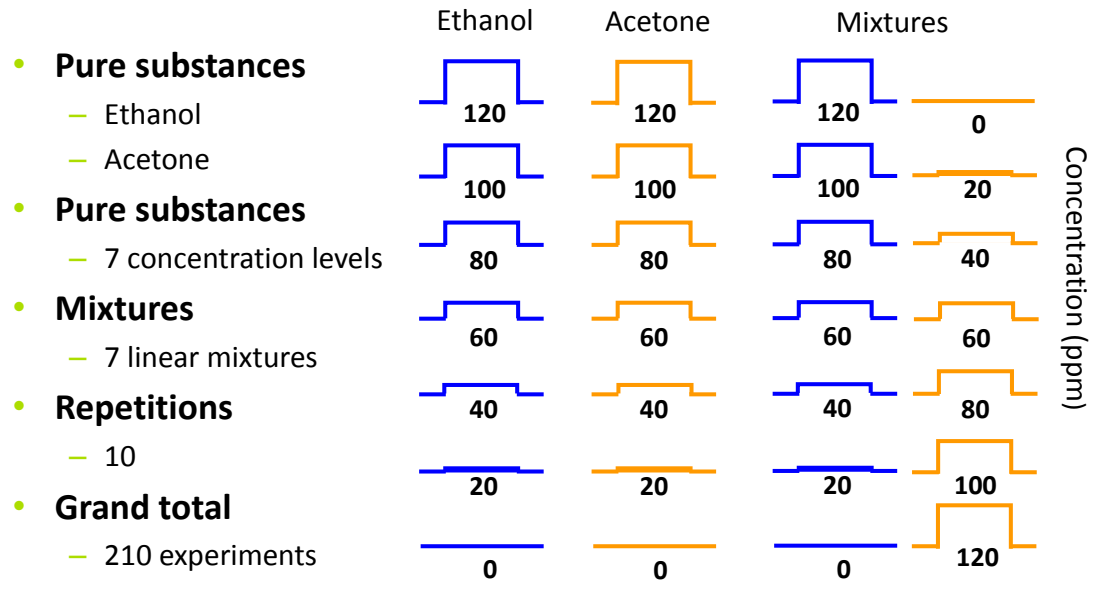

Fig. 49. Experimental dataset used in Chapter V.

Using this dataset we have performed three experiments (Table 1). First experiment (I) illustrates the method presented in Section 2, for two MOX sensor units. The concepts of hyper-volume of accessible Sensor space (V_S), hyper-volume of noise on the Sensor Space (V_N), and Number of discriminable odour features (N_O), are revised to enhance the reader's comprehension of the odour to sensor transformation and the effect noise on it. No feature selection is realized in this experiment. In a second experiment (II) we perform a temperature optimization to maximize odour discrimination. In particular, we search the best binary combination of temperatures from two MOX units. In order to prevent spurious results caused by feature collinearity, we introduce here a regularization of the fitness parameter N_O. We emphasize that temperature optimization is directly performed using the sensor readings. And that the array response was expressed in sensor voltage (V). However, sometimes it is desirable to realize a more systematic approach modelling the sensor response (i.e. for avoiding the data acquisition of new odour samples). For this reason, a third experiment is proposed (III). There, we model the sensor response of three MOX sensors to binary gas mixtures at different temperatures. Though, this time the array response was calculated in terms of sensor resistance (Ω). In addition to this, we generate reliable models of sensor noise studying how it co-varies along temperature. Then, the optimum set of temperatures is found employing our methodology, for a given simulated Odour Space.

Table 1. Depiction of the three experiments performed in Chapter VI. Sensors*: S1=TGS-2602 S2=TGS-2610, S3=TGS-2620

Experiment	I	II	III
Sensors*	S2, S3	S2, S3	S1, S2, S3
Data	Real	Real	Real
Magnitude	Voltage	Voltage	Resistance
# Features	200	2	237
#Latent Variables	2	2	2
Parameters	V_S, V_N, N_O	V_S, V_N, N_O, $\bar{N}_O$	V_S, V_N, N_O,$\bar{N}_O$

V.2.2. Illustration of the method

In this experiment we project the acquired Odour Space onto a reduced Sensor Space built from the sensor features of two commercial sensor units (TGS-2610 and TGS-2620). This new Sensor Space corresponds to the latent variable scores obtained from a PLSR regression between the array of sensor features (200 features) and the training samples of the odour dataset. The number of latent variables is selected to be 2 in order to capture the intrinsic dimensionality of the Odour Space. This criterion is also followed on the rest of experiments of this chapter. Nevertheless, it is possible to perform cross-validation stage to select a suitable number of latent variables for the PLSR model. This is recommendable for datasets composed of a large number of pure compounds. The hyper-volume of the Odour Space is simply calculated as the area of the triangle spanned by the odour mixtures of the odour set. The parameters V_S, V_N and $\hat{S}$ are computed from

the latent variable scores of the training samples according to equations (2), (3) and (4), respectively. Since the number of latent variables is 2, m takes this value in (2). Also in (2), k is selected to be 3 in order to ensure that around the 89.0% of the samples of the noise matrix are confined within the estimated V_N.

V.2.3. Regularization of the parameter N_O

Employing the same set of odour samples and sensor features as in Experiment I, we perform an exhaustive search of the best 2 temperatures (one per sensor type) in terms of odour separation. To do it we create 1000 PLSR models. That is one model per binary combination of sensor temperatures. Then we compute V_S, V_N N_O for each of these models. Temperature selection is firstly performed using N_O as a figure of merit of odour discrimination. In parallel, the condition number of the linearized sensitivity matrix (Cond($\hat{S}$)) is calculated for the 1000 data models. The condition number of a matrix provides information about is closeness to singularity. That information is related to the degree of 'orthogonality' presented in its row vectors (Turing, 1948). Noteworthy, these row vectors correspond to the set of array responses to different mixtures in our particular case. Low values of the condition number (close to 1) denote linear different arrays responses to a variety of odour mixtures. On the other hand, large condition numbers indicate sensor response collinearity on the linearized sensitivity matrix. This situation eventually leads to poor odour discriminability. To prevent from selecting very much correlated features we realize the optimization of the sensor array temperatures again, but this this time using the ratio No/Cond($\hat{S}$) as a figure of merit of odour separability.

V.2.4. Optimization through sensor modelling

In the last experiment, we optimize the temperatures of three sensor units (TGS-2602, TGS-2610 and TGS-2620) so as to maximize the discrimination of samples from the following simulated Odour Space: [80-40; 80-60; 80-80; 60-40; 60-60; 60-80; 40-40; 40-60; 40-80]. Where first component represents ethanol, second one acetone, and pure odour concentrations are expressed in ppm. This task is divided in three different sub-tasks: sensor response modelling, sensor noise modelling, and temperature selection.

V.2.4.1. Sensor model for mixtures with two pure compounds

We present a model of sensor response for 2-compound gas mixtures inspired by the Clifford-Tuma model of sensor conductance (Clifford and Tuma, 1983a). This model states that the sensor conductance is modified in presence of a gas species following an almost potential relationship with the gas concentration:

$$\bar{\sigma}_g = \frac{\sigma_g}{\sigma_0} \sim \left(K_g C_g\right)^{\beta_g}, \qquad K_g C_g \gg 1 \tag{5.5}$$

where σ_0 is the conductance of the sensor exposed to air, Cg is the gas concentration, and Kg and βg, gas-dependent parameters. In our model, we propose that the sensor conductance corresponding to a 2-compound gas mixture is:

$$\bar{\sigma}_m = 1 + \bar{\sigma}_{g1} + \bar{\sigma}_{g2} + \epsilon\left(C_{g1}, C_{g2}\right) \tag{5.6}$$

being $\overline{\sigma}_m$ the normalized conductance to the gas mixture, $\overline{\sigma}_i$ the normalized conductance to the pure gas compounds and ε a correcting term that depends on the concentration of both odours. In particular, we assume that ε explicitly takes the form:

$$\epsilon\left(C_{g1}, C_{g2}\right) = K_{g1,g2} C_{g1}^{\alpha_{g1}} C_{g2}^{\alpha_{g2}} \tag{5.7}$$

where α_{g1}, α_{g2} and $K_{g1,g2}$ are constants characteristic of the specific gas mixture. Notice that the sensor response to a binary mixture equals the response of the pure compounds if no mixture is produced (C_{gl}= 0 and C_{g2} > 0 or vice-versa). In addition to this, mixtures generated at low concentrations tend to produce sensor responses similar to those obtained exposing the sensor to air. Finally, the sensor resistance to a mixture can be obtained just inverting the normalized sensor conductivity and multiplying this value by the sensor conductivity to air:

$$R_m = \frac{\sigma_0}{\bar{\sigma}_m} \tag{5.8}$$

V.2.4.2. Model of sensor noise

In order to build realistic models of sensor noise we need to know how the different sensor features co-vary with the experimental noise, N (see section V.1.2). To do it, we proceed to compute the covariance matrix of N^T. This can be done by means of the Singular Value Decomposition (SVD) of N^T:

$$N^T = UDV^T \tag{5.9}$$

where N^T is an m x n matrix, U is an m x m unitary matrix, D an m x n rectangular diagonal matrix of singular values, and V^T and n x n unitary matrix. Simple algebraic manipulations allow obtaining the covariance matrix of N^T from (5.9):

$$Cov(N^T) = \frac{1}{m-1}(UD^2U^T) \tag{5.10}$$

This approach has the advantage of preventing instable calculations of the covariance matrix by setting to zero the singular values of D that lesser contribute to the decomposition of N^T. Once the covariance of noise is obtained, we can generate the simulated noise employing a generator of multivariate normal random numbers.

V.2.4.3. Temperature selection

The optimization of sensor array temperatures is performed using Genetic Algorithms (GA). In particular, we employ the regularized number of discriminant odour features as

fitness function to maximize with the selected features. The process is performed as follows: **(i)** We generate an initial population of p=100 samples, allowing only 3 possible features activated per individual. The position of these features follows a uniform random distribution between the first and the last array feature indexes. We do this way for two reasons. First, we prevent the selection of spurious features limiting their number in the initialization step, and second, we ensure that (in average) features of the three sensors are present in each individual of the population. **(ii)** This population is tested against the fitness function and its median value is computed. **(iii)** The individuals below this value are removed from the population. On the other hand, the individuals above the median are randomly grouped in pairs for breeding. **(iv)** We perform single point breeding. That means that each pair of parents is divided in two sections at a random position. The position of the cut also follows a uniform distribution. Next, a pair of children individuals is created interchanging analogous sections between parents. Note that once the breeding stage is performed for each couple of parents we retrieve the original size of the population. **(v)** Additionally, each individual of the population is allowed to mutate one of their features with randomly selected. The probability of mutation of an individual is 0.001. After that, we return to the step **(ii)** and repeat the sequence until some convergence criterion is achieved. Our criterion consists in stopping the iterations of GA when the current average fitness of the population does not increase more than a 1% with respect the previous iteration. Then, we obtain the best individual of the population. In order to avoid a solutions corresponding to local minima, the entire procedure is repeated

from **(i)** to **(v)** 5000 times. Finally, the set of selected features is obtained looking for the most repeated features present on the pool of the best individuals from different populations.

Table 2. Parameters for the Genetic Algorithms feature subset selection

Population Size	# Populations	Breeding	Probability of Mutation	Fitness Parameter
100	5000	Single Point	0.001	$\bar{N}_O$

V.3. RESULTS

The results of first experiment are presented in Fig.50, and Fig.51. Fig.50 shows a scatter plot of the Odour Space, where each of the figure axes corresponds to a pure odour compound (x-axis for ethanol and y-axis for acetone).

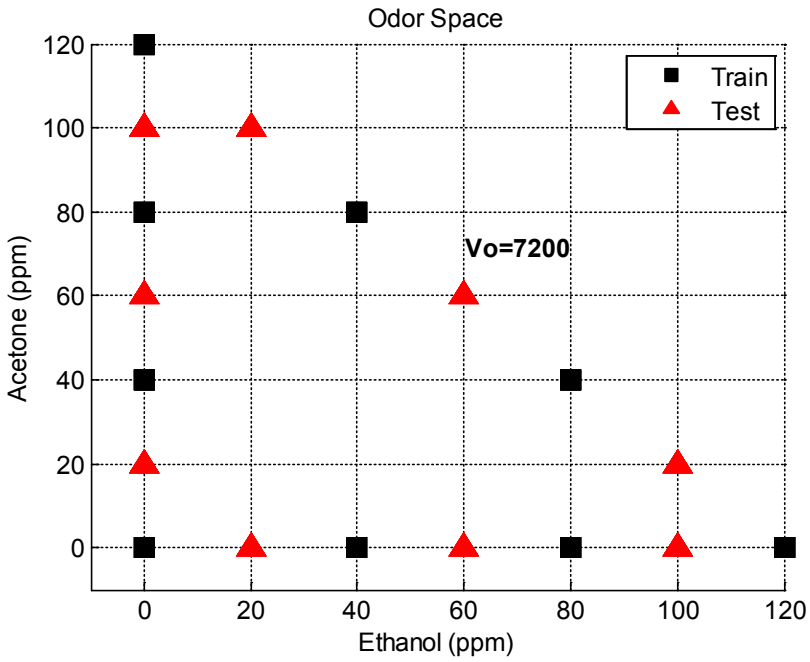

Fig. 50. Representation of the Odour Space. On the figure, each of the axes defines the amount of pure substance present on an odour mixture (x-ethanol, y-acetone). Note that black squares and red triangles represent, respectively, the training and test samples for the subsequent PLSR model. The hyper-volume on the Odour Space is 7200 ppm^2.

Black squares and red triangles represent, respectively, samples of the training and test set. Note that the Odour Space is an isosceles right triangle with a leg length of 120 ppm. Thus, V_O is the area of this triangle, which is 7200 ppm2. If we turn our attention to Fig. 51, we can see the projection Odour Space onto the reduced Sensor Space (that is the latent variable scores of the PLSR model).

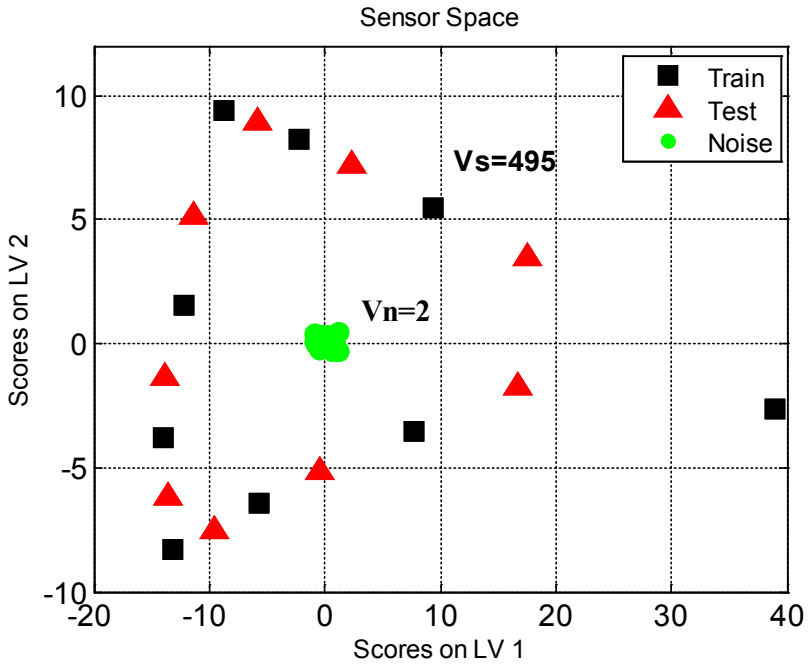

Fig. 51. Projection of the Odour Space onto the Reduced Sensor Space. This space corresponds to the latent variable scores of PLS regression, where sensor response is expressed in voltage. The notation of fig1.a is preserved on this figure. The Hyper-volume on the Sensor Space is around 495. This plot also includes the scores for the noise matrix in green circles. The corresponding Hyper-volume of Noise on the Sensor Space is 2.

The mean of each sample class is showed on a score plot. The marker notation for training and test samples of the previous figure is preserved. Additionally, the noise matrix N after dimensionality reduction is plotted in green circles. The values for V_S and V_N are also displayed on the figure. The estimated Number of Discriminant Odour Features N_O is around 248, for a condition number of $\hat{S}$ of 4.6. Comparing the areas spanned by the odour dataset and the noise on the scores plot, the value obtained for N_O seems a reasonable approximation.

Regarding the second experiment, we present the computations of N_O, Cond($\hat{S}$), and N_O/Cond($\hat{S}$), for the pair-wise combinations of sensor temperatures in the contour plots of Fig.52(a-b) and in Fig.53. These parameters are represented in logarithmic scale on the figures so as to enhance the visualization of the most relevant sensor temperatures. Colours biased towards red tones denote high parameter values. On the contrary, blue tones indicate low ones. According to Fig. 52a, where the temperature selection is performed using N_O, the best region for odour for separation seems close to the upper-right corner of the plot (that is beyond the 250 ºC for both sensors). Though, there are two additional narrow areas which are apparently significant for odour discrimination. First area is around 250ºC of the TGS-2620 unit and follows the low-temperature range of the TGS-2610 sensor (between 25 ºC and 160ºC). Similarly, the second area is situated around the 300ºC of the TGS-2610 unit and follows the temperature axis of the TGS-2620 sensor from 25ºC to 250ºC. The situation is quite different if we consider the

results shown in Fig. 52b. We can see that the system of equations that defines the odour to sensor space transformation is ill-defined for some pairs of temperature combinations. In particular, the largest values of Cond(Ŝ) virtually overlap to the largest values of N_O, so must be down-weighted. This is done in Fig. 53, where we show the ratio N_O/Cond(Ŝ). On the figure, we observe that the most discriminant temperature pairs are placed around 250ºC for the TGS-2610 unit and 340ºC for the TGS-2620. The value of N_O at this point is 384. Furthermore, the contrast between good and bad temperatures for odour discrimination is enhanced.

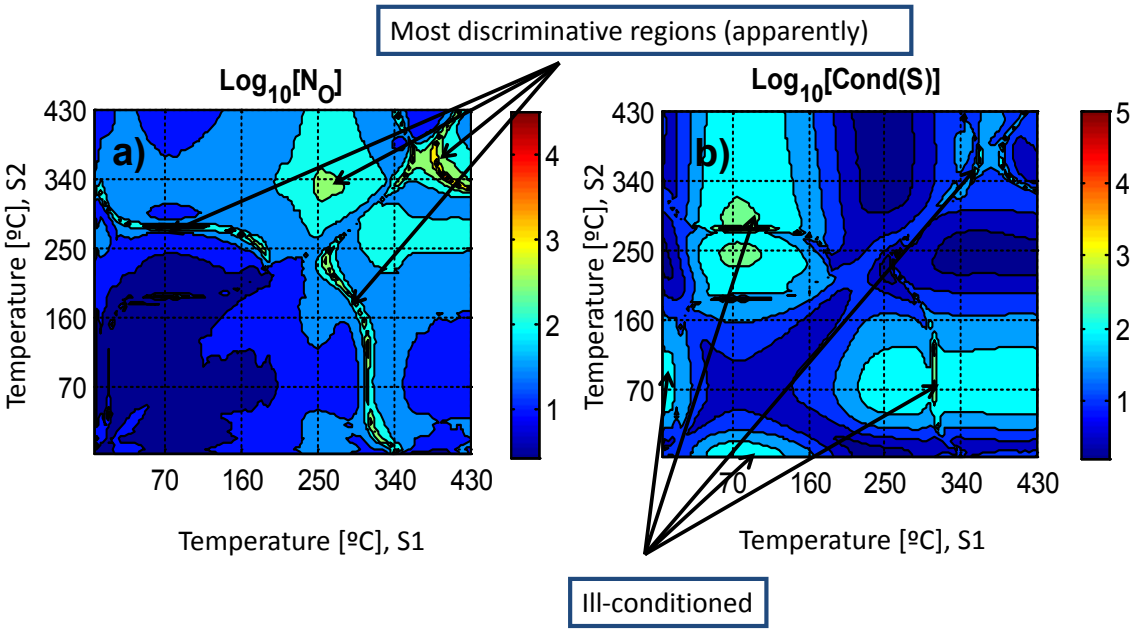

Fig. 52. Example of wrong feature selection. Contour maps for the (a) Number of Odour Discriminant Features (b) the Condition Number of Ŝ, obtained from all binary combination of temperatures from the sensors TGS-2610 and TGS-2620.

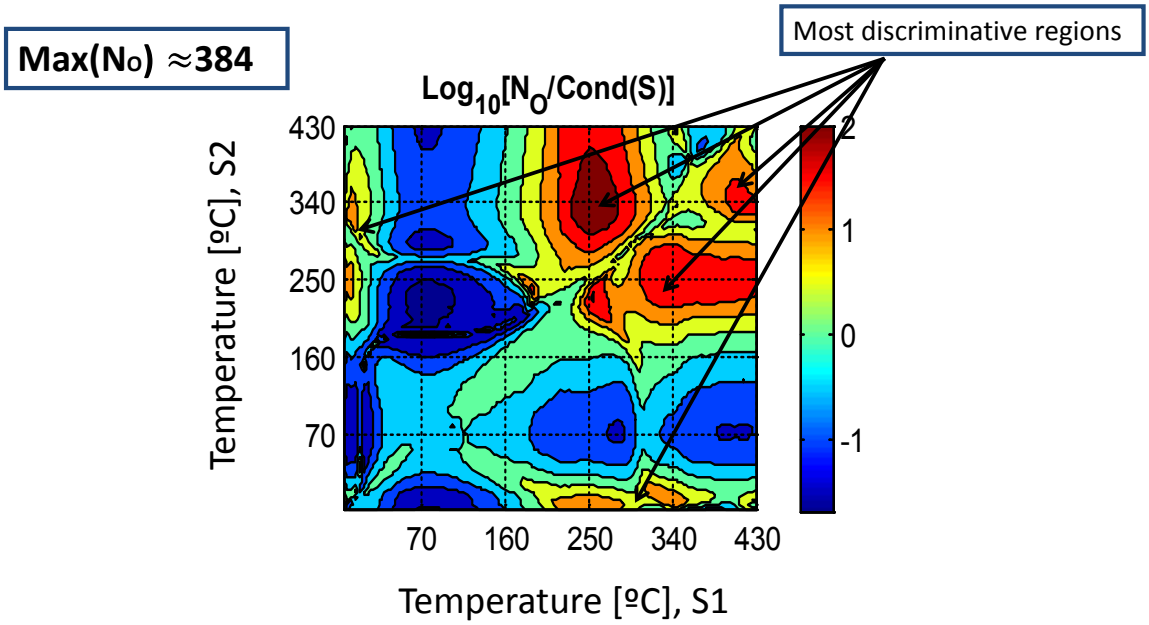

Fig. 53. Regularized Number of Odour Discriminant Features. We obtained this parameter from all binary combination of temperatures from the sensors TGS-2610 and TGS-2620.

Finally, in experiment 3 we perform temperature optimization to enhance the discrimination of ethanol and acetone mixtures. Though, this time temperature optimization is realized employing the simulated sensor responses of the TGS-2602, TGS-2610, and TGS-2620 units. In particular, we generate a Sensor Space that corresponds to an Odour Space of 9 samples: [80-40; 80-60; 80-80; 60-40; 60-60; 60-80; 40-40; 40-60; 40-80]. Thus our current Odour Space is a square with an area of V_O=1600 ppm^2. Sensor models are built according to section V.2.3.1. Note that in the previous Sensor Space the contribution of noise is not included. To obtain a more realistic set of

sensor responses, we add to these signals the sensor noise calculated as in section V.2.3.2. This process is repeated 10 times in order to obtain a set 90 noise-affected sensor responses. To estimate the goodness of our approach, we compare the real sensor readings with the simulated ones. This is done on the on the PLSR latent variables scores plot shown in Fig.54. There we can see the samples used to create and test the sensor models in, respectively, black squares and red triangles. Blue asterisks correspond to the modelled sensor responses to our simulated Sensor Space. We only consider the mean of each sample class odour sample to help visualization. Interestingly, sensor readings corresponding to the mixtures of 80-40, 60-60 and 40-80, almost overlap with the simulated sensor responses. The plot also includes the noise matrix N of the simulated samples represented by green circles. Comparing the sizes of the simulated Sensor Space ($V_S=2.6\cdot10^{10}$) and the sensor noise ($V_N=8.0\cdot10^{8}$), it is evident that an optimization of the sensor temperatures is needed to increase the signal to noise ratio ($N_O=32$).

Temperature optimization is performed using Genetic Algorithms (GA) for feature selection, where the fitness function is the regularized number of discriminable odour features. The frequency of selection of sensor temperatures obtained from 5000 randomly initialized GA populations is found on Fig.56. The results on this figure suggest that the most discriminant temperatures tend to be clustered around T=225ºC for the TGS-2610 and TGS-2620 units, whereas that for the TGS-2602 sensor several discriminant regions appear superimposed between 80ºC o 150 ºC. In order to limit the

number of selected temperatures, we compare the distribution of frequencies obtained with our method with that one corresponding to a random selection of features (3 temperatures per individual, uniformly distributed along the feature vector). By virtue of the Central Limit Theorem (CTL) the latter distribution of frequencies tends to be Gaussian (see the histogram on Fig.55).

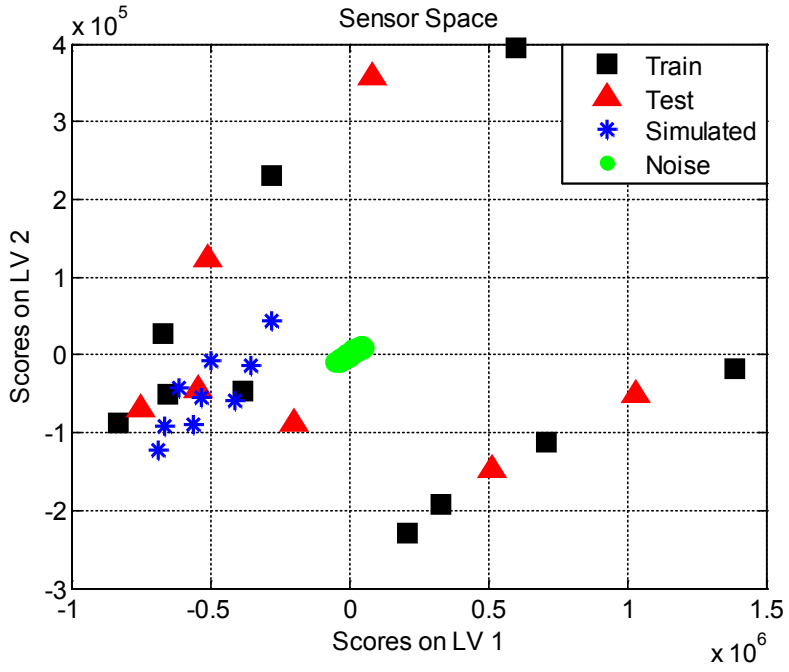

Fig. 54. Reduced Sensor Space for real and simulated samples. Data features were expressed in terms of sensor resistance. Black squares represent the training samples utilized to generate the sensors models, whereas the red triangles are used as a test samples. Blue asterisks correspond to the class centres of the simulated odour mixtures. Finally, the simulated noise matrix is included on the plot in green circle markers.

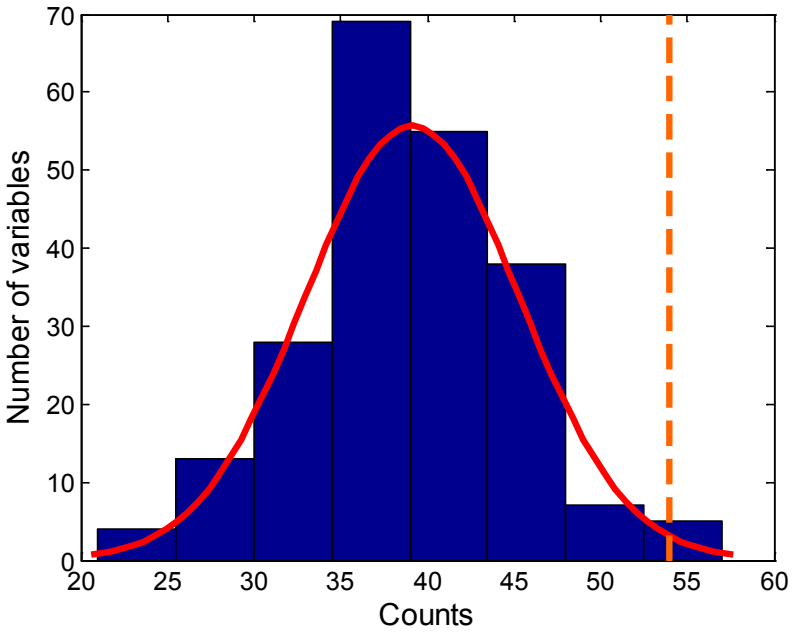

Fig. 55. Histogram corresponding to a random selection of sensor temperatures. By virtue of the Central Limit Theorem, the distribution of counts tends to be Gaussian. The orange dashedline indicates the number of counts where the 99% of the features have been selected by chance

That fact allows us performing a test of hypothesis to either accept or reject sensor array features. The null hypothesis is that the selection of temperature is performed by chance (that is that the frequencies of selection are within this normal distribution). We accept this hypothesis with a confidence of 99%.This calculation provides the threshold value plotted on the figure in a blue dashed line (53 counts). After variable selection, the regularized number of sensor features is N_O=236.

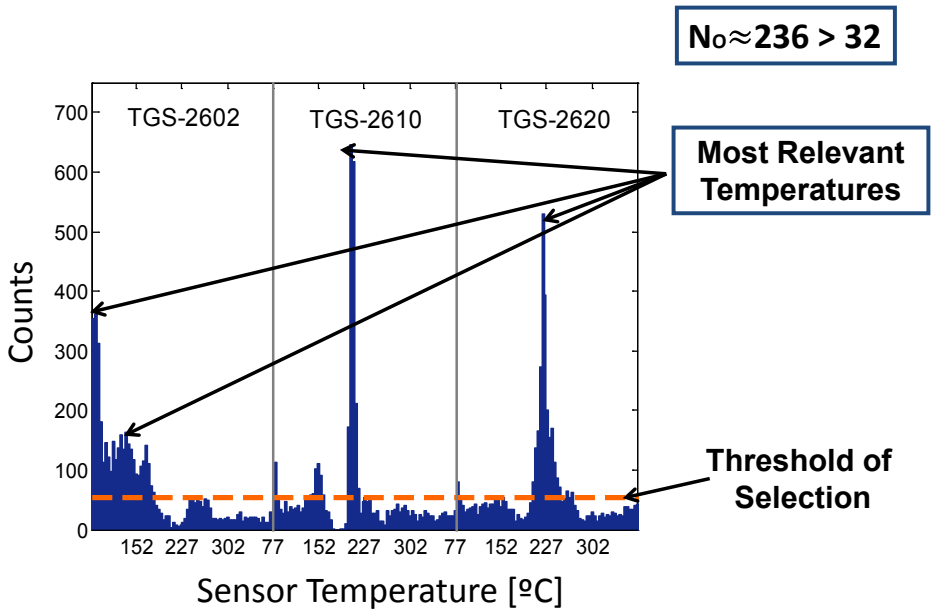

Fig. 56. Bar plot representing the counts for the selected features. Again, the orange dashed line is the threshold that discriminates a random from systematic feature selection.

V.4. DISCUSSION

In this work we have presented a methodology to optimize arrays of temperature modulated MOX sensors for odour discrimination. This methodology was inspired by the feature selection method created by Pearce and Sanchez-Montañes, and consists in maximizing the Odour to Sensor Space volume transformation, considering the effect of noise.

In our opinion, the main limitation of the original method consisted in the Sensor Space dimension couldn't exceed the dimension of the Odour Space in order to apply the technique. Thus, part of the discriminant of information provided by the array of sensors

was merely neglected. The reason for that limitation was that the Odour Space preserved its intrinsic dimensionality (the number of pure compounds) when projected onto a Sensor Space of higher dimension. This issue can be understood with a simple example: Imagine an Odour Space of dimension 2. In such as Odour Space, the odour samples are confined on a plane, and V_O is an area. Now, try to represent our 2-dimensional Odour Space on a 3-dimensional Sensor Space. The odour samples on the Sensor Space will be confined on surface defined by the readings of three sensors. Consequently, V_S, which is a volume, will be 0. To overcome this problem we proposed the use of multivariate regression methods (such as PLSR) before to perform the Odour to Sensor Space volume transformation. Firstly, we took advantage of a dimensionality reduction stage by using the latent variable scores of the PLSR model as a new sensor space. In other words, we combined those sensor features that exhibited very much correlated responses enhancing the signal to noise ratio. Note that, the dimension of the Odour Space limited the number of latent variables of the PLSR model. Furthermore, the array linearization performed though the PLSR regression simplified considerably the application of the method. Since the odour to sensor transformation became a constant matrix after dimensionality reduction, the calculus of the hyper-volume on the sensor space was not dependent of the specific operational point of the odour space.

Though, the original method presented an additional drawback: an inaccurate calculation of the hyper-volume of noise, V_N. Basically, the authors didn't consider any noise contribution from the Odour Space. Besides that, noise on the Sensor Space was

supposed to be independent and Gaussian. That is to approximate the hyper-volume of noise to the area of a hyper-rectangle with sides of length σ_i, where σ is the sensor standard deviation and *i* denotes the sensor index. To correct this issue, we took into account the common sources of noise present on the Sensor Space (for instance sensor drift) computing V_N as the generalized variance of sensor noise. In such a case, the V_N corresponded to area rectangle built from the principal axis of the covariance matrix of noise. It is follow that the more the sensor noise co-varies; the worse is the estimation of V_N considering this noise independent.

Another key improvement of our version consisted in regularizing N_O. We performed this regularization simply dividing N_O by cond($\hat{S}$). The condition number was a powerful tool to rank the 'quality' of Odour to Sensor transformation. Large condition numbers involved ill-defined transformations. That meant that even slight tolerances on the Odour Space samples caused large differences of response on the Sensor Space. As a result, the different odour classes (odour quality and quantity) became mixed when represented on the Sensor Space. As we mentioned somewhere, Cond($\hat{S}$) was related with the degree of orthogonality of the row vectors of $\hat{S}$. Matrices (not necessary square) with almost orthogonal row vectors tend to have conditions numbers close to 1. Noteworthy, N_O and N_O/Cond($\hat{S}$) converged to the same value in such a case. So the most discriminative sensor temperatures (that is those that provided the most 'orthogonal' response to odours) weren't down-weighted. Curiously, one might think that we had already checked the

degree of collinearity of the row vectors of $\hat{S}$ when we computed V_S (we remember the reader that V_S is proportional to the determinant of $\hat{S}$). This is because it is usually stated that ill-conditioned matrices must exhibit determinant values close to zero, and vice-versa. Nonetheless, although both concepts are closely related they are not equivalent. In fact, we can always build matrices corresponding to equivalent systems of equations with arbitrary large values of their determinant, but the same condition number. This can be done as follows: Imagine a matrix A associated to system of equations whose determinant is det(A), and its condition number, Cond(A). It is known from linear algebra theory that $\det(cA)=c^n\det(A)$, where c is a constant and n is the number of rows (or columns) of A. Thus, the value of the determinant can be trivially increased selecting $c>>1$. However, this operation doesn't alter the value of Cond(A).

This methodology has been utilized to select the most relevant sensor temperatures in two different scenarios of odour discrimination. First scenario consisted in obtaining the maximum separability of ethanol, acetone and their linear mixtures within a given range of pure substance concentration. There, sensor responses corresponded to the output voltages of the sensors at different temperatures. We wondered if these sensor readings could be used to optimize temperature selection for unseen ethanol-acetone mixtures. That led us to build a model of sensor response to binary mixtures across temperature. Notice that this time, sensor responses were expressed in terms of sensor resistance. Then the second scenario was defined. We tried to enhance odour discrimination of ethanol-

acetone mixtures around a particular operational point of the Odour Space. As we saw in fig.54, sensor models were in agreement with the real measurements. Tough, we want to emphasize that those sensor models were mere interpolations built from a limited collection of experiments. Therefore, large discrepancies between real and modelled responses should be expected for odour samples far from the initial Odour Space. Still, only two additional models of odour mixtures for MOX sensors were found in the literature (Clifford and Tuma, 1983a; Chaiyboun et al., 2006) so we considered appropriate to include our interpolation-based model in this study. Regarding the modelling of noise, we followed the rationale that sensor noise was correlated across temperature. We believe that this point was crucial, because we approximate to the true nature of noise. A naïve approach would have been, for instance, considering an independent Gaussian noise for each sensor temperature. Comparing the results obtained from the experiments, we find two issues to be discussed. First, the collection of sensor temperatures selected in each experiment was very different. That may seem shocking at first sight, but it can be simply explained. The point is considering that sensor readings were expressed in voltage or resistance depending on the experiment. Since the functional relationship that converts sensor voltage to sensor resistance values is non-linear, the shape of the corves as a function of one and another magnitude is quite different. Consequently, the most discriminative temperature combinations didn't match in different scenarios. This distortion on the sensor's response waveform was reflected on the PLSR score plots of Fig.51 and Fig.54. There we can see that, although both plots

showed a projection on the initial Odour Space onto a reduced Sensor Space, the arrangement of the odour samples on their respective latent variable planes was totally different. The second matter to discuss is the tendency of adjacent sensor temperature combinations to be clustered in accordance to the value of N_O. That happened because the sensor responses at nearer temperatures were very much correlated. Thus, best V_S values were found around specific combinations of sensor temperatures whose averaged response reduced the parameter V_N. As a final comment, we feel interesting to have found a solution for combining a variety of sensors responses in an optimum manner that is analogous to the architecture of the olfactory epithelium. Were the olfactory receptor neurons (ORN) expressing the same receptor type converge to pseudo-spherical structures called glomeruli. Following the analogy, the different glomeruli (cluster centres of sensor temperatures) encode for the odour quality, whereas the population of redundant ORN receptors within each cluster (sensor responses at adjacent temperatures) reduces independent sensor noise.

In conclusion, the power of our updated feature selection method lies in exploiting the benefits of sensor diversity and redundancy, factors that at the end of the day a responsible for odour discrimination. The method seems to capture efficiently the most relevant temperatures for odour separation using MOX sensors. Future work includes comparing the performance of our method with other feature selection techniques.

CHAPTER VI

CALIBRATION TRANSFER

Shifts in working temperature prevent direct calibration transfer between instruments (Lin, 1998). That is to say that calibration models built for instrument I_1 working at a temperature T_1 experience an important degradation on prediction when applied to data samples of instrument I_2 at T_2 ($T_2 \neq T_1$). This is a matter of the utmost importance for temperature modulated metal oxide gas sensor arrays (Lee and Reedy, 1999) where tolerances in heater resistances values, variations on the working flow conditions, and environmental fluctuations can give rise to a global shift ΔT of the sensor nominal temperature profile, and therefore of the sensor response waveform. A naïve approach to overcome invalid calibration transfer is to create independent calibration models for each of the arrays. However this is an impractical solution, since implies costly, labour-intensive measurement campaigns. A preferable methodology is the use of instrument standardization techniques (Wang and Veltkamp, 1991), to correct the temperature shift in sensor arrays as compared to a reference array (from now on slave and master arrays respectively) calibrated for a complete set of experimental conditions and a proper temperature profile. The calibration transfer relies then on the measurement of only a small subset of experimental points in the slave array (herein called transfer samples).

According to (Marco and Gutierrez-Galvez, 2012) calibration transfer can be realized in three different ways: **(i)** by transforming the slave instrument readings to keep the calibration model of the master instrument still valid on the slave instrument, **(ii)** by modifying the target labels of the samples from the slave instrument so as to match with those obtained from the master instrument, and **(iii)** by forcing master and slave readings to become more similar to create the calibration model. Direct Standardization (DS) and Piecewise Direct Standardization (PDS) are the most used approaches to standardize slave instrument response (Bouveresse and Massart, 1996; Walczak1 et al., 1997). With respect to the slave instrument target values correction, the most frequent method is univariate Multiplicative Signal Correction (MSC) (Feudale et al., 2002). Finally, Component Correction (CC), Orthogonal Signal Correction (OSC) and Generalized Least Squares Weighting (GLSW) are the usual techniques used to remove instrument-to-instrument variability (Sjöblom et al., 1998; Padilla et al., 2010; Fu et al., 2012).

Although many different investigations on instrument standardization have been dedicated to Near Infrared Spectroscopy (NIRS), there is a noticeable lack of contributions to standardize gas sensor arrays. Still, three essential references addressing the issue can be found in chemical sensing literature. (Balaban et al., 2000) attempted to transfer a model trained to identify milk samples by age from a 12 conducting polymer to a slave sensor array endowed with the same set of sensors. In their work, they transformed the slave array response into master array readings by applying three

different types of corrections: Univariate Regression, Multivariate Regression (MLR) and Multilayer Perceptrons (MLP). This calibration transfer methods were evaluated comparing the classification rates of master and the transformed master arrays. Multivariate regression showed the best performance in standardizing the instruments. In a similar study, (Tomic et al., 2004) tried to compensate the effect of sensor replacement in a hybrid sensor array composed of 12 MOX (metal-oxide semiconductor) sensors and 5 MOSFET (metal-oxide semiconductor field-effect transistor) so as to distinguish between off-flavor and suitable for feeding milk samples. They acquired twice the complete dataset, prior to and after the sensor replacement, and modelled the data of the old sensor array, which was selected as the master instrument. Measurements obtained from the new array were adapted to be used in the master classification model with two different techniques: Component Correction (CC) and Multiplicative Drift Correction (MDC), being the latter slightly more efficient in rectifying the slave instrument response. The comparison between master and corrected slave instruments was referred to the classification rate obtained for the test set samples. In a more recent paper, (Shaham et al., 2005) showed the possibility of constructing mappings between two different sensor technology arrays, a 32 conducting polymer array (CP) and an 8 sensor quartz microbalance module (QMB), which were exposed to a set of 23 pure chemicals. The authors built a PCA model for each instrument and tried to classify test samples according to the distance to the centroid of the nearest class. After that, they converted the projected data from one sensor array to the other in both directions. To perform the

task, they investigated three different approaches: Multivariate Regression (MLR, PCR, PLS), Neural Networks (NN) and Tesselation-based Linear Interpolation (TLI). Again, the classification rate was the figure of merit used to compare master and the standardized slave instruments. Their results showed that the performance of the different standardization methods was dependent on the mapping direction, obtaining the best results for the conversion from CP to QMB using NN, and applying TLI in the reverse mapping. In all these previous works the complete set of calibration samples used to create the data models was transferred from the master to the slave instrument.

Beyond these valuable contributions, we have identified four important open questions for calibration transfer in e-noses. **(i)** E-nose arrays can tune their operational parameters so as to enhance their sensitivity to different compounds (Hierlemann and Gutierrez-Osuna, 2008). Therefore, instrument dissimilarities due to tolerances on the operational parameters must be corrected accordingly. **(ii)** In order to make an efficient calibration transfer, a limited subset of experiments should be run in the slave instruments. To the best of our knowledge, no systematic study comparing the performance of different calibration transfer techniques with respect to the number of transfer samples is found in the literature for e-noses. **(iii)** Continuous calibration models (regressors) provide a more sensitive measure of the calibration transfer performance than discrete calibration models (classifiers). However, in the literature you can only find classification models transferred from one instrument to another. **(iv)** It is necessary to define a clear criterion, lacking in

the literature, to either accept or reject a calibration transfer based on its performance.

In this chapter, we address these four open questions with the following study. We have explored the calibration transfer problem for temperature modulated metal oxide sensor arrays when a global shift of temperature occurs **(i)**. In an exhaustive study that includes 132 master-slave instrument combinations, we will evaluate the quality of the calibration transfer obtained from several instrument standardization techniques. We will compare master and slave errors (RMSEP) for different temperature shifts and sizes of the transfer sample set **(ii)** on concentration prediction **(iii)**. We propose a new statistical method to evaluate the quality of the calibration transfer based on the bias variance trade-off **(iv)**.

VI.1. THEORY

In this chapter we follow two of the three different strategies proposed in the literature for calibration transfer (Marco and Gutierrez-Galvez, 2012). The first one is to transform the sensor responses of the slave instrument so it resembles those of the master instrument. In this way, we can directly use the calibration model built on the sensor responses of the master instrument with the transformed slave sensor responses. In this strategy, we work on the space of responses of the master instrument. To transform the sensor responses of the slave instrument, we used Direct Standardization (DS) and Piece-wise Direct Standardization (PDS). The second strategy consists of transforming not only the sensor responses of the slave instrument but also those of the master instrument to a joint master-slave space. Thus, the calibration model is built in this joint space. The sensors response transformation methods used in this strategy are Generalized Least Squares Weighting (GLSW) and Orthogonal Signal Correction (OSC). Fig. 57 illustrates both strategies. In addition to this, we realized a sample subset selection to sort out the samples used to study the performance of the calibration transfer in terms of the number of samples considered from the slave instrument. We test two different approaches: select samples before or after creating the calibration model of the master instrument. In the following subsections we describe the main features of the different calibration transfer techniques used in this paper, as well as the two methodologies used to perform sample subset selection.

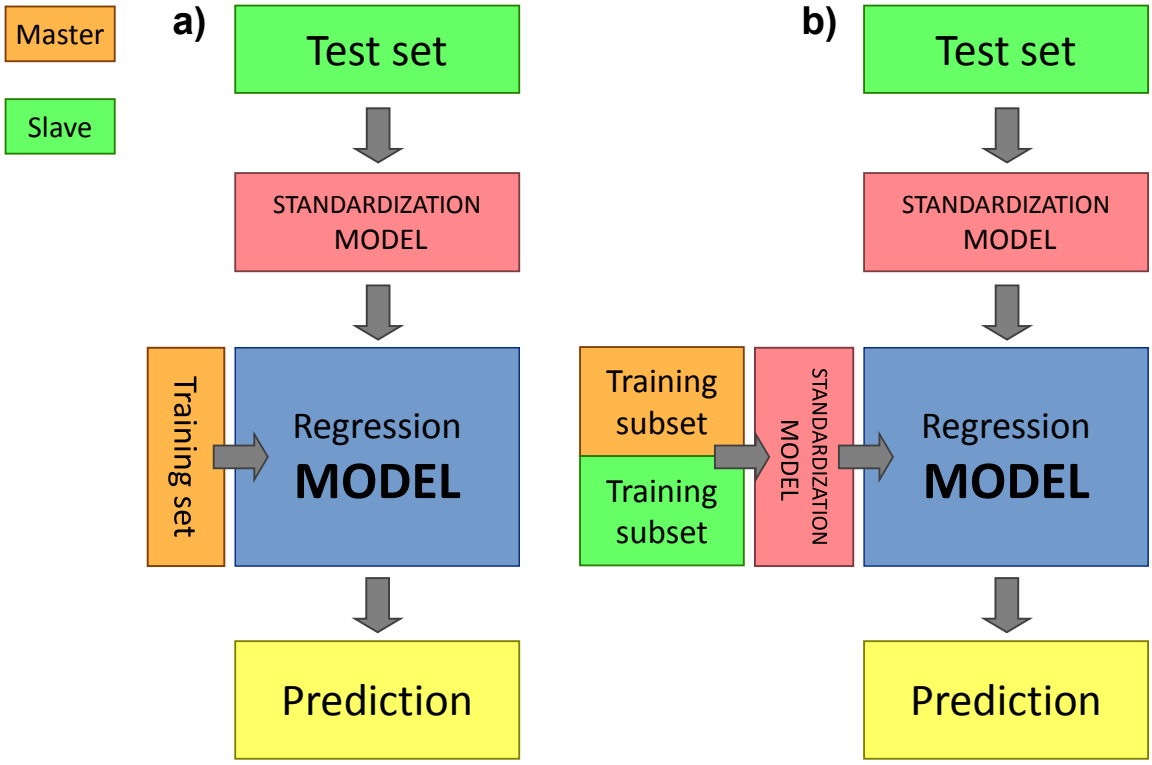

Fig. 57. Block diagram of the calibration transfer process: (a) to transform the responses of the slave instrument so as to work on the space of responses of the master instrument (DS and PDS), and (b) to transform the responses of the master and slave instrument in order to work on a joint master-slave space (OSC, GLSW).

VI.1.1. Calibration transfer techniques

VI.1.1.1. Direct Standardization (DS)

Direct Standardization (Tauler et al., 2009) is a calibration transfer technique that relates the readings of the slave instrument to those of the master according to the following linear transformation:

$$\overline{S}_M = \overline{S}_S \cdot F \tag{6.1}$$

where $\overline{S}_M$ and $\overline{S}_S$ are the mean-centered response matrices of master and slave instruments and *F* the slave-to-master transformation matrix, which is estimated as the product $\overline{S}_M$ and the pseudo-inverse of $\overline{S}_S$:

$$F = \overline{S}_S^{+} \cdot \overline{S}_M \tag{6.2}$$

In this way, samples from the slave instrument can be projected onto the master instrument response space:

$$x_M^T = x_S^T \cdot F \tag{6.3}$$

VI.1.1.2. Piece-wise Direct Standardization (PDS)

The DS method has the limitation of not properly transform the responses from slave to master instruments when the number of variables per sample is greater than the number of samples. Thus, the transformation matrix *F* (6.2) becomes underdetermined (Feudale et al., 2002). Piece-wise Direct Standardization (Wang et al., 1992) avoids this problem using local PLS models. It creates local linear models f_j that relate the response of the master instrument variables within a window of size **w** centered at the *j*th variable to the

*j*th variable on the slave array. The resulting transformation matrix for the method *F* has a diagonal structure:

$$F = diag(f_1^T \dots f_2^T \dots f_k^T) \tag{6.4}$$

where *k* is the number of variables on both instruments. The projection of data from the master onto the slave instrument is performed following (6.3).

VI.1.1.3. Ortohgonal Signal Correction (OSC)

Orthogonal Signal Correction (Fearn, 2000) aims to remove the sources of variance of the slave instrument that are orthogonal to the master array. The OSC algorithm starts calculating the scores vector $\mathbf{t_1}$ of the first Principal component of the slave array data matrix, $\mathbf{S_S}$. That vector is then orthogonalized against the master instrument response matrix $\mathbf{S_M}$, giving raise to $\mathbf{t_1'}$**:**

$$t_1' = (1 - S_M \cdot (S_M^T \cdot S_M)^{-1} \cdot S_M^T) \cdot t_1 \tag{6.5}$$

After that, the weights $\mathbf{w_1}$ of the product $\mathbf{S_S \cdot w_1}$ are calculated for the maximum projection onto the orthogonal scores vector $\mathbf{t_1'}$:

$$w_1 = \overline{S}_S^+ \cdot t_1' \tag{6.6}$$

Being $\mathbf{S}_S^+$ the pseudo-inverse of **X**. The scores vector $\mathbf{t}_1$ is then updated:

$$t_1 = S_S \cdot w_1 \tag{6.7}$$

Next, the algorithm returns to (6.5), where the determination of the orthogonal score vector is repeated until convergence. At this point, the loading vector corresponding to the first orthogonal score is computed as:

$$p_1 = S_S^T \cdot t_1 (t_1^T t_1)^{-1} \tag{6.8}$$

and the first OSC component can be removed from the original **X** matrix obtaining the deflated data matrix $\mathbf{X}_1$:

$$S_{S,1} = S_{S,1} - t_1 p_1^T \tag{6.9}$$

Finally, the complete process can be repeated until the *N-th* Orthogonal Signal Component as follows:

$$S_{S,N} = S_S - \sum_{i=1}^{i=N} t_i p_1^T \tag{6.10}$$

VI.1.1.4. Generalized Least Squares Weighting (GLSW)

Generalized Least Squares Weighting (Martens et al., 2003) method identifies and down-weights the instrument channels (variables, features) responsible for the major sources of variance between master and slave instruments. To build the filter, the covariance matrix ***C*** from the difference between the mean-centered master and slave responses is computed:

$$C = \left(\overline{S}_M - \overline{S}_S\right)^T \left(\overline{S}_M - \overline{S}_S\right) \tag{6.11}$$

Next, ***C*** is factorized as the product of three matrices through singular value decomposition (SVD):

$$C = VS^2V^T \tag{6.12}$$

where **V** and **S** are, respectively, the eigenvector and the singular value matrices. After that, the **S** matrix is weighted in the following way:

$$D = \sqrt{\frac{S^2}{\alpha} + I} \tag{6.13}$$

Being **D** the matrix of the weighted eigenvalues, **α** the weighting parameter and **I** the identity matrix. The parameter **α** controls the degree of dissimilarity allowed to the

instruments. While high values of **α** increase the down weighting, lower values of **α** reduce its effect. The filtering matrix **G** is then calculated using the inverse of the weighted eigenvalues:

$$G = VD^{-1}V^T \tag{6.14}$$

VI.1.2. Sample subset selection

Sample subset selection can be conducted in two manners: a) by looking for the non-characteristic samples (with respect the multivariate mean) on the master instrument matrix $\overline{R}_M$ through the calculus of the leverage matrix **H** (Sharaf et al., 1986):

$$H = \overline{R}_M \overline{R}_M^T \tag{6.15}$$

And b) by seeking for the most influent samples of the master's instrument calibration model, approaching **H** as the leverage matrix for the inverse calibration model $\overline{R}_M^+$, also mean-centered:

$$H = \overline{R}_M \overline{R}_M^+ \tag{6.16}$$

In both cases, the maximum diagonal element of **H** corresponds to the most relevant sample in the dataset. Once the first sample is obtained, the rest of the dataset is

orthogonalized against it, a new leverage matrix **H** is created, and the next most influent sample can be selected. Table 3 shows the first 12 samples selected using both methods.

VI.2.METHODS

VI.2.1. Experimental

To perform this study, we used a set of three different types of Figaro metal oxide semiconductor sensors (TGS2600, TGS2610, TGS2620) replicated 12 times. In all experiments, one of the sets of three sensors was used as a master instrument to find a calibration model and the rest treated as slave arrays to study the calibration transfer. The read out of the sensors is performed through a load resistor (R_L=6.1 KΩ) in a half bridge configuration. We modulated the sensor temperatures with a ramp profile ranging from ambient temperature to 495°C ± 5°C (Lee and Reedy, 2000) in a period of 90 seconds. The 36 sensors were exposed during 900 seconds to three analytes (ethanol, acetone, 2-butanone) at six different concentrations (20, 40, 60, 80, 100, 120) ppm plus synthetic air. After each measurement block, the sensor chamber was cleaned in synthetic air over a period of 1800 seconds. The experiments with concentration levels of 0, 40, 80 and 120 ppm were acquired 7 times (84 samples) as a calibration (training) set, while the ones with concentration levels of 20, 60, 100 ppm were acquired 3 times (27 samples) and used for testing the calibration models. This information is summarized in Fig.58. The selected temperature window used for the calibration of the master instruments was [200-300] ºC.

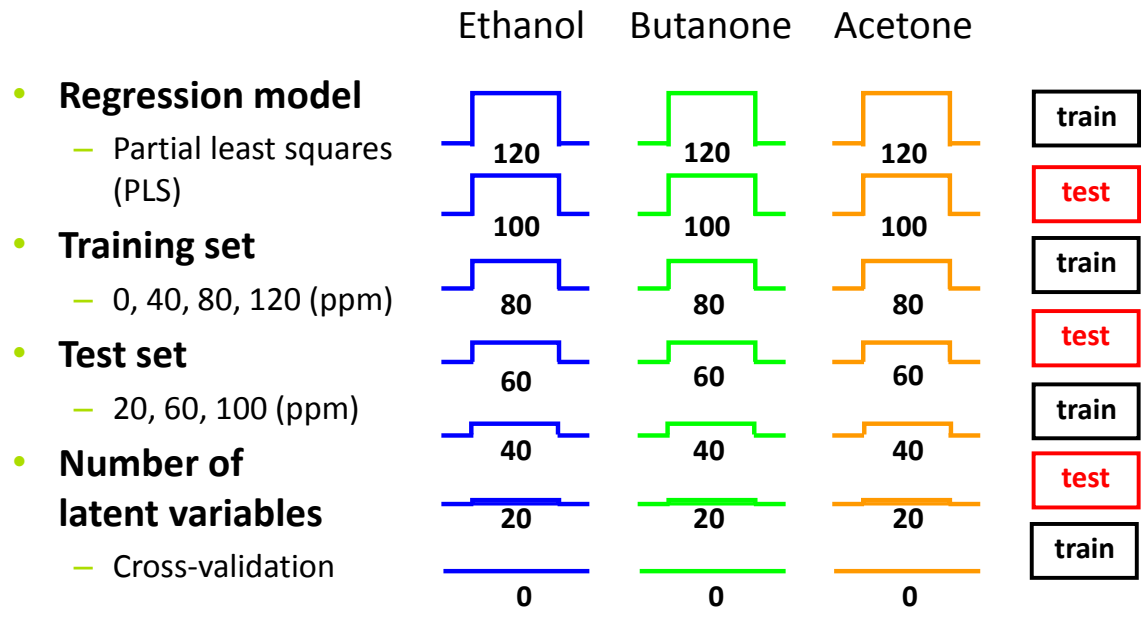

Fig. 58. Set of experiments used in Chapter VI.

VI.2.2. Calibration model

We have approached the calibration of our instruments as a regression problem to provide more sensitivity when transferring the calibration model to another instrument. In particular, we have used partial least squares regression (PLSR). The level of complexity of the PLSR master instrument calibration model (i.e. the number of latent variables) was set through a cross-validation stage based on the Leave One Block Out (LOBO) approach. This method calculates the $RMSECV_M$ as the average of the RMSE obtained from predicting each of the different blocks of calibration conditions using the complementary blocks of samples to generate the PLSR model:

$$RMSECV_M = \frac{1}{C}\sum_{k=1}^{C}\sqrt{\frac{\sum_{i=1}^{N_V}\sum_{j=1}^{M}\left(\tilde{y}_{i,j,k} - y_{i,j,k}\right)^2}{N_V \cdot M}} \quad (6.17)$$

where $\tilde{y}_{i,j,k}$ and $v_{i,j,k}$ are, respectively, the observed and the predicted concentration values for the sample *i*-th sample the *j*-th pure substance and the k-th data partition, N_V is the number of samples for each partition of the validation set (7), M the number of substances present in the dataset (3) and C the number of blocks of calibration conditions (12). The number of latent variables of the calibration model was determined calculating the $RMSECV_M$ (lv) for an increasing number of latent variables (lv from 1 to 10). When the current $RMSECV_M$ (lv=r) did not reduce the previous $RMSECV_M$ (lv=r-1) value more than a 1%, the selected number of latent variables was determined lv=r-1.

The measure of the model's performance fitting the test data for the master array was the Root Mean Squared Error of Prediction ($RMSEP_M$):

$$RMSEP_M = \sqrt{\frac{\sum_{i=1}^{N_T}\sum_{j=1}^{M}\left(\tilde{y}_{i,j} - y_{i,j}\right)^2}{N_T \cdot M}} \quad (6.18)$$

where $\tilde{y}_{i,j}$ and $y_{i,j}$were, respectively, the observed and the predicted concentration values for the sample i-th sample the j-th pure substance, N_T is the number of samples of test set (27), M the number of substances present in the dataset (3). The RMSEP was also used as a measure of goodness of fit for the transformed slave readings ($RMSEP_S$).

VI.2.3. Calibration transfer

In this study, we have evaluated the ability of four techniques (DS, PDS, OSC, GLSW) to counteract the effect of temperature shift on calibration transfer. A series of experiments were conducted where the temperature of the slaves was shifted according to the following temperature values: $\Delta T = 0°C, \pm 10°C, \pm 20°C, \pm 30°C, \pm 40°C, \pm 50\ °C$. Fig. 60 shows the dramatic change on MOX sensor waveforms due to temperature shifting ($\Delta T = -50\ °C$), for a temperature modulated TGS 2620 sensor exposed to the 3 test set ethanol concentrations.

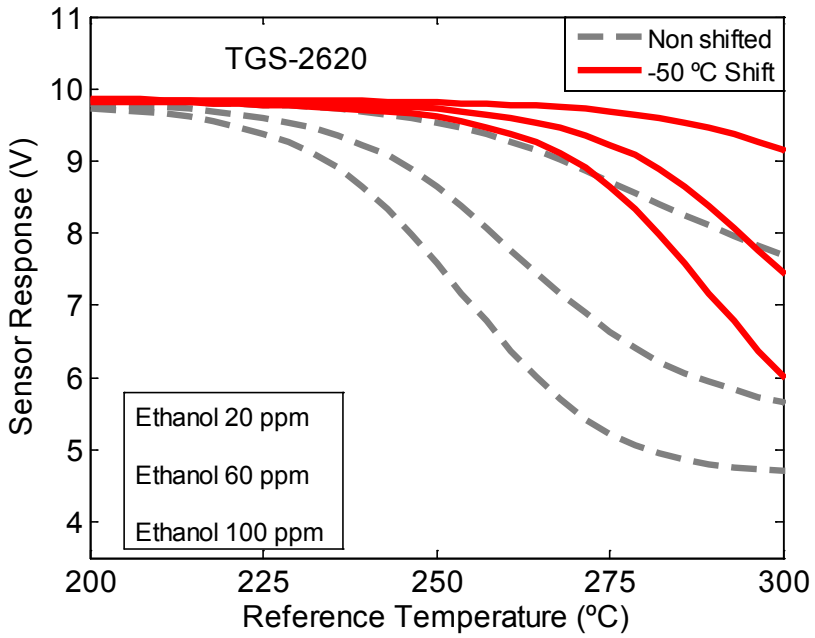

Fig. 59. Global temperature shift on the sensor waveform. Response of a TGS 2620 sensor unit to 20, 60, 100 ppm of ethanol within a nominal temperature window of 200-300 °C for a) no temperature shift (gray-dashed corves) and b) for a temperature shift of $\Delta T = -50°C$ (red corves).

Transfer sample subset was selected using methods 1 and 2 (see Table 3). The effect of the number of transfer samples (from 1 up to 12) on the calibration transfer quality was studied, giving rise to a total of 17424 different calibration models transferred (12 masters x 11 slaves x 11 temperature shifts x 12 calibration samples) per instrument standardization technique. An example of the calibration transfer process is shown in figures (60a-c) using Direct Standardization, for a temperature shifting of ΔT =-50 °C and 12 transfer samples.

Table 3. Selection of the transfer samples of the calibration dataset. These samples were selected using methods 1 and 2.

	Method 1				Method 2			
Transfer Samples	Sample Replicate	Concentration (ppm)			Sample Replicate	Concentration (ppm)		
		Eth	Acet	But		Eth	Acet	But
1	9	0	120	0	10	120	0	0
2	10	0	0	0	2	0	120	0
3	6	120	0	0	5	0	0	120
4	1	0	0	120	7	0	0	40
5	8	40	0	0	10	80	0	0
6	10	80	0	0	10	0	40	0
7	6	0	0	40	3	0	0	80
8	9	0	0	120	2	40	0	0
9	2	0	120	0	7	0	80	0
10	7	40	0	0	7	0	0	120
11	5	0	0	120	4	120	0	0
12	5	0	0	40	8	0	80	0

These figures show the scores plot of a PCA model for the master array (60a), the uncorrected slave array (60b) and corrected slave array (60c). Calibration transfer allows placing test samples back to its original position or nearby. Finally, predictions from master and corrected slave instruments were compared through a statistical test based on the bias-variance trade-off, where the null hypothesis was that master and slave instruments presented the same error (RMSEP) and the alternative hypothesis that the slave instrument showed a higher error level than the master.

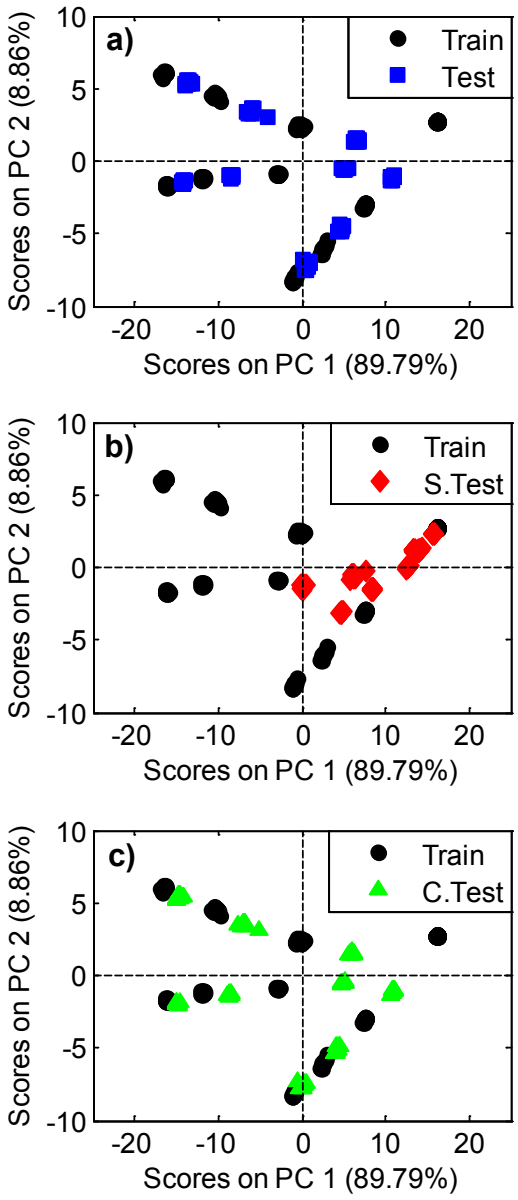

Fig. 60. Example of calibration transfer. PCA plot of the sensor response for the training (black circles) and test sets with interleaved concentrations for: (a) the master experiments (blue squares), (b) the uncorrected slaves (red diamonds) and (c) the corrected slaves after performing a Direct Standardization (green triangles), (ΔT=-50ºC).

VI.2.3.1. Parameter optimization

We optimized the 4 calibration transfer methods minimizing the difference between the master and the corrected slave array readings. This procedure optimized the parameters of the different calibration transfer algorithms selecting them among a set of possible values. Thus, the window size **w** was selected from a list of 1 to 31 channels for PDS; the weighting parameter **α** within the collection of values 1, 0.5, 0.1, 0.05, 0.01, 0.05, 0.001 for GLSW; and finally, the number of iterations, the tolerance and the number of orthogonal components respectively, from 1 to 10, within the set 90, 95, 98, 99, 99.9, and in the range of 1 to 12, for OSC. The validation started performing data correction for each technique and set of parameter values. The calibration model of the master instrument was then applied on the transformed calibration set of the slave instrument and the concentration predictions of both instruments were compared. The comparison was performed through the calculation of the Root Mean Squared Error of Calibration ($RMSEC_{M\text{-}S}$):

$$RMSEC_{M-S} = \sqrt{\frac{\sum_{i=1}^{N_C}\sum_{j=1}^{M}\left(y_{i,j}^{M} - y_{i,j}^{S}\right)^2}{N_{TC}\cdot M}} \tag{6.19}$$

where $y^{M}_{i,j}$ and $y^{S}_{i,j}$ are the predicted concentration values of the master and slave instruments for the sample *i*-th sample and the *j*-th pure substances, N_C (84) is the number of calibration samples and M the number of substances present in the dataset (3). The set

of parameter values whose $RMSEC_{M-S}$ was not able to be reduced in more than 1% by any other set was selected to build the calibration transfer model, for each calibration transfer algorithm.

VI.2.3.2. Evaluation criterion

A method to either accept or reject a calibration transfer between instruments based on the bias-variance trade-off is proposed. According to this result, the RMSE is decomposed in the sum of two terms:

$$E[(y-\tilde{y})^2] = (E[y]-\tilde{y})^2 + E[(y-E[y])^2] \tag{6.20}$$

where y and ỹ are, respectively, the vectors for the measured and theoretical predictions, given a set of samples. First addend on (6.20) explains how biased the calibration model prediction is with respect its theoretical value, whereas the second term describes the dispersion on the measured prediction. That means that two instruments I_A and I_B with the same expected value and variance for the prediction (mean(y_A) = mean (y_B), var(y_A)= var(y_B)) show equals error in prediction. We can easily expand this concept to matrices in the following way:

$$Tr\left(E\left[\left(Y-\tilde{Y}\right)^T\left(Y-\tilde{Y}\right)\right]\right) = \tag{6.21}$$

$$Tr\left(\left(E[Y]-\tilde{Y}\right)^T\left(E[Y]-\tilde{Y}\right)\right) + Tr(E[(Y-E[Y])^T(Y-E[Y])])$$

So now we use the multivariate mean and the covariance matrix of the prediction matrix. We compare the multivariate means through the Hotteling's T^2 test, and the covariance matrices using the Box's M test, for a significance level of 95%. The Null Hypotheses were a) both instruments present the predictions matrices with the same multivariate mean and b) both instruments present prediction matrices with the same covariance. If none of the independent tests rejects its null hypothesis, we accept the calibration transfer between two instruments as success. Conversely, if any of the independent tests rejects its Null hypothesis, we assume that the calibration transfer fails.

VI.3. RESULTS

To gain some insight on the effect of temperature shift on calibration model transfer, we will show first results of the master calibration model applied directly on the slave without correction. This will provide a baseline performance from where to improve. Then, we will present the results of the slave RMESP for an increasing number of transfer samples and also as temperature shifts varies in the range of [-50,50] °C. Finally, the results of the exhaustive statistical analysis will provide a comprehensive picture of the performance of the different calibration transfer techniques.

In this study, each of the array replicates was used both as master instrument for the other replicates or as slave array to be corrected by other master array. When acting as master instruments, the array replicates produced similar calibration models in terms of complexity and model performance. Most of the array replicates built a 4 latent variable

PLSR model (9 out of 12) whereas the remaining (4) needed 5 latent variables to achieve the specifications set for cross-validation. The average $RMSEP_M$ for the set of master instruments was (4.7±1.1) ppm. The direct application of the master calibration model in the slave arrays leaded, as anticipated, to high $RMSEP_S$. Fig. 61 shows the average prediction error of uncorrected slave arrays ($RMSEP_S$) along temperature shift, for all possible master-slave combinations. The $RMSEP_S$ was substantially higher than the $RMSEP_M$. The minimum difference between instruments was found when no temperature shift was produced ($RMSEP_{S|\Delta T=0}$=29.1 ±18.9 ppm). As can be expected, the $RMSEP_S$ increased as the temperature shift between instruments increased. Though, this effect was not symmetric: shifts towards higher temperatures exhibited a greater penalty on the $RMSEP_S$ than shifts in the opposite direction. Comparing the most extreme temperature shifts in both directions we found that the error of prediction at ΔT=+50ºC was $RMSEP_{S|\Delta T=+50ºC}$=128.2 ±41.4 ppm, whereas at ΔT=--50ºC was $RMSEP_{S|\Delta T=-50ºC}$=40.6 ±6.1 ppm.

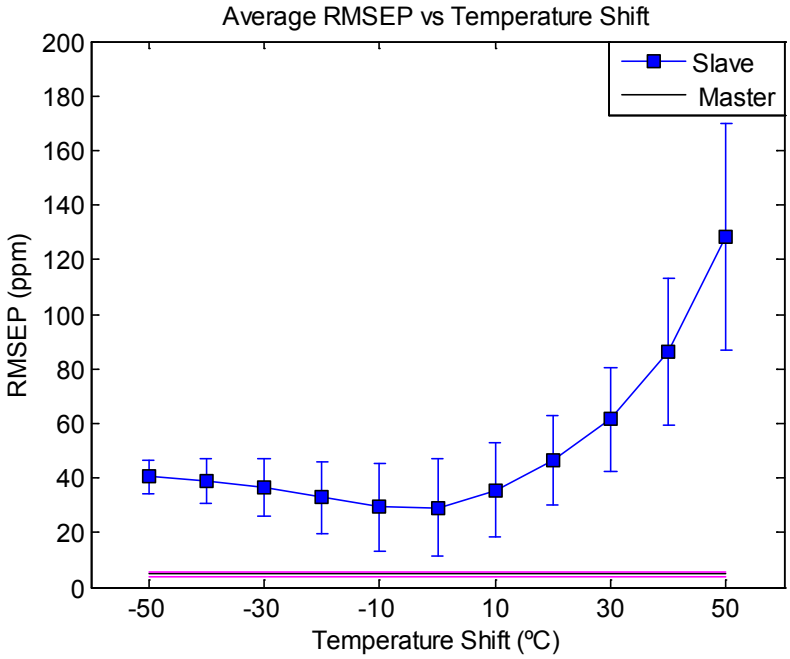

Fig. 61. Average $RMSEP_S$ as function of the temperature shift. Note that the worst predictions are biased towards positive temperature shifts.

After data correction, the $RMSEP_S$ of the slave arrays was considerably reduced. The degree of error reduction depended on the amount of transfer samples and the shift of temperature. As a general trend, the $RMSEP_S$ decreased gradually until saturation as the number of transfer samples increased, for any temperature shift and calibration transfer technique. The influence of the transfer sample subset size on the quality of the calibration transfer is illustrated in figure 62(a-d). The figure shows the average $RMSEP_S$ of the corrected slave instruments of the different calibration transfer techniques, for an increasing number of transfer samples and a fixed temperature shift of ΔT=-20ºC. DS and PDS obtained the lowest $RMSEP_S$ levels (6.3 ±2.1 ppm, and 6.1 ±1.4

ppm, respectively) although PDS needed a fewer number of samples to reach error saturation (five instead of eleven). OSC and GLSW showed higher $RMSEP_S$ values (around 8 ppm, for both techniques) and slower transitions to saturation.

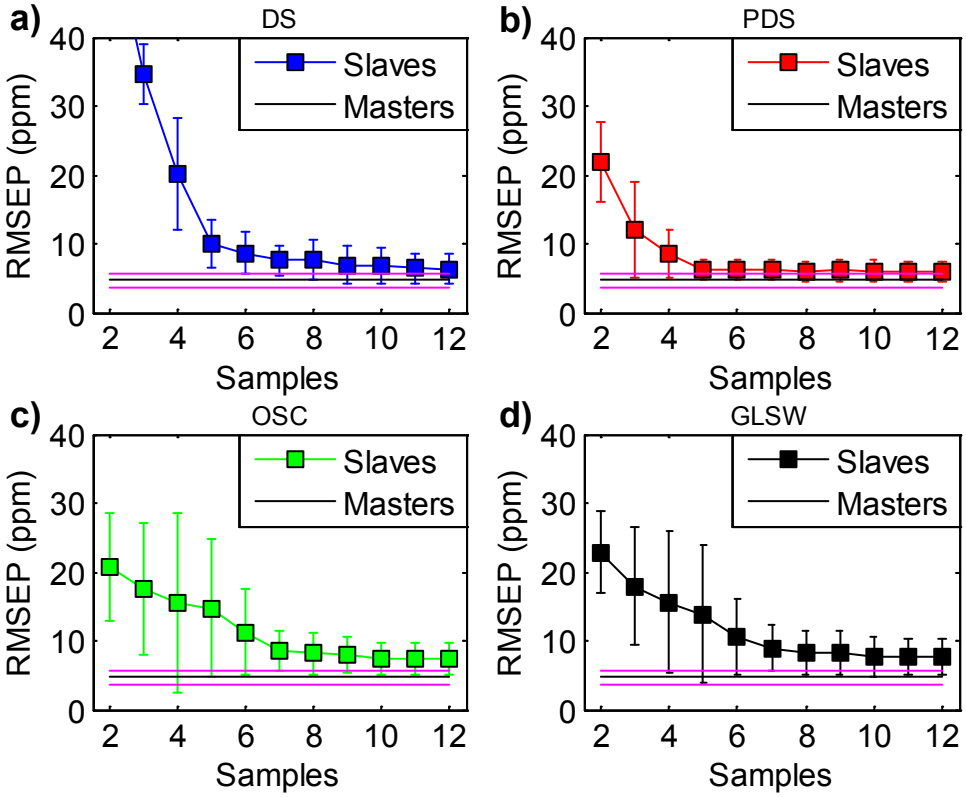

Fig. 62. Effect of the number of transfer samples. Average $RMSEP_S$ of the corrected slave instruments as function of the number of transfer samples, for a fixed temperature shift of ΔT=-20ºC. Data correction was performed using a) Direct Standardization (blue-dotted line), b) Piece-wise Direct Standardization red-dotted line), c) Orthogonal Signal Correction (green-dotted line), and d) Generalized Least Squares Weighting (black-dotted line). The averaged $RMSEP_M$ is included in each of the plots with comparative purposes.

Table 4. Parameter optimization of the CT models 1. Median, first quartile and third quartile of the optimized set of parameters used compensate for a temperature shift of -20ºC in the slave arrays, for a different number of transfer sample and calibration transfer technique. Note that for OSC only the number of orthogonal components (ncomp) was shown.

Transfer Samples	PDS (w)			OSC (ncomp)			GLSW (α)		
	Q1	Median	Q3	Q1	Median	Q3	Q1	Median	Q3
2	1	9	11	2	2	2	0.1	0.1	0.1
3	3	9	12	3	3	3	0.1	0.1	0.1
4	5	9	17	2	4	4	0.01	0.1	0.1
5	8	12	19	2	5	5	0.01	0.05	0.1
6	7	13	21	2	6	6	0.01	0.05	0.05
7	7	15	23	3	5	7	0.01	0.01	0.05
8	9	15	23	3	5	8	0.005	0.01	0.05
9	9	15	27	3	6	9	0.005	0.01	0.01
10	11	17	27	3	6	8	0.005	0.01	0.01
11	13	21	27	3	6	8	0.005	0.01	0.01
12	13	21	27	3	6	8	0.003	0.01	0.01

Concerning the influence of temperature shift, we found that the lowest $RMSEP_S$ were biased towards negative shifts, for any number of transfer samples and calibration transfer technique. However, PDS demonstrated to be the most robust technique against this direction-dependent effect. An example of this behaviour can be seen on Fig. 63(a-d), where we show the average $RMSEP_S$ of the corrected slave arrays using the four instrument standardization methods, for the complete set of the temperature shifts, fixing to 5 the number of transfer samples. The minimum $RMSEP_S$ value for DS and PDS is obtained for a temperature shift of ΔT=-30ºC (9.4±4.0 ppm, and 6.2 ±1.6 ppm,

respectively). On the other hand, OSC and GLSW presented their minimum $RMSEP_S$ value for $\Delta T=0^{o}C$ (8.7±2.8 ppm for OSC and 9.1±3.3 ppm for GLSW).

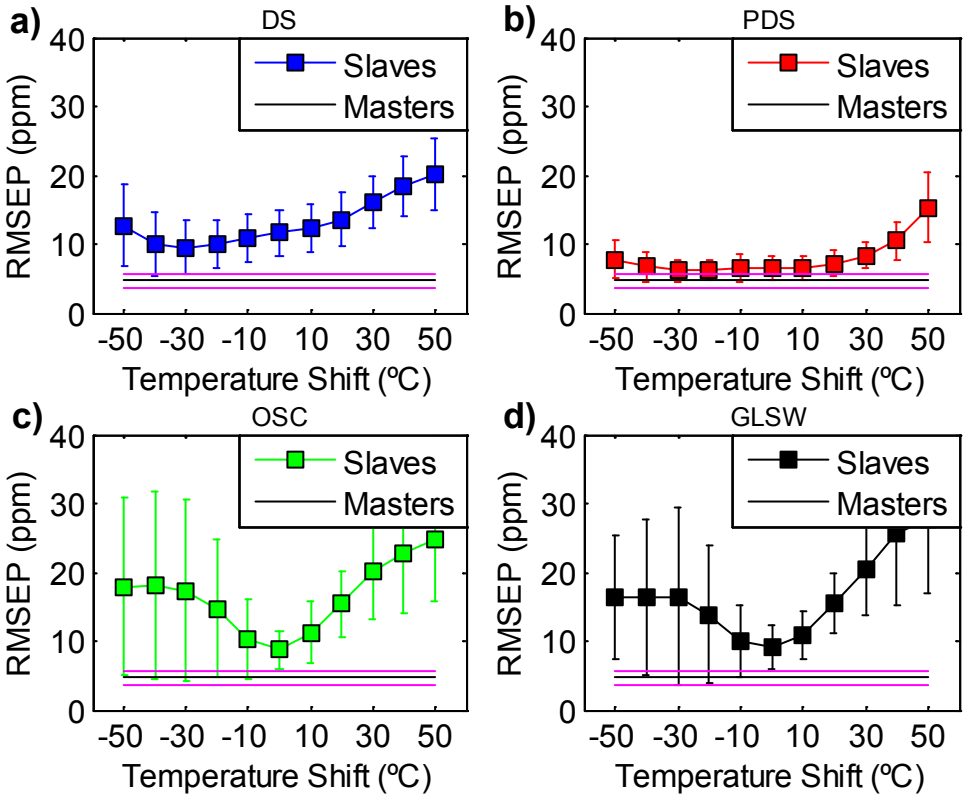

Fig. 63. Effect of the global temperature shift. Average $RMSEP_S$ of the corrected slave instruments as function of the temperature shift, for a number of 5 transfer samples. Data correction was performed using a) Direct Standardization (blue-dotted line), b) Piece-wise Direct Standardization red-dotted line), c) Orthogonal Signal Correction (green-dotted line), and d) Generalized Least Squares Weighting (black-dotted line). The average $RMSEP_M$ is included in each of the plots with comparative purposes.

Table 5. Parameter optimization of the CT models 2. Median, first quartile and third quartile of the optimized set of parameters used to correct the readings slave arrays, for the different temperature shifts and calibration transfer technique and fixing to 5 the number of transfer samples.

Temp. Shift (ºC)	PDS (w)			OSC (ncomp)			GLSW (α)		
	Q1	Median	Q3	Q1	Median	Q3	Q1	Median	Q3
-50	17	19	29	5	5	5	0.01	0.05	0.1
-40	13	21	31	5	5	5	0.01	0.05	0.1
-30	9	21	27	5	5	5	0.01	0.05	0.1
-20	8	13	22	3	5	5	0.01	0.05	0.1
-10	7	11	20	2	4	5	0.01	0.05	0.1
0	5	9	13	2	3	5	0.01	0.01	0.05
10	5	7	13	3	5	5	0.01	0.05	0.1
20	7	9	11	2.5	5	5	0.01	0.1	0.1
30	11	13	15	3	5	5	0.01	0.1	0.1
40	11	13	16	5	5	5	0.01	0.1	0.1
50	15	13	19	5	5	5	0.01	0.1	0.1

The outcome of the contrast of hypothesis test is in agreement with the previous results. Applying the master calibration directly into the slave arrays, none of them satisfied the null hypothesis (the slave and its corresponding master had the same RMSEP level). After calibration transfer, a number of them fall within the strict criteria of the test varying with the number of transfer samples, the temperature shift and the calibration transfer technique applied. Figure 64(a-d) shows the number of transformed slaves within the null hypothesis normalized to the total number of slaves (132) arrays, for each number of transfer samples, temperature shift and calibration transfer technique.

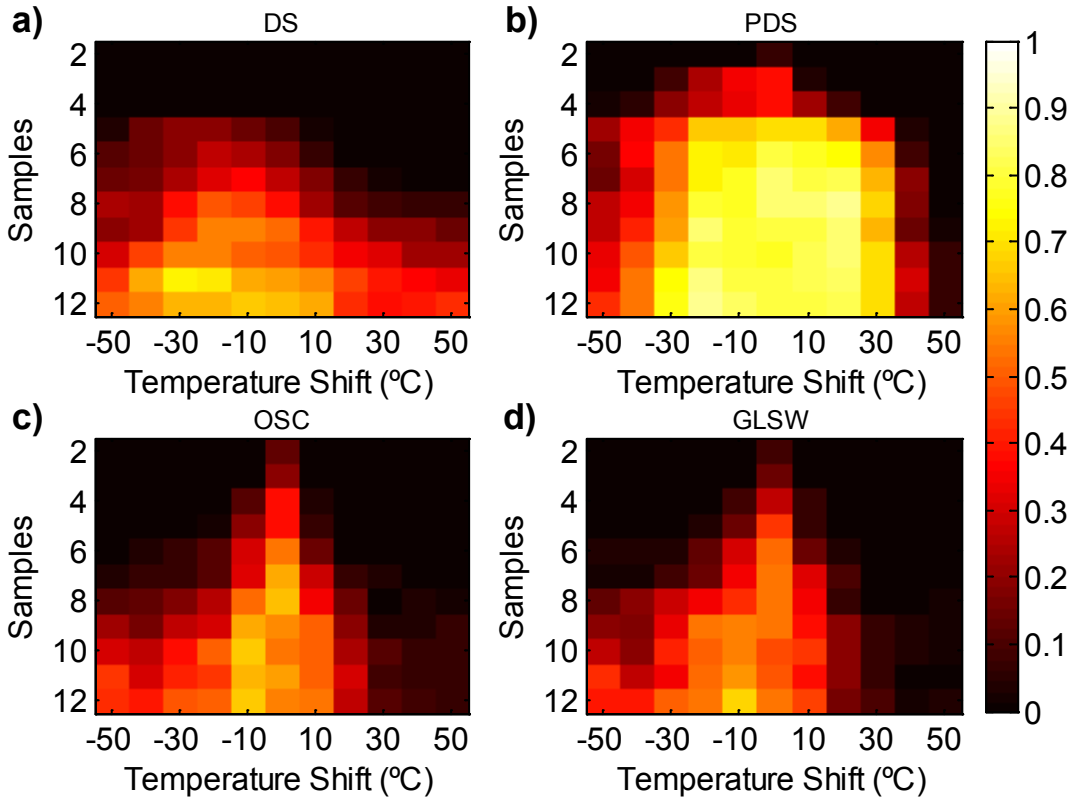

Fig. 64. Evaluation criterion. Plot of the normalized number of corrected slave arrays showing the same predictive performance as their corresponding master instrument, for each temperature shift and number of transfer samples. Data correction was performed using a) Direct Standardization, b) Piece-wise Direct Standardization, c) Orthogonal Signal Correction, and d) Generalized Least Squares Weighting.

To compare the different instrument standardization methods we propose to find how many transfer samples are necessary to reach 70% of accepted slave arrays corrections. DS was better correcting the slave arrays when they were biased towards negative shifts of temperature. Still the technique needed 10 transfer samples to obtain more than a 70%

of the slaves arrays properly corrected (that occurs at ΔT=-20ºC). Regarding OSC and GLSW, they exhibited a similar behaviour in the sense they experienced difficulties to correct the shifts of temperature. Note that both techniques needed 4 transfer samples to have any slave instrument correction accepted, for the closest temperature shift (ΔT=±10ºC). In any case, none of these techniques reached the 70% of accepted calibration transfers, even for no temperature shifting. Again, PDS presented the best performance, since the technique provided the highest number of acceptable slave corrections, using the lesser number transfer samples to build the calibration model and minimizing the RMSEP error contribution due to the temperature shift direction. For instance, PDS only needed 5 transfer samples to obtain more than 70% of the corrected slave arrays accepted in the range of temperature shifts that goes from ΔT=-20ºC to ΔT=20ºC.

VI.4. DISCUSSION

The reason why PDS performed better corrections than DS is that PDS creates local corrective models for each of the channels of the slave array, whereas DS generates a single global model, lesser flexible and complex. This seems to be so also for OSC and GLSW. In addition to this, PDS detected which channels of the master array (within a window) were more correlated to the particular channel on the slave array, down-weighting the contribution to the correction of the non-important channels. As a consequence, the number of transfer samples between master and slave arrays needed to achieve the same error level tended to be lower for PDS. That suggests that the piece-

wised extensions of OSC and GLSW may outperform the results obtained from the global versions of the algorithms, although this discussion is beyond the scope of this paper.

The performance of a calibration model with a high degree of complexity is directly related with the availability of a large number of samples. Effectively, as we know from figure 62(a-d), an increment on the number of transfer samples provides, up to a point, an enhancement of the corrected RMSEP. This improvement is reflected on the structure of the calibration transfer models (Table 4), where the parameters that govern the sample transformations are gradually modified until reaching saturation. The reason for error saturation on the corrected slave arrays can be deduced from the selection of the calibration transfer sample subset, shown in Table 3. Basically, for a certain number of selected samples we start to find samples that belong to a previously acquired category (substance and concentration). In consequence, no new information is added to the transfer models and the error of prediction for the corrected slave arrays cannot decrease significantly. The transition to error saturation is faster when the option for selecting the transfer samples is Method 2. That occurs because it includes a representative of each of the categories present on the calibration set (with the exception of the air samples) before adding sample replicates, while Method 1 discards three sample categories. In reference to the calibration transfer models, those methods that performed data correction before to build the calibration model (GLSW and OSC) exhibited their best results employing the

sample subset method 1, whereas those methods that applied data correction after the creation of the calibration model (DS and PDS) showed their best performance for the sampling subset method 2.

A special comment deserves the asymmetry in sensor response with respect to temperature shift. Revisiting the results of figure 63 (a-d) we observe that an increase on the temperature shift forces an increment on the model's specifications (see Table 5). Interestingly, the asymmetry showed by the $RMSP_S$ for opposite temperature shift positions is also present on the parameter values of all the calibration transfer techniques. This is in agreement with the results obtained in Fig. 61 for a direct calibration transfer between instruments shifted in temperature, where the higher prediction errors were found towards positive temperature shifts. The asymmetry on the error due to temperature shifting was produced because the uncorrected slave array response tends to saturate to the highest voltage level (10 V) for any substance and concentration, as review in Fig. 59. Projecting the response of test set samples of a slave array shifted towards negatives increments of temperature (ΔT=-50ºC) on a PCA model built from the calibration set of a master array (Fig.60b) we see that these samples approximate to the master array response to air. Taking that result as a reference we can estimate the lower bound for the uncorrected slave array substituting the slave array samples by air measurements of the master array. That gives rise to a lower error bound around the 68 ppm. Towards positive temperature shifts, no saturation on the uncorrected slave array

response is produced, so the test samples tend to spread on the PCA space and the error is continuously increasing.

VI.5. CONCLUSIONS

In the present study, it was demonstrated that the effect of temperature shifts between homologous MOX sensor arrays leads to invalid calibration transfers featured with low predictive performance and direction-dependent error magnitudes. To overcome instrument dissimilarities, the use calibration transfer is required. Among the four different calibration techniques used in this chapter, the Piece-wise Direct Standardization procedure showed the best performance in reducing the slave array prediction error for any temperature shift direction and using fewer transfer samples. This result was first explored inspecting the corrected $RMSEP_S$ and confirmed using statistical method based on the error's bias-variance trade-off. The main advantage of the PDS method lied in its ability to correct individually each of the slave instruments channels through the use of multivariate local models, fact that provided less complexity and more flexibility to whole calibration transfer model.

CHAPTER VII

CONCLUSIONS OF THIS THESIS

In this dissertation we have studied the role of sensor diversity and redundancy in odour information encoding. Also, we have used these properties of the sensor arrays to address some of the open problems in artificial olfaction, namely sensor failure, feature selection, and calibration transfer.

To this end, we designed and built an advanced prototype of electronic nose based on an array of MOX gas sensors, and inspired by the architecture of the olfactory epithelium. We considered sensor diversity as the number of distinct sensor types present in a sensor array, and sensor redundancy the average number of sensor copies along the different sensor types. We proposed to increase the diversity of our sensor array combining different types of MOX sensors along with a modulation of their operating temperatures, and its sensor redundancy by using multiple copies for each sensor type and modifying the sensor's measurement circuits (voltage dividers) with different load resistances. Noteworthy, we implicitly linked sensor diversity to sensor features that caused variations on the array response due to chemical interaction. Similarly, sensor redundancy was related to sensor features that not provided any new chemical information to the array response but decreased the contribution of sensor. We considered these types of sensor diversity and redundancy as structural, in the sense that they were

present in the array by construction. We showed that structural sensor diversity and redundancy tended to increase, respectively, the ability of our sensor array to discriminate odours, and to estimate odour concentration. Tough, these claims deserve some comments. Sensor diversity couldn't increase indefinitely the performance of the sensor array. A progressive increment of the array size (for a given size of the calibration set of samples) eventually leads to bad estimations of the prediction model parameters, and thus, to overfitting. On the other hand, the capacity of sensor redundancy to enhance odour concentration estimation depended on the nature of sensor noise. Independent sensor noise was efficiently rejected from the sensor array, whereas common sources of sensor noise fixed the limit for noise reduction.

At a higher level of abstraction, the separation between diverse and redundant features in our sensor array was actually more diffuse. The reason for that was a product of three factors. First factor was sensor response correlation. Different commercial sensor types exhibited very similar responses to a set of odours. The same happened for adjacent sensor responses along the temperature modulation profile on a single sensor unit. In these cases, sensor features that we first considered as diverse were, in fact, redundant. Second factor was related to sensor response variability within the same sensor type. A modification of the sensor's measuring circuit using different load resistors altered the dose-response curve of the sensor. As we showed elsewhere, an increment on the array response variability caused by a better odour quantity mapping tended to increase the

coding power of the sensor array. From this point of view, different load resistors should be considered diverse features, instead of redundant. We believe that only equivalent sensor features belonging to different sensor copies can be considered strictly redundant. Third, sensor diversity and redundancy were not absolute array magnitudes. Simple datasets, composed of few and very distinct odour samples, doesn't take advantage of the potential sensor diversity of the array, so the major part of sensor features can be regarded as redundant. On the contrary, as the complexity of the dataset increases, sensor diversity becomes highlighted, and the level of sensor redundancy decreases. Therefore, data characteristics determine the degree of similarity between sensor features. At this point, we were in conditions to suggest functional definitions for sensor diversity and redundancy based on sensor feature clustering. Our proposal was to group sensor features according to their contribution to the variance of a dataset. In particular, we considered as similar sensor features those than spanned the same angle in the loading space of PCA decomposition. Thus, sensor diversity was defined as the number of clusters, and sensor redundancy as the average number of sensor features along the clusters. We believe that these definitions actually captured the essence of sensor diversity and redundancy, since sensor features that exhibit a similar behaviour are clustered regardless the physical sensor units they stemmed from.

The second half of the thesis treated the applications of sensor diversity and redundancy in machine olfaction. First application was robustness to sensor damage. We asked ourselves under which conditions sensor redundancy could bear a massive turn-off of

sensors units in terms of data model performance. We found that not only the level of sensor redundancy, but the distribution of sensor faults across the different sensor types was crucial to prevent the degradation of data models. Such a fault distribution had to maintain the level of sensor diversity of the sensor array so as to bear the performance of data models. In other words, sensor fault distribution had to be independent of the sensor type so has to prevent the accumulation of damaged sensors in only a few sensor types. This result has an important implication for the design of large arrays of highly redundant sensors. It is recommendable to spread the different sensor types across the sensor array rather than distribute the sensors by areas of the same sensor type. Second application was feature selection in gas sensor arrays. We detected that this dimensionality reduction approach tended to optimize the sensor diversity of the array subset, disregarding sources of sensor redundancy. We identified this issue as a potential weak point of the approach, since sensor redundancy counteracts to some degree the effect of noise, and should be considered somehow in sensor array optimization. We proposed to include a feature extraction stage based on PLSR multivariate regression within the feature selection process to both compress the redundant sensor information and minimize the curse of dimensionality. This strategy was employed to enhance a feature selection search performed with Genetic Algorithms. In particular, we wanted to optimize operational sensor temperatures of an array of MOX gas sensors modulated in temperature for odour mixture discrimination. The optimal solution consisted in a set of temperature clusters spread along the different sensor types. These clusters were defined by a central sensor

temperature, which we took as a cluster representative, and its adjacent sensor temperatures. Sensor array optimization conducted only using the cluster representatives produced substantially worse results that employing all the cluster elements. This fact reinforced our idea that sensor response correlation was just another facet of sensor redundancy. Finally, we explored the application of instrument standardization techniques (DS, PDS, OSC, and GLSW) to transfer calibration models between e-noses. More specifically, we corrected global temperature shifts between instruments in temperature modulated sensor arrays. This task was realized exploiting the high degree of sensor redundancy exhibited by our sensor array, at two different levels. First level of redundancy was achieved by simple instrument replication (we employed 12 copies of an array of 3 different MOX gas sensors). We took advantage of this type of sensor redundancy to perform multiple instrument standardizations, warranting the generality of the results. Second level of redundancy was obtained from correlations on the sensor's waveform responses between master and shifted instruments. Our results showed that PDS was the best technique for rectifying instrumental differences. The reason for that was that PDS sought the most correlated sensor features between instruments within a region, and related them by means of local transformations. That gave rise to simple and flexible calibration transfer models, with a high capacity to generalize sample transfer beyond the transfer sample set. In contrast, the other techniques provided global and complex instrument transformations that usually leaded to invalid calibration transfer models.

CHAPTER VIII

RESUMEN DE LA TESIS

VIII.1. INTRODUCCIÓN

La nariz electrónica (e-nose) es un instrumento de propósito general para la detección química de olores. Este instrumento está inspirado en los sistemas olfativos naturales, donde la discriminación de los olores se realiza sin necesidad de receptores altamente especializados. En lugar de esto, los sistemas olfativos naturales extraen la información de los olores a través de un conjunto de receptores pobremente selectivos, organizados de manera convergente. Tal arquitectura de detección permite combinar de las respuestas de las diferentes unidades de la matriz de receptores, dando lugar a representaciones particulares para diferentes estímulos olfativos. Este enfoque de la detección química, basada en la codificación de olores por parte de una población de receptores en conjunto, tiene como principal ventaja que es más robusta y eficiente que la codificación de olores llevada a cabo por cualquiera de sus elementos individuales.

Una población de receptores obtiene su máximo rendimiento en la codificación olores al combinar los beneficios de la diversidad y la redundancia sensorial. Por *diversidad sensorial* entendemos los diferentes tipos de sensores que son responsables de incrementar la variabilidad de la población a un conjunto de olores. Del mismo modo, por la *redundancia sensorial* nos referimos al promedio de sensores replicados en una

población. El papel de la redundancia sensorial es proveer robustez a la codificación del olor contra el daño sensorial y el ruido. Esta gran variedad de tipos de receptores junto con su destacado su número son características fundamentales de los sistemas olfativas. Lamentablemente, la nariz electrónica tradicional suele contar con un número limitado de sensores, con respuestas muy correlacionadas con los estímulos olfativos. Varias estrategias para mejorar la representación del olor usando matrices de sensores de gas se basan incrementar la diversidad y la redundancia sensorial. Sin embargo, sólo muy recientemente la implementación de estas estrategias en plataformas de detección química ha sido tecnológicamente viable.

El objetivo de este trabajo consiste en desarrollar una de estas matrices de nueva generación para investigar las ventajas de representar estímulos olfativos mediante codificación poblacional. En particular, proponemos construir un sistema de detección química basado en una matriz de óxido metálico (MOX) sensores de gas, y dotados de un alto grado de diversidad sensorial y redundancia. Proponemos usar esta arquitectura de detección de bio-inspirada junto técnicas de reconocimiento de patrones estadísticos para hacer frente a algunos de los problemas sin resolver en olfacción artificial. Entre otros, esta tesis aborda los siguientes temas: optimización de la temperatura en matrices de sensores modulados por éste parámetro, robustez al daño sensorial para matrices altamente redundantes, y, de transferencia de calibración entre narices electrónicas.

VIII.2. LA NARIZ ELECTRÓNICA

El amplio poder discriminatorio demostrado por el olfato biológico para la detección química de olores es la fuente de inspiración de la olfacción artificial (Persaud and Dodd, 2000). La olfacción artificial (una simulación automatizada del sentido del olfato) es una aplicación emergente de la ingeniería que tiene como objetivo detectar, identificar o cuantificar los olores. El instrumento icónico de la olfacción artificial tiene como nombre llama nariz electrónica. La nariz electrónica está formada por un conjunto de sensores parcialmente selectivos, combinado con un sistema de reconocimiento de patrones capaz de determinar ciertas propiedades de olor, tales como la identidad, la composición y la concentración (Gardner and Bartlett, 1994a).

VIII.2.1. Tecnologías de sensores

En olfacción artificial se utilizan diferentes tecnologías de sensores para la detección de gases. Entre ellas figuran los sensores óxido metálico (MOX), los polímeros conductores, (CP), los transistores de óxido metálico (MOSFET), las microbalanzas de cuarzo (QCM), los sensores de onda acústica superficial (SAW) y los sensores ópticos (Arshak et al, 2004). A pesar de las diferencias tecnológicas, todos estos tipos de sensores tienden a ser poco selectivos, sufrir derivas y envenenamientos, y ser sensibles a gases interferentes o a modificaciones ambientales (cambios de humedad y la temperatura).

En este resumen incluimos información más detallada sobre los sensores MOX, pues son la base de nuestro sistema de detección químico. El principio de funcionamiento del

sensor MOX se basa en su cambio de la conductividad en respuesta a un gas (Albert and Lewis, 2000, Barsan et al., 2007). Las principales ventajas de los sensores MOX son sus respuesta rápida y sus pequeños tiempos de recuperación, así como su alta sensibilidad (Pearce et al., 2003). Sin embargo, exhiben selectividades pobres, tienden a tener un alto consumo de energía y sufren de envenenamiento irreversible cuando se exponen a compuestos sulforosos (Dickinson et al., 1998).

La selectividad del sensor MOX depende de su temperatura de funcionamiento, ya que este parámetro gobierna la cinética de las reacciones de redox que tienen lugar en su superficie (Clifford and Tuma, 1983a; Clifford and Tuma, 1983b). La relación existente entre temperatura y selectividad puede explotarse mediante técnicas de modulación de temperatura que permiten aumentar la información discriminatoria proporcionada por el sensor (Lee and Reedy, 1999; Benkstein et al., 2009; Rogers et al., 2011; Rogers et al., 2012). Existen dos estrategias para la modulación en temperatura: los transitorios térmicos y los ciclos de temperatura (Gutierrez-Osuna et al., 2003).

VIII.2.2. Generación de volátiles

Las técnicas de generación de volátiles más empleadas en olfacción artificial son el barrido del espacio de cabeza, los tubos de permeación, los burbujadores, los sistemas estáticos y la dilución de sustancias volátiles en un flujo de gas portador (Pearce et.al, 2003). Estás técnicas son más o menos efectivas en su función dependiendo de las especificaciones requeridas a nuestro sistema. Por ejemplo, el espacio de barrido de

cabeza no es recomendable cuando se desea controlar de manera fina la concentración de muestra de volátil, como tampoco lo son los sistemas estáticos sin esperamos conseguir muestras de olores de forma continuada.

En este apartado, explicamos el método de dilución de un volátil en un flujo de gas portador, pues nuestro sistema de generación de volátiles está inspirado en él. Esta técnica consiste en diluir un flujo odorante de concentración conocida en una corriente de gas portador (Mandayo et al., 2003). Una vez que se alcanza el estado de equilibrio de fluidos dentro de la cámara de medición, la concentración de odorante es igual a la razón entre el flujo odorante y el caudal total de la corriente. Este método proporciona concentraciones estables, pero requiere un diseño consciente del circuito de fluido para evitar tiempos transitorios excesivos hasta alcanzar el estado estacionario de la concentración.

VIII.2.3. Procesado del señal

Las técnicas de reconocimiento de patrones permiten caracterizar la respuesta multivariante de un conjunto de sensores con el fin de detectar, identificar y cuantificar los olores. Procesar la señal de estos sensores es necesario para obtener tanto buenos descriptores olfativos como predicciones fiables para tales descriptores. El procesado de datos suele concebirse como en serie de etapas ordenadas en el tiempo (Gutierrez-Osuna, 2002): pre-procesado (Gardner et al, 1998), reducción de dimensionalidad (Marco and

Gutierrez-Galvez, 2012). Predicción (Gutierrez-Osuna, 2003) y validación (Ripley, 1996; Efron and Tibshirani, 1993)..

VIII.2.4. Grandes matrices de sensores

La redundancia de un conjunto de sensores puede ser incrementada replicando los diferentes tipos de sensor de la matriz de sensores en grandes cantidades. Sin embargo, no ha sido hasta hace poco que la construcción de estas grandes matrices de sensores ha sido tecnológicamente posible. En la siguiente sección, se presentan cuatro prototipos de nariz electrónica basados en grandes conjuntos de sensores homogéneos.

Estas narices electrónicas de nueva generación utilizan las tecnologías de sensores ópticos o poliméricos. La primera de estas grandes matrices de sensores, es un sistema de detección basado en un conjunto óptico de alta densidad (Dickinson et al, 1999), con miles de sensores en forma de pequeñas perlas de tres clases discretas (Nilo Rojo / poli, Rojo Nilo / sílice y Sensidye) dispersos en toda la cara de una fibra óptica grabada. Otra gran matriz basada en sensores de gas ópticos consiste en un conjunto de sensores cuya capa sensible es continua y está formada por indicadores de color (ZnTTP, MnTTP, CoTPP y PtTTP) disueltos en una matriz de PVC (Di Natale et al., 2009). Los sensores poliméricos también se han utilizado para el desarrollo de grandes matrices de sensores de gas (Gardner et al., 2009). Un ejemplo es de esto es un sistema de olfacción artificial que combina 3 matrices replicadas de 300 sensores compuestos por material polimérico conductor polímero de material compuesto conductor (24 tipos de polímeros) con dos

columnas remanentes recubiertas con compuestos polares y no polares. Finalmente, el último sistema de medida que vamos a presentar está compuesto por una matriz a gran escala de 16.384 polímeros conductores de 24 clases diferentes (Bernabei et al., 2012).

VIII.2.5. Nuestra matriz de sensores

Nuestro sistema de detección química comprende dos bloques: el bloque de medida y, el sistema de transporte de volátiles.

El sistema de medida, se encarga de la adquisición y el almacenamiento de la información química de los compuestos volátiles obtenidos de sensores MOX. Este bloque incluye la matriz de sensores, y la electrónica para el control de fuente de alimentación del sensor y para polarizar los circuitos de medida. El sistema de adquisición de datos está formado por los sensores de gas, una placa de medida, dos multiplexores y una tarjeta de adquisición de datos. Utilizamos 8 tipos diferentes de sensores MOX proporcionados por las casas comerciales FIGARO (TGS-2600, TGS-2602, TGS-2610, TGS-2620) y FIS (SB-11B-00, SB-1500, SB-41 a 00, SB-AQ1-04), con 12 repeticiones para cada tipo. Estos 96 sensores se colocan en placa de medición de 8 columnas y 12 filas. Cada columna es independiente de los otros y corresponde a la alimentación de un tipo de sensor. El circuito básico de medida de nuestro sistema es el divisor de tensión. Cada unidad de sensor se mide a través de una batería de 16 resistencias de carga (0.10K, 0.25K, 0.40K, 0.87K, 1.30K, 3.01K, 6.19K, 9.09K, 21.00K, 30.01K, 40.20K , 51.10K, 68.10K, 82.5K, 90.90K, 105.K). Los divisores de

tensión se construyen por medio de un módulo con dos multiplexores de alta velocidad Estos multiplexores permiten conmutar la conexión de los sensores a las resistencias de carga. El punto de conexión entre los multiplexores se toma para adquirir la respuesta del sensor. Este proceso se realiza utilizando una tarjeta de adquisición de datos.

El bloque de potencia y control comprende dos fuentes independientes de energía y una placa de control hecho a mano. El circuito básico para la distribución de energía de la placa de control consta de un amplificador operacional conectado a la terminal de puerta de un transistor de potencia PMOS. El control se realiza mediante la comparación de la señal digital proporcionada por un DAQ en el terminal de entrada negativo de la OA con una señal de referencia constante de 2.5V en el positivo. Los sensores MOX se modulan en temperatura mediante perfil de rampa de voltaje generada por una fuente DC, mientras que los diferentes divisores de tensión están polarizados a 10 V usando otra fuente de alimentación de DC.

La función del sistema de generación de volátiles es generar mezclas de olores a diferentes concentraciones y transmitirlos a la cámara de sensor. El sistema de transporte de volátiles incluye un generador de compuestos volátiles, dos distribuidores de gas, una batería de 8 electro-válvulas, y una cámara de medida de aluminio. El generador de los compuestos volátiles se basa en la evaporación controlada de compuestos líquidos en un flujo de gas. Después del generador de compuestos volátiles, uno de los distribuidores de

gas divide el flujo de odorante en 8 flujos iguales (uno por cámara tipo canal de sensores). Otras configuraciones de distribución de flujo son posibles mediante el uso de las electro-válvulas. A la salida de la cámara de sensores, los 8 flujos correspondientes a cada canal de sensores se unifican usando el segundo distribuidor de gas.

VIII.2.6. Bases de datos

Usando nuestro sistema hemos adquirido tres bases de datos. La primera de ellas contiene las respuestas matriz de sensores a 7 concentraciones diferentes de acetona distribuidos a lo largo de 3 décadas de concentración (10, 50 100 500, 1000, 5000 y 10000 ppm). La segunda, comprende las lecturas de la matriz de sensores a 6 concentraciones diferentes (0, 20, 40, 60, 80, 100 y 120 ppm) de 3 sustancias puras (etanol, acetona y butanona.). Por último, la última base de datos consiste en las respuestas de la matriz de sensores a las mezclas binarias de etanol, acetona y butanona en el rango de 0 a 120 ppm de cada substancia pura. Los experimentos se diseñaron para tener una transición desde un primer analito a segundo analito en seis pasos, para cada uno de 3 combinaciones binarias de los 3 analitos.

VIII.3. DIVERSIDAD SENSORIAL Y REDUNDANCIA

El sistema olfativo es el ejemplo arquetípico de una matriz sensorial que codifica la información de los estímulos químicos utilizando una vasta población de estímulos sensoriales (Friedrich and Stopfer, 2001; Korsching, 2002; Miura et al., 2012; Buck and Axel, 1991). La razón por la evolución ha seleccionado la codificación de estímulos

mediante poblaciones de sensores para adquirir está vinculado a su robustez. La combinación de gran número de receptores con una arquitectura altamente convergente da lugar al fenómeno emergente de la hiper-agudeza sensorial (Bialek, 1987). Dos formas de hiper-agudeza están presentes en los receptores olfativos (Pearce et al., 2001). La primera de ellas está relacionada con la variabilidad de respuestas de los receptores de población (diversidad sensorial) y es responsable de mejorar en la estimación de la cualidad del olor (Buck and Axel, 1991). El segundo tipo de hiper-agudeza es producto de la gran cantidad de copias que existe para los diferentes tipos de receptores (redundancia sensorial), y mejora en la estimación de la cantidad del olor (Drongelen, 1978; Boeckh and Ernst, 1987; Duchamp-Viret et al., 1989; Shier, 2004).

Este capítulo se centra en el estudio de la diversidad de sensor y redundancia en nuestra matriz de sensores de gas. En primer lugar, mostramos fuentes de diversidad estructural sensor y redundancia presente en nuestra matriz. Después ilustramos que la diversidad de sensor y redundancia soportan la codificación de la información olfativa en matrices de sensores de sensores. Finalmente proponemos una definición más general de diversidad y redundancia en matrices de sensores.

VIII.3.1. Diversidad y redundancia en nuestra matriz

En este apartado, mostramos una variedad de ejemplos de cómo la diversidad de sensores y la redundancia mejoran en cierta medida la calidad de las predicciones obtenidas a

partir de una matriz de sensores de gas. En particular, comprobamos esto para las diferentes fuentes de diversidad estructural y redundancia de nuestro sistema de medida.

Empezamos con la diversidad sensorial. Al incrementar en número de la variabilidad del conjunto de respuestas de los sensores, ya fuera mediante el uso de sensores diferentes o mediante la técnica de modulación de temperatura de los sensores, la capacidad de predicción de nuestro sistema de detección química tiende mejorar. Esto lo chequeamos mediante la tasa de clasificación de un clasificador cuadrático (para el caso de diferentes sensores) y usando el área bajo la curva ROC (para el caso de modulación de temperatura). También, comprobamos que existe una relación inversa entra la diversidad sensorial y la correlación de la respuesta de los sensores, analizando los *loadings* de la descomposición PCA, para el caso de modulación en temperatura. En cuanto a la redundancia de sensores, estudiamos como el error de predicción de concentración debido a la presencia de ruido independiente tiende a disminuir al promediar la respuesta de sensores (para el caso copias de sensores) u optimizar la respuesta de la matriz trabajando en condiciones de máxima sensibilidad (para el caso de las diferentes resistencias de carga)

VIII.3.2. Codificando la información olfativa

Hemos visto de una manera intuitiva cómo la diversidad y redundancia sensorial soportan la codificación de la información de olores en nuestra matriz de sensores. Ahora, presentamos un enfoque más formal para abordar esta cuestión sobre la base de

estadísticas y medidas de Teoría de la Información. Aquí tratamos de evaluar capacidad de codificación para las matrices de sensores dotados con diferentes grados de diversidad sensorial y estudiamos en profundidad el papel de la redundancia sensorial en la reducción de ruido.

Para el caso de diversidad sensorial, calculamos la Información Mutua de un conjunto de sensores virtual al que dotamos con dos niveles de variabilidad en la respuesta. El primer nivel de diversidad viene dado por el rango receptivo molecular de los sensores (RR). El segundo, con las variaciones de las curvas dosis-respuesta que presenta la población de sensores. En nuestro experimento, vamos incrementando paulatinamente el número de sensores de la población. Observamos que, si nuestra matriz de sensores sólo tiene uno de los dos niveles de diversidad (tener diferentes RRs), tiende a codificar peor la información olfativa que si tiene ambos niveles. Por otro lado, podemos intuir dos tipos de codificaciones olfativas: Una basada en optimizar las respuestas de los sensores a una serie de estímulos odoríferos dados. Esta codificación estaría basada en la identificación de los componentes puros que forman parte del olor, y sería típica sistemas olfativos naturales. Otra, que se basaría en codificar los olores en función de cómo los sensores responda a su concentración, y aparecía en sistemas de detección química artificiales.

En referencia a la redundancia de sensores, trabajamos con dos aproximaciones diferentes: Agregación de sensores y optimización de la matriz. La agregación de

sensores la estudiamos a partir de métodos estadísticos. En esencia, comprobamos que la respuesta ruidosa del agregado de sensores disminuye con el número de sensores agregados. Sin embargo, está disminución depende de la naturaleza del ruido de los sensores y su nivel de independencia. También, ponemos en evidencia la existencia de fuentes de ruido común en nuestra matriz de sensores. Respecto a la optimización de la matriz, realizamos un análisis de la Información de Fisher obtenida usando diferentes resistencias de carga para codificar la concentración de un analito en condiciones ruidosas (ruido Gaussiano de media 0). Vemos que encontrar la resistencia de carga que optimiza la Información de Fisher para cada concentración equivale trabajar en condiciones de máxima sensibilidad del divisor de tensión. Esta solución es mejor que el simple promediado de sensores.

VIII.3.3. Definición funcional de la diversidad y la redundancia

En la introducción de esta tesis doctoral, definimos la diversidad sensorial como el número de diferentes tipos de sensores responsable de provocar la variabilidad de respuesta de sensores a matriz a una colección de olores; y la redundancia sensor, como el número promedio de copias de sensores en una población. Observamos que las definiciones anteriores implican una agrupación de los receptores de matriz de acuerdo con un criterio de similitud. De esta manera, los grupos de receptores similares se consideran del mismo tipo. El número de grupos de sensores corresponde entonces a la diversidad sensor de la matriz, y el número promedio de receptores a lo largo de las agrupaciones a su redundancia sensor.

Para caracterizar la diversidad y la redundancia, se propone un método para estimar el grado de diversidad de sensor y redundancia de una serie de sensores basados en la agrupación de sus unidades sensoriales. Más específicamente, se realiza un agrupamiento por el ángulo según los *loadings* de un PCA de los datos de los sensores. Nuestro razonamiento es el siguiente. Tenemos en cuenta que un modelo PCA de los datos es una proyección de éstos originales sobre un nuevo conjunto de ejes correspondientes a los vectores propios de la matriz de covarianza de los datos (las direcciones en el espacio de características donde los datos varían más). Estos vectores propios expresados en los ejes originales son llamados generalmente los *loadings* del modelo PCA. Los sensores de la matriz que explican la varianza de los datos de manera similar contribuyen de manera similar a los *loadings*. Por lo tanto, las características de los sensores que son redundantes tienden a abarcar el mismo ángulo sólido en el espacio los *loadings* y ser agrupados en el mismo clúster. Del mismo modo, el número direcciones "eficaces" que agrupan el conjunto características representan su diversidad sensor.

VIII.4. ROBUSTEZ AL FALLO SENSORIAL

El envejecimiento, el envenenamiento, y el fallo eléctrico son las principales causas para el fallo sensorial en una matriz de sensores de gas. El fallo sensorial constituye una desventaja en detección química porque degrada los resultados de los modelos de predicción formados en ausencia estos fallos. Para asegurar predicciones fiables, los sensores dañados deben ser reemplazados por sensores libres de fallos y la matriz tiene que ser recalibrada, lo cual es un proceso largo y costoso. Un enfoque posible para evitar

el efecto pernicioso fallo sensorial consiste en explotar la información redundante obtenida a partir de grandes matrices de sensores. Este enfoque se inspira en la redundancia sensorial masiva mostrada por el epitelio y el bulbo olfativo (Bozza and Kauer, 1998, Firesten, 2001). Sólo unas pocas matrices de sensores de gas dotadas con un gran número de unidades receptoras se han fabricado hasta la fecha (Dickinson et al, 1999; Di Natale et al., 2009; Gardner et al., 2009; Bernabei et al., 2012). Nuestra hipótesis es que la distribución de sensores dañados a través de los tipos de sensores y no sólo el nivel de redundancia es la clave para hacer que el sistema robusto al fallo sensorial. El objetivo de este capítulo es estudiar el efecto de la distribución de sensores dañados en la degradación del rendimiento de un sistema conjunto de sensores, para diferentes escenarios de fallo (fallo de sensores dependiente e independiente) y tipos de fallo (envejecimiento, envenenamiento y fallo eléctrico).

VIII.4.1. Materiales y métodos

Para realizar esta tarea, utilizamos los datos experimentales de nuestra matriz altamente redundante de sensores MOX modulados en la temperatura. Recordamos que nuestra matriz esta dotada con dos niveles de redundancia: 1) 12 réplicas de cada tipo de sensor para un total de 96 sensores, y 2) 16 resistencias de carga para medir cada uno de los sensores. Esto hace un total de 1.536 medidas por segundo. Los datos experimentales usados provienen de la base de datos II.

Con el fin de determinar la degradación del rendimiento del sistema se llevan a cabo dos experimentos en los que las unidades sensoriales se ven obligadas a fallar, considerando dos escenarios diferentes de distribución de fallo del sensor. En el primer experimento, se caracteriza la evolución de la diversidad del sistema y la redundancia para un fallo progresivo de unidades sensoriales. Para ello, usamos la definición funcional de la diversidad y la redundancia que propusimos en el capítulo II. El segundo experimento se diseña para determinar específicamente la degradación del rendimiento de los modelos predictivos. El sistema está capacitado para separar el etanol, acetona y butanona a diferentes concentraciones usando un modelo que combina PCA y LDA. Las muestras de test se corrompen sintéticamente por medio de tres tipos diferentes de tres tipos diferentes de fallos (fallo eléctrico, envenenamiento y variación de la sensibilidad del sensor). Para evaluar la tolerancia de la matriz contra el fallo del sensor, se utiliza una medida de la separación de las clases de olor tales como la puntuación de Fisher, ya que proporciona una medida mucho más sensible que la clasificación.

VIII.4.2. Resultados y discusión

Para caracterizar nuestra serie de sensores en términos de diversidad y redundancia, se realiza un experimento en el que eliminamos al azar unidades sensoriales mientras se monitorea el número de grupos activos restantes (diversidad) y el número medio de unidades sensoriales por clúster activo (redundancia). Consideramos clústeres activos aquellos que transmiten información discriminatoria. Para determinar qué clústeres están todavía activos, definimos un umbral fijando el porcentaje de unidades sensoriales vivas

en clúster dentro de un grupo por debajo del cual el clúster ya no está activo. Para el caso independiente, la diversidad del sistema se mantiene en un nivel alto para cualquier nivel de umbral hasta que decae abruptamente cuando el porcentaje de sensores dañados alcanza el umbral. A continuación, la diversidad cae abruptamente. Esto es debido a que aproximadamente todos los clústeres se inactivan al mismo tiempo al alcanzar el valor de umbral. Para el caso dependiente, la diversidad decae de paulatinamente en torno al valor de umbral. Este comportamiento es coherente con la manera diferente en que se retiran las unidades sensoriales cuando consideramos dependientes. Cada sensor físico contiene un número unidades sensoriales adyacentes, es decir que es probable muchas pertenezca al mismo clúster. En consecuencia, el fallo de cada sensor físico se concentra en un número reducido de clústeres. Esto explica la distribución asimétrica de unidades sensoriales defectuosas entre clústeres y por lo tanto la inactivación progresiva de las agrupaciones. Si estudiamos ahora de la redundancia, vemos que ésta disminuye progresivamente en ambos escenarios, observándose un comportamiento casi lineal. Este comportamiento se mantiene para los valores más altos del umbral en ambos escenarios, mientras que para valores bajos del umbral el escenario dependiente se aleja de la linealidad. Esto sucede para valores bajos de la redundancia. La causa de este fenómeno parece ser las diferentes distribuciones de terminación de clústeres en los dos escenarios.

En el segundo experimento se estudia la evolución del Fisher Score en términos del número de sensores dañados para los 3 tipos de fallo y los 2 escenarios de unidades

sensoriales dañadas. Los resultados muestran que para cualquier tipo de fallo en el sensor, el rendimiento es mucho más robusto en el escenario independiente que en la dependiente. En las curvas de escenarios independientes, el FS se mantiene sin casi ninguna pérdida hasta que un 60-80% de los sensores dañados y cae abruptamente después de eso. Esto muestra un alto comportamiento robusto para esta distribución de las fallas. Las curvas del escenario dependiente degradan suavemente. Esto hace que el sistema mucho menos robusto para la misma cantidad de fallo del sensor. En cuanto a los tipos de fallo, el fallo eléctrico es la más leve de los fallos ya que el sistema es capaz de lidiar mejor con él que con los otros dos fallos para ambos escenarios. Por el contrario, el envejecimiento es el tipo de fallo más grave para la matriz de sensores. Estos resultados muestran que un cambio de sensibilidad de los sensores tiene un impacto negativo más fuerte sobre la capacidad del sistema para diferenciar los olores que un sensor insensible que siempre proporciona el mismo valor.

Nuestros resultados muestran que el rendimiento de nuestra matriz es radicalmente diferente dependiendo de la distribución de los defectos sensoriales. Vemos que ésta obtiene el mejor rendimiento cuando las unidades sensoriales defectuosas se distribuyen uniformemente a través de los diferentes tipos de sensores. También, que el rendimiento de la matriz disminuye cuando las unidades sensoriales defectuosas se concentran en algunos tipos de sensores.

Esta diferente degradación del rendimiento puede ser explicado observando los resultados del experimento sobre caracterización de la diversidad y la redundancia. Comprobamos que el nivel de redundancia de la matriz es prácticamente igual para los dos escenarios de daño sensorial. Esto significa que, sorprendentemente, la diferencia en el rendimiento en ambos escenarios no es directamente debido al nivel de redundancia de la matriz. Hemos visto que los dos escenarios exhiben una notable diferencia entre el nivel de diversidad del sistema en ambos escenarios. Esto muestra claramente que la diferencia en el rendimiento del sistema bajo ambos escenarios es debido al nivel de la diversidad que el sistema es capaz de mantener en cada nivel del proceso de daños sensor.

Finalmente, podemos adquirir una mayor compresión de los efectos diferenciales de cada fallo mediante el estudio de la proyección PCA-LDA de los datos. Todos los fallos provocan un encogimiento más un corrimiento de la proyección de los datos de test en este espacio. Además de esto, el envenenamiento incrementa la dispersión dentro de clase datos. Sumado a estos dos efectos, el envejecimiento añade una distorsión del patrón proyectado. En consecuencia, el orden de fallos según lo dañinos que resultan la estabilidad de los patrones de olores obtenidos con el sistema es, de menos a más: fallo eléctrico, envenenamiento y envejecimiento.

VIII.5. SELECCIÓN DE CARACTERÍSTICAS

Una posible estrategia para aumentar la selectividad de los sensores MOX consiste en modificar su temperatura operativa. Este parámetro modifica la sensibilidad del sensor a

través de olores, y por lo tanto, el grado de selectividad de un sensor de gas MOX cuando se expone a una mezcla de olores (Clifford and Tuma, 1983a; Clifford and Tuma, 1983b).

En este apartado presentamos otra posible aproximación para la discriminación de olores usando matrices de sensores MOX moduladas en temperatura. Nuestro método se basa en el marco teórico establecido por los autores Pearce y Sánchez-Montañés (Pearce 2000, Pearce and Sanchez-Montanes, 2003) para optimizar el rendimiento de detección de los sistemas de detección química, cuyo principal objetivo consiste en maximizar el Número de Características Olfativas Discriminables (N_O), un parámetro semejante a una relación señal ruido del sistema. La principal contribución de nuestro trabajo consiste en el uso de una versión mejorada de su método para hacer frente a grandes conjuntos de datos con sensores no lineales y redundantes. En particular, proponemos el uso de regresión de mínimos cuadrados parciales (PLSR) tanto para linearizar la transformación que relaciona el espacio de los olores con el espacio de los olores, como para el olor al reducir la dimensionalidad del espacio de los sensores. Adicionalmente, proponemos reformular el cálculo del volumen que ocupa el ruido en el espacio de los sensores. El método se basa en computar el determinante de la matriz del ruido.

VIII.5.1. Materiales y métodos

Utilizamos la respuesta de 3 de sensores pertenecientes a nuestro sistema de detección química (TGS-2602 y TGS-2610, y TGS-2620, de la casa comercial Figaro Inc.), modulados en temperatura con un perfil rampa (de 0 a 5 V durante 90 segundos). Para

adquirir la respuesta de los 3 sensores se conecta cada uno de a una resistencia de carga de 6.1 KΩ, en configuración de medio puente. Medimos la tensión de salida de los sensores al ser expuestos a 6 concentraciones diferentes de etanol y acetona (0, 20, 40, 60, 80,100 y 120 ppm) y sus mezclas lineales (20-100, 40-80, 60-60, 80-40, 100-20 ppm), obtenidas de combinar las bases de datos I y 2. Por lo tanto, el total de las mediciones por muestra olor es 300 (3 tipos de sensores x 100 temperaturas).

N_O se calcula después de realizar una regresión PLSR que relaciona la respuesta de los sensores con la composición de las muestras. Este parámetro se obtiene dividiendo el volumen del espacio de los olores visto desde el espacio de los sensores (V_S), entre el volumen de ruido de los sensores (V_N). V_S, en el espacio de los scores de la PLSR, se computa como el determinante de la matriz sensibilidad reducida $\hat{S}$. Esta matriz, a su vez, puede conocerse a partir de la matriz de regresión (Q). V_N es proporcional al determinante de la matriz del ruido.

Hemos realizado tres experimentos usando los datos previamente descritos. El primer experimento (I) ilustra el método para dos unidades de sensor MOX (TGS-2610, y TGS-2620). En un segundo experimento (II) buscamos la mejor combinación binaria de las temperaturas de dos unidades de MOX (TGS-2610, y TGS-2620). Para ello, debemos regularizar el parámetro N_O, dividiéndolo por su matriz el número de condición de $\hat{S}$, para hacerlo robusto a colinearidad de la respuesta de los señores de la matriz. En el

tercer experimento (III), se modela la resistencia de tres sensores MOX a diferentes temperaturas como respuesta a mezclas de gases binarias (TGS-2602, TGS-2610, y TGS-2620). Encontramos el conjunto óptimo de temperaturas que maximiza la separación de olores para un espacio de olores simulado combinando nuestra metodología con una selección de características basada en algoritmos genéticos.

VIII.5.2. Resultados y discusión

Los resultados del primer experimento estiman que Número de Características Olfativas Discriminantes (N_O) es aproximadamente de 248, para un número de condición de la matriz de sensibilidad reducida $\hat{S}$ de 4.6. Si comparamos las áreas ocupadas por el volumen accesible por los sensores y el volumen ocupado por el ruido, vemos que este resultado es una buena aproximación para N_O. En relación con el segundo experimento, calculamos de N_O, Cond ($\hat{S}$), y N_O/Cond ($\hat{S}$), para las combinaciones por parejas de las temperaturas de los sensores. De acuerdo con una selección de características basada sólo en el parámetro N_O, las mejores temperaturas para separar las muestras de olores están más allá de los 250 º C, para ambos sensores. Sin embargo, estos resultados son espurios y son debidos a un mal condicionamiento de las matrices $\hat{S}$, tal y como podemos saber al calcular a partir de su número de condición. Tras regularizar N_O, encontramos que las mejores temperaturas están alrededor de 250ºC para la unidad de TGS-2610 y 340ºC para el TGS-2620. El valor de N_O en este punto es 384. Por último, en el experimento III realizamos una optimización de la temperatura para mejorar la discriminación de las mezclas de etanol y acetona. Esta optimización temperatura se realiza sobre respuestas de

sensores simulados modeladas a partir de las lecturas de los sensores TGS-2602, TGS-2610, y TGS-2620. Más específicamente, se genera un espacio de sensores que se corresponde a un espacio de los olores de 9 muestras: [80-40; 80-60; 80-80; 60-40; 60-60; 60-80; 40-40; 40-60; 40-80]. Sin realizar ninguna selección de características el valor de N_O para esta base de datos simulada es de N_O=32. Combinado múltiples repeticiones de algoritmos genéticos (5000) con nuestro método de selección, obtenemos que el valor final de N_O es de 236.

En nuestra opinión, la principal limitación del método original consiste en que éste no es aplicable en una base de datos cuyo número de sensores supere al número olores puros. Por lo tanto, parte de la información discriminante proporcionada por el conjunto de sensores simplemente no puede ser utilizada. Para superar este problema hemos propuesto usar métodos de regresión multivariante (tales como PLSR) para disminuir la dimensionalidad del espacio de los sensores, combinado las características del sensor más correlacionadas. Así el parámetro N_O se calcular sobre un espacio de sensores reducido, cuya matriz de sensibilidad ha sido linearizada y que, además, presenta una mejor relación señal a ruido. Como mejora adicional del método calculamos el determinante de la matriz del ruido para conocer el volumen del ruido en el espacio de sensores. De esta manera volumen de ruido es computado teniendo en cuenta que éste puede co-variar para diferentes combinaciones de sensores.

Otra de las mejoras clave de nuestra versión del método de selección de características consiste en la regularización N_O. Esta regularización se realiza simplemente dividiendo N_O por Cond (s). Números de condición grandes involucran transformaciones mal definidas. Esto significa que incluso tolerancias leves en las muestras del espacio olores causan grandes diferencias de respuesta en el espacio de los sensores. Cond ($\hat{S}$) se relaciona con el grado de ortogonalidad de los vectores fila de la $\hat{S}$. Matrices con vectores fila casi ortogonales tienden a tener condiciones números cercanos a 1. Notamos que, en consecuencia, N_O y N_O / Cond ($\hat{S}$) convergen al mismo valor en dichas condiciones. Así que las temperaturas de los sensores más discriminativos (que son los que proporcionan la respuesta más "ortogonal" a los olores) quedan realzadas.

Como comentario final, creemos interesante recalcar que nuestra optimización de temperaturas de sensor ha llevado a resultados análogos a los que se obtendría imitando la arquitectura del epitelio olfativo. Siguiendo la analogía, los diferentes glomérulos (clústeres de temperatura) codifican el olor, mientras que los sensores redundantes dentro de cada grupo (respuestas del sensor a temperaturas adyacentes) mejorar la estimación de la calidad del olor.

VIII.6. TRANSFERENCIA DE CALIBRACIÓN

Los cambios en la temperatura de trabajo impiden la transferencia de calibración directa entre los instrumento (Lin, 1998). Este tema cobra una gran importancia cuando tratamos con matrices de sensores de gas de óxido metálico modulados en temperatura (Lee and Reedy, 1999), en los que un cambio global en el perfil de temperatura nominal del sensor

perfil modifica drásticamente la forma de onda de respuesta del sensor. Una metodología conveniente para superar este problema consiste en usar técnicas de estandarización instrumental (Wang and Veltkamp, 1991) para corregir el cambio de temperatura comparando estas matrices con una matriz de referencia (desde ahora matrices esclava y maestra, respectivamente) calibrada para un conjunto completo de las condiciones experimentales y un perfil adecuado de temperatura.

Hemos identificado cuatro preguntas abiertas importantes para la transferencia de calibración entre narices electrónicas. **(i)** Las narices electrónicas pueden ajustar los parámetros de funcionamiento de sus sensores a fin de aumentar su sensibilidad a diferentes compuestos. Por lo tanto, las diferencias entre instrumentos que son debidas a las tolerancias existentes entre sus parámetros operacionales deben corregirse en consecuencia. **(ii)** Para realizar una transferencia de calibración eficiente, ésta debe ejecutarse usando un subconjunto limitado de experimentos en los instrumentos de esclavos. Hasta dónde sabemos, ningún estudio sistemático comparativo del rendimiento de diferentes técnicas de transferencia de calibración con respecto al número de muestras de transferencia ha sido realizado para narices electrónicas. **(iii)** Los modelos de calibración continua (regresores) proporcionan una medida más sensible del rendimiento de la transferencia de calibración de modelos de calibración discretas (clasificadores). Sin embargo, en la literatura sólo se puede encontrar modelos de clasificación transferidos de un instrumento a otro. **(iv)** Es necesario definir un criterio claro para aceptar o rechazar

una transferencia de calibración en función de su rendimiento. En este capítulo, tratamos de aportar soluciones que resuelvan estas cuatro preguntas abiertas.

VIII.6.1. Materiales y métodos

Hemos explorado el problema de transferencia de calibración para matrices de sensores de óxido de metal modulados en temperatura cuando se produce entre ellas un cambio global temperatura. Para realizar este estudio, hemos utilizado un conjunto de tres tipos diferentes de sensores semiconductores de óxido metálico Figaro (TGS2600, TGS2610, TGS2620) replicados 12 veces. Los 36 sensores fueron expuestos durante 900 segundos a tres analitos (etanol, acetona, 2-butanona) a los seis concentraciones diferentes (20, 40, 60, 80, 100, 120) ppm además de aire sintético (base de datos II). La lectura de los sensores se realiza a través de una resistencia de carga (R_L = 6,1 KΩ) en una configuración de medio puente. La temperatura de los sensores es modulada con un perfil de rampa que va desde la temperatura ambiente hasta 495 ° C ± 5 ° C [20] en un período de 90 segundos. Los experimentos con niveles de concentración de 0, 40, 80 y 120 ppm conforman el conjunto de calibración, mientras que los que tienen niveles de concentración de 20, 60, 100 ppm) se utilizan para probar los modelos de calibración. La ventana de temperatura seleccionada utilizado para la calibración de los instrumentos de maestros era [200-300] ºC.

En todos los experimentos, uno de los conjuntos de tres sensores se utiliza como instrumento maestro para encontrar un modelo de calibración (una regresión PLS) y el

resto de los conjuntos como instrumentos para estudiar la transferencia de calibración. En un estudio exhaustivo que incluye 132 combinaciones de instrumentos maestro-esclavo, evaluamos la calidad de la transferencia de calibración obtenida de varias técnicas de normalización de instrumentos. Estas técnicas son: Estandarización Directa (DS), Estandarización Directa por partes (PDS), Ponderación por Mínimos Cuadrados (GLSW) y Corrección Ortogonal del Señal (OSC). Nuestro interés fundamental consiste en encontrar la mejor técnica de trasferencia de calibración en función de número de muestras transferidas (en el rango de 1 a 12) y el desplazamiento global de temperatura ($\Delta T = 0°C, \pm 10°C, \pm 20°C, \pm 30°C, \pm 40°C, \pm 50$ °C).

Para realizar este estudio, es necesario crear los diferentes modelos PLS de calibración; seleccionar las muestras a transferir entre instrumentos maestros y esclavos; y optimizar los parámetros de cada una de las técnicas de transferencia de calibración utilizadas. El número de variables latentes de los modelos de calibración se obtiene mediante una validación cruzada tipo LOBO (Leave One Block Out). Las muestras de transferencia entre modelos se pueden conseguir de dos maneras diferentes: ordenando las muestras que tienen más influencia (1) en la base de datos, o (2) en la creación de los modelos PLS de instrumento maestro. Finalmente, los parámetros de las técnicas de transferencia de calibración se optimizan minimizando el error cuadrático medio de calibración para el subconjunto de muestras transferidas entre instrumentos. Para aceptar o rechazar la

transferencia de calibración entre instrumentos utilizamos un método basado en la descomposición sesgo-varianza del error cuadrático medio de predicción.

VIII.6.2. Resultados y discusión

En este estudio, cada una de las repeticiones de matriz se utiliza como instrumento maestro para las otras repeticiones o como matriz esclavo de ser corregido por otra matriz maestra. La aplicación directa del modelo de calibración maestro en las matrices de esclavos conduce a altos errores de predicción. Como se puede esperar, este error aumenta a medida que se incrementa el cambio de temperatura entre instrumentos. Sin embargo, este efecto no es simétrico: los cambios hacia temperaturas más altas provocan una penalización mayor en el error de predicción que los cambios en la dirección opuesta. Después de la corrección de datos, los errores de predicción de las matrices de esclavas se reducen considerablemente. El grado de reducción del error depende de la cantidad de muestras transferidas y del cambio de la temperatura. Como tendencia general, los errores disminuyen gradualmente hasta la saturación a el número de muestras de transferencia aumenta, para cualquier cambio de temperatura y técnica de transferencia de calibración. DS y PDS obtienen los niveles más bajos de error de predicción, aunque PDS necesitan un menor número de muestras para alcanzar la saturación de error. OSC y GLSW exhiben unos valores más altos de error de predicción y transiciones más lentas a la saturación. En cuanto a la influencia del cambio de temperatura, observamos que los valores más bajos del error de predicción están sesgados hacia desplazamientos de temperatura negativos, para cualquier número de muestras de transferencia y técnica de

transferencia de calibración. Sin embargo, PDS demuestra ser la técnica más robusta frente a este efecto dependiente de la dirección.

Si consideramos los resultados de la prueba de contraste basada en la descomposición sesgo-varianza del error, vemos que ningún instrumento sin corregir pasa la prueba de aceptación de transferencia de calibración. Después de la transferencia de calibración, sólo un número de estos instrumentos supera los estrictos criterios de la prueba. Éste número depende de la cantidad de muestras de transferencia, del cambio de temperatura y de la técnica de transferencia de calibración aplicada. Una vez más, PDS presenta el mejor rendimiento, ya que la técnica proporciona el mayor número de correcciones de esclavos aceptables, usando un menor número de muestras para construir el modelo de transferencia de calibración y minimizado la contribución la contribución al error debida a la dirección de desplazamiento de la temperatura.

La razón por la PDS realizan mejores correcciones de DS es que PDS crea modelos correctivos locales para cada uno de los canales de la matriz del esclavos mientras que DS genera un solo modelo global, menos flexible y complejo. Este parece ser válido también para OSC y GLSW. Además de esto, PDS detecta que los canales de la matriz principal (dentro de una ventana) más correlacionados con el canal en particular en la matriz de esclavo, reduciendo la contribución de los canales poco importantes a la corrección. Como consecuencia, el número de muestras necesarias para lograr el mismo nivel de error entre la matriz maestra y esclava tiende a ser menor para PDS.

El rendimiento de un modelo de calibración con un alto grado de complejidad está directamente relacionado con la disponibilidad de un gran número de muestras. Efectivamente, nuestros resultados muestran que un incremento en el número de muestras de transferencia ofrece, hasta cierto punto, una mejora del error corregido. La razón de la saturación de error en las matrices esclavas corregidas se debe a que a partir de un determinado número de muestras de transferencia empezamos a encontrar muestras que pertenecen a una categoría que ya ha sido previamente adquirida (substancia y concentración). En consecuencia, no se añade nueva información a los modelos de transferencia y el error de predicción para las matrices esclavas corregidas no puede disminuir de manera significativa.

VIII.8. CONCLUSIONES DE LA TESIS

En esta tesis hemos estudiado el papel de la diversidad sensor y redundancia en la codificación de la información odorífera. Además, hemos utilizado estas propiedades de las matrices de sensores para abordar algunos de los problemas abiertos en la olfacción artificial, a saber, tolerancia al fallo sensorial, selección de características, y transferencia de calibración.

Para ello, hemos diseñado y construido un prototipo avanzado de nariz electrónica basada en un conjunto de sensores de gas MOX, e inspirado en la arquitectura del epitelio olfatorio. Consideramos la diversidad sensorial como el número de distintos tipos de sensores presentes en una matriz de sensores, y su redundancia como el número medio de

copias de sensores por tipo de sensor. Nos propusimos aumentar la diversidad de nuestra matriz de sensores combinando diferentes tipos de sensores MOX modulados en temperatura modulación, y su redundancia mediante el uso de múltiples copias para cada uno de los tipos de sensor y la modificación de sus circuitos de medida (divisores de tensión) con diferentes resistencias carga. Cabe destacar, que ligamos implícitamente la diversidad sensorial a las características de los sensores que provocaban variaciones en la respuesta de la matriz debidas a la interacción química entre los analitos y los sensores. Del mismo modo, relacionamos la redundancia sensorial con características que no proporcionaban ninguna información química nueva a la respuesta de la matriz, pero disminuían la contribución del ruido de los sensores. Consideramos este tipo de diversidad sensor y redundancia estructural, en el sentido de que estaban presentes en la matriz por construcción. Hemos mostrado que la diversidad y redundancia estructurales tendían a aumentar, respectivamente, la capacidad de nuestro conjunto de sensores para discriminar olores, y para estimar la concentración de estos. Sin embargo, estas afirmaciones merecen algunos comentarios. La diversidad sensorial no podría aumentar de manera indefinida el rendimiento de la matriz de sensores. Un incremento progresivo de la tamaño de la matriz (para un tamaño dado de la calibración conjunto de muestras) eventualmente conduce a malas estimaciones de los parámetros del modelo de predicción, y por lo tanto, a sobreajuste. Por otro lado, la capacidad de la redundancia sensorial para mejorar la estimación de la concentración de los olores depende de la naturaleza del ruido del sensor. El ruido sensorial independiente fue rechazado de

manera eficiente por la matriz de sensores, mientras que las fuentes comunes de ruido sensorial fijaron el límite para la reducción de ruido.

A un nivel más alto de abstracción, la separación entre características diversas y redundantes en una matriz de sensores fue en realidad más difusa. La razón para esto radica en tres factores. En primer factor fue la correlación entre respuestas de los sensores. Diferentes tipos de sensores comerciales exhibieron respuestas muy similares a un conjunto de olores. Lo mismo ocurrió para las respuestas de los sensores adyacentes a lo largo del perfil de modulación de la temperatura para un sensor individual. De este modo, características sensoriales que en un principio consideramos como diversas eran, de hecho, redundantes. El segundo factor, estaba relacionado con la variabilidad de la respuesta de un sensor dentro del mismo tipo de sensor. Una modificación del circuito de medida del sensor utilizando diferentes resistencias de carga altera la curva dosis-respuesta del sensor. Como ya demostramos, un incremento en la variabilidad de la respuesta de la matriz causada por una mejor cuantificación de la concentración del olor tiende a aumentar el poder de codificación de la matriz de sensores. Desde este punto de vista, diferentes resistencias de carga deben considerarse como características diversas, en lugar de redundantes. Creemos que solamente características equivalentes de los equivalentes pertenecientes a diferentes copias sensores pueden ser consideradas como estrictamente redundante. En tercer lugar, la diversidad sensorial y la redundancia no eran magnitudes absolutas de la matriz. Conjuntos de datos simples, compuestos por pocas y

muy distintas muestras de olor, no aprovechan el potencial de la diversidad del sensor de la matriz, por lo que la mayor parte de las características del sensor puede considerarse como redundantes. Por el contrario, al incrementar la complejidad de los conjuntos de datos, la diversidad sensorial queda resaltada y el nivel de redundancia del sensor disminuye. Así pues, la naturaleza de los datos determina el grado de similitud entre las características del sensor. Llegados a este punto, propusimos definiciones funcionales para la diversidad y la redundancia sensoriales basadas en la agrupación de las características de los sensores. Nuestra propuesta consistió en agrupar las características de los sensores en función de su contribución a la varianza del conjunto de datos. En particular, consideramos que características similares de sensores abarcan el mismo ángulo en el espacio de los loadings de una descomposición PCA. Por lo tanto, la diversidad sensorial se definió como el número de grupos de sensores obtenidos, y la redundancia como el número medio de características en estos grupos. Creemos que estas definiciones realmente capturan la esencia de la diversidad y redundancia sensoriales, puesto que las características de sensores que exhiben un comportamiento similar se agrupan con independencia a los sensores físicos de las que surgieron.

La segunda mitad de la tesis trata de las aplicaciones de la diversidad y redundancia sensoriales en olfacción artificial. La primera aplicación que tratamos fue la robustez al daño de sensores. Nos preguntamos bajo qué condiciones la redundancia sensorial podría soportar el daño sensorial en términos del rendimiento de los modelos predictivos

construidos a partir de datos sin fallos. Encontramos que no sólo el nivel de redundancia sensorial, sino también la distribución de fallos del sensor a través de los diferentes tipos de sensores eran cruciales para prevenir la degradación de modelos predictivos. Tal distribución de fallos tenía que mantener el nivel de diversidad de la matriz de sensores para mantener el rendimiento de los modelos. En otras palabras, la distribución de fallos tenía que ser independiente del tipo de sensor para evitar la acumulación de fallos en sólo unos pocos tipos de sensores. Este resultado tiene una implicación importante para el diseño de grandes conjuntos de sensores altamente redundantes. Es recomendable distribuir los diferentes tipos de sensores a través de la matriz en lugar de hacerlo por áreas del mismo tipo de sensor. La segunda aplicación fue selección de características en matrices de sensores de gas. Detectamos que este enfoque de reducción de dimensionalidad tendía optimizar la diversidad sensorial del subconjunto matriz de la matriz seleccionado, sin tener en cuenta las fuentes de la redundancia del sensor. Identificamos este problema como un potencial punto débil de esta aproximación, ya que la redundancia del sensor contrarresta en cierta medida el efecto del ruido, y debería considerarse de alguna manera en la optimización del conjunto de sensores. Hemos propuesto incluir una etapa de extracción de características basada en la regresión multivariante PLSR en el proceso de selección características para comprimir la información de los sensores redundantes y reducir al mínimo el problema de la maldición de la dimensionalidad. Esta estrategia fue empleada para mejorar una selección de características realizada con algoritmos genéticos. En particular, quisimos optimizar las

temperaturas de trabajos de una serie de sensores de gas MOX modulados en temperatura para una mejor discriminación de mezclas de dos olores. La solución óptima consistió en diferentes grupos de temperatura repartidos a lo largo de los sensores. Estos grupos se definían por una temperatura central, que tomamos como representante del clúster, y sus temperaturas adyacentes. La optimización de la matriz de sensores realizada utilizando sólo los representantes de cada clúster condujo a resultados sustancialmente peores que aquellos en los que se emplearon todos los elementos de los clústeres. Este hecho refuerza nuestra idea de que la correlación de la respuesta de sensores no es más que otra faceta de la redundancia del sensor. Finalmente, hemos explorado la aplicación de técnicas de estandarización de instrumentos (DS, PDS, OSC y GLSW) para transferir modelos de calibración entre narices electrónicas. Más específicamente, corregimos los cambios de temperatura globales entre instrumentos basados en matrices de sensores moduladas en temperatura. Esta tarea se realizó aprovechando el alto grado de redundancia sensorial exhibido por nuestra matriz de sensores, a dos niveles diferentes. En primer nivel de redundancia se logró mediante la simple replicación de instrumentos (se emplearon 12 copias de una matriz de 3 sensores diferentes de gas MOX). Aprovechamos de este tipo de redundancia para realizar múltiples estandarizaciones instrumentales, lo que justifica la generalidad de nuestros resultados. El segundo nivel de redundancia se obtuvo a partir de las correlaciones en la respuestas de la forma de onda del sensor entre el los instrumentos maestro y esclavo desplazado en temperatura. Nuestros resultados mostraron que PDS era la mejor técnica para rectificar diferencias

instrumentales. La razón para ello es que PDS buscó las características de los sensores más correlacionados entre los instrumentos, y las relaciona por medio de transformaciones locales. Eso dio lugar a modelos de transferencia de calibración simples, flexibles, y con una alta capacidad de generalizar la transferencia de muestras para experimentos no usados en el modelo de transferencia de calibración. Por el contrario, las otras técnicas crearon transformaciones globales y complejos, que por lo general con condujeron a modelos no válidos de transferencia de calibración.

CHAPTER IX

LIST OF PUBLICATIONS AND CONFERENCES

IX.1. PUBLICATIONS

IX.1.1. Journals

- **Fernández, L**., S. Marco, and A. Gutiérrez-Galvez. "Robustness to sensor damage of a highly redundant gas sensor array." *Sensors and Actuators B: Chemical* (2015).

- Ziyatdinov, Andrey, J. Fonollosa, **L. Fernández,** A. Gutiérrez-Gálvez, S. Marco, A. Perera. "Bioinspired early detection through gas flow modulation in chemo-sensory systems." *Sensors and Actuators B: Chemical* 206 (2015): 538-547.

- Ziyatdinov, Andrey, J. Fonollosa, **L. Fernández,** A. Gutiérrez-Gálvez, S. Marco, A. Perera. "Data set from gas sensor array under flow modulation." *Data in Brief* 3 (2015): 131-136.

- Fonollosa, Jordi, **L. Fernández**, R. Huerta, A. Gutiérrez-Gálvez, S. Marco. "Temperature optimization of metal oxide sensor arrays using mutual information." *Sensors and Actuators B: Chemical* 187 (2013): 331-339.

XIX.2. PARTICIPATION IN CONFERENCES

XIX.2.1. Oral

- **Fernández, L.**, A. Gutierrez-Galvez, and S. Marco. "Robustness to Sensor Damage of a Highly Redundant Gas Sensor Array." *Procedia Engineering* 87 (2014): 851-854.

- **Fernández, L.**, S. Guney, A. Gutiérrez-Gálvez, and S. Marco. "Calibration transfer in temperature modulated sensor arrays". Proceedings of the 15th International Symposium on Olfaction and Electronic Nose (ISOEN), Daegu (Korea), 2013.

- Gutiérrez-Gálvez, Agustín, **L. Fernández**, and S. Marco. "Study of sensory diversity and redundancy to encode for chemical mixtures." Olfaction and Electronic nose: Proceedings of the 14th International Symposium on Olfaction and electronic nose (ISOEN), New York (USA). Vol. 1362. No. 1. AIP Publishing, 2011.

- **Fernández, L.,** A. Gutiérrez-Gálvez, and S. Marco. "Gas sensor array system inspired on the sensory diversity and redundancy of the olfactory epithelium." *Procedia Engineering* 5 (2010): 25-28. ". In XXIV Eurosensors, Linz (Austria)

XIX.2.2. Poster

- **Fernández, L.**, A. Gutiérrez-Gálvez, and S. Marco. "Multi-way analysis of diversity and redundancy factors in large MOX gas sensor data." *Proceedings of 14th International Meeting on Chemical Sensors–IMCS*. Vol. 2012. 2012.

- **Fernández, L.,** A. Gutiérrez-Gálvez, J. Fonollosa, and S. Marco. "A biomimetic gas sensor array system designed to test computational olfaction models." *CHEMICAL SENSES*. Vol. 36. No. 1. OXFORD UNIV PRESS, 2011.

REFERENCES

Albert, Keith J., et al. "Cross-reactive chemical sensor arrays." *Chemical reviews* 100.7 (2000): 2595-2626.

Alkasab, Tarik K., Joel White, and John S. Kauer. "A computational system for simulating and analyzing arrays of biological and artificial chemical sensors." *Chemical senses* 27.3 (2002): 261-275.

Arshak, K., et al. "A review of gas sensors employed in electronic nose applications." *Sensor review* 24.2 (2004): 181-198.

Baby, R. E., M. Cabezas, and EN Walsöe De Reca. "Electronic nose: a useful tool for monitoring environmental contamination." *Sensors and Actuators B: Chemical* 69.3 (2000): 214-218.

Bailey, Arthur LPS, Anna Maria Pisanelli, and Krishna C. Persaud. "Development of conducting polymer sensor arrays for wound monitoring." *Sensors and Actuators B: Chemical* 131.1 (2008): 5-9.

Balaban, M. O., et al. "Transportability of data between electronic noses: mathematical methods." *Sensors and Actuators B: Chemical* 71.3 (2000): 203-211.

Barsan, N., D. Koziej, and U. Weimar. "Metal oxide-based gas sensor research: How to?." *Sensors and Actuators B: Chemical* 121.1 (2007): 18-35.

Bartlett, Phillip N., Joe M. Elliott, and Julian W. Gardner. "Electronic noses and their application in the food industry." *Food technology (USA)* 51.12 (1997):44-48.

Benkstein, K. D., et al. "Inducing analytical orthogonality in tungsten oxide-based microsensors using materials structure and dynamic temperature control." *Sensors and Actuators B: Chemical* 137.1 (2009): 48-55.

Bernabei, Mara, et al. "Large-scale chemical sensor array testing biological olfaction concepts." *Sensors Journal, IEEE* 12.11 (2012): 3174-3183.

Bialek, William. "Physical limits to sensation and perception." *Annual review of biophysics and biophysical chemistry* 16.1 (1987): 455-478.

Bishop, Christopher M. *Neural networks for pattern recognition*. Oxford university press, 1995.

Boeckh, J., and K-D. Ernst. "Contribution of single unit analysis in insects to an understanding of olfactory function." *Journal of Comparative Physiology A* 161.4 (1987): 549-565.

Bouveresse, E., and D. L. Massart. "Improvement of the piecewise direct standardisation procedure for the transfer of NIR spectra for multivariate calibration." *Chemometrics and intelligent laboratory systems* 32.2 (1996): 201-213.

Bozza, Thomas C., and John S. Kauer. "Odorant response properties of convergent olfactory receptor neurons." *The Journal of neuroscience* 18.12 (1998): 4560-4569.

Branca, Andrea, et al. "Electronic nose based discrimination of a perfumery compound in a fragrance." *Sensors and Actuators B: Chemical* 92.1 (2003): 222-227.

Brian D. Ripley. *Pattern recognition and neural networks*. Cambridge university press, 1996.

Brown, W. Michael, and Alex Bäcker. "Optimal neuronal tuning for finite stimulus spaces." *Neural computation* 18.7 (2006): 1511-1526.

Buck, Linda, and Richard Axel. "A novel multigene family may encode odorant receptors: a molecular basis for odor recognition." *Cell* 65.1 (1991): 175-187.

Carey, W. P., K. R. Beebe, and B. R. Kowalski. "Selection of adsorbents for chemical sensors arrays by pattern recognition." *Anal. Chem* 59 (1987a): 1529-1534.

Carey, W. Patrick, Kenneth R. Beebe, and Bruce R. Kowalski. "Multicomponent analysis using an array of piezoelectric crystal sensors." *Analytical chemistry* 59.11 (1987b): 1529-1534.

Chaiyboun, Ali, et al. "Modular analytical multicomponent analysis in gas sensor arrays." *Sensors* 6.4 (2006): 270-283.

Cheng, Z. J., et al. "An electronic nose in the discrimination of breath from smokers and non-smokers: a model for toxin exposure." Journal of breath research 3.3 (2009): 036003.

Clifford, P.K. and Tuma D.T., "Characteristics of Semiconductor gas sensors I. Steady state gas response", *Sensors and Actuators*, 3 (1982a) 233–254.

Clifford, P.K. and Tuma D.T., "Characteristics of Semiconductor gas sensors II. Transient response to temperature change", *Sensors and Actuators*, 3 (1982b) 255–281.

Covey, Ellen. "Neural population coding and auditory temporal pattern analysis." Physiology & behavior 69.1 (2000): 211-220.

Dickinson, Todd A., et al. "Current trends in artificial-nose technology." *Trends in Biotechnology* 16.6 (1998): 250-258.

Dickinson, Todd A., et al. "Convergent, self-encoded bead sensor arrays in the design of an artificial nose." *Analytical chemistry* 71.11 (1999): 2192-2198.

Di Natale, Corrado, Arnaldo D'Amico, and Fabrizio AM Davide. "Redundancy in sensor arrays." *Sensors and Actuators A: Physical* 37 (1993): 612-617.

Di Natale, Corrado, et al. "Human skin odor analysis by means of an electronic nose." *Sensors and Actuators B: Chemical* 65.1 (2000): 216-219.

Di Natale, Corrado, et al. "Lung cancer identification by the analysis of breath by means of an array of non-selective gas sensors." *Biosensors and Bioelectronics* 18.10 (2003): 1209-1218.

Di Natale, C., et al. "An artificial olfaction system based on the optical imaging of a large array of chemical reporters." *Sensors and Actuators B: Chemical* 142.2 (2009): 412-417.

Dragonieri, Silvano, et al. "An electronic nose in the discrimination of patients with asthma and controls." *Journal of Allergy and Clinical Immunology* 120.4 (2007): 856-862.

Drongelen, W. van. "Unitary recordings of near threshold responses of receptor cells in the olfactory mucosa of the frog." *The Journal of physiology* 277.1 (1978): 423-435.

Duchamp-Viret, Patricia, R. Duchamp, and M.Vigouroux. "Amplifying role of convergence in olfactory system a comparative study of receptor cell and second-order neuron sensitivities." *Journal of neurophysiology* 61.5 (1989): 1085-1094.

Duda, Richard O., Peter E. Hart, and David G. Stork. *Pattern classification*. John Wiley & Sons, 2012.

Efron, Bradley, and Robert J. Tibshirani. *An introduction to the bootstrap*. CRC press, 1994.

Eklöv, Tomas, Per Mårtensson, and Ingemar Lundström. "Enhanced selectivity of MOSFET gas sensors by systematical analysis of transient parameters." *Analytica Chimica Acta* 353.2 (1997): 291-300.

Fearn, Tom. "On orthogonal signal correction." *Chemometrics and Intelligent Laboratory Systems* 50.1 (2000): 47-52.

Feudale, Robert N., et al. "Transfer of multivariate calibration models: a review." *Chemometrics and Intelligent Laboratory Systems* 64.2 (2002): 181-192.

Figaro USA, http.//www.figarosensor.com/

Firestein, Stuart. "How the olfactory system makes sense of scents." *Nature* 413.6852 (2001): 211-218.

Fonollosa, Jordi, Alexander Vergara, and Ramón Huerta. "Algorithmic mitigation of sensor failure: Is sensor replacement really necessary?." *Sensors and Actuators B: Chemical* 183 (2013a): 211-221.

Fonollosa, Jordi, et al. "Temperature optimization of metal oxide sensor arrays using mutual information." *Sensors and Actuators B: Chemical* 187 (2013b): 331-339.

Frank, LLdiko E., and Jerome H. Friedman. "A statistical view of some chemometrics regression tools." *Technometrics* 35.2 (1993): 109-135.

Freund, Michael S., and Nathan S. Lewis. "A chemically diverse conducting polymer-based" electronic nose". *Proceedings of the National Academy of Sciences* 92.7 (1995): 2652-2656.

Friedman, Jerome H. "Regularized discriminant analysis." *Journal of the American statistical association* 84.405 (1989): 165-175.

Friedrich, Rainer W., and Mark Stopfer. "Recent dynamics in olfactory population coding." Current opinion in neurobiology 11.4 (2001): 468-474.

Fu, Qingbo, et al. "Short-wave near-infrared spectrometer for alcohol determination and temperature correction." *Journal of analytical methods in chemistry* 2012 (2012).

Gardner, Julian W. "Detection of vapours and odours from a multisensor array using pattern recognition Part 1. Principal component and cluster analysis." *Sensors and Actuators B: Chemical* 4.1 (1991): 109-115.

Gardner, Julian W., and Philip N. Bartlett. "A brief history of electronic noses." *Sensors and Actuators B: Chemical* 18.1 (1994a): 210-211.

Gardner, Julian W., et al. "A multisensor system for beer flavour monitoring using an array of conducting polymers and predictive classifiers." *Sensors and Actuators B: Chemical* 18.1 (1994b): 240-243.

Gardner, Julian W., and Philip N. Bartlett. "Performance definition and standardization of electronic noses." *Sensors and Actuators B: Chemical* 33.1 (1996): 60-67.

Gardner, J. W., et al. "The prediction of bacteria type and culture growth phase by an electronic nose with a multi-layer perceptron network." *Measurement Science and Technology* 9.1 (1998): 120-127.

Gardner, J. W., and P. N. Bartlett. "Electronic noses. Principles and applications." *Measurement Science and Technology* 11.7 (2000): 1087.

Geladi, Paul, and Bruce R. Kowalski. "Partial least-squares regression: a tutorial." *Analytica chimica acta* 185 (1986): 1-17.

Gosangi, Rakesh, and Ricardo Gutierrez-Osuna. "Active temperature programming for metal-oxide chemoresistors." *Sensors Journal, IEEE* 10.6 (2010): 1075-1082.

Gosangi, Rakesh, and Ricardo Gutierrez-Osuna. "Active temperature modulation of metal-oxide sensors for quantitative analysis of gas mixtures." *Sensors and Actuators B: Chemical* 185 (2013): 201-210.

Grate, Jay W., and Michael H. Abraham. "Solubility interactions and the design of chemically selective sorbent coatings for chemical sensors and arrays." *Sensors and Actuators B: Chemical* 3.2 (1991): 85-111.

Grosmaitre, Xavier, et al. "Odorant responses of olfactory sensory neurons expressing the odorant receptor MOR23: a patch clamp analysis in gene-targeted mice." *proceedings of the national Academy of Sciences of the United States of America* 103.6 (2006): 1970-1975.

Gutierrez-Osuna, Ricardo. *Signal processing and pattern recognition for an electric nose*. North Carolina State University, 1998.

Gutierrez-Osuna, Ricardo, H. Troy Nagle, and Susan S. Schiffman. "Transient response analysis of an electronic nose using multi-exponential models." *Sensors and Actuators B: Chemical* 61.1 (1999a): 170-182.

Gutierrez-Osuna, Ricardo, and H. Troy Nagle. "A method for evaluating data-preprocessing techniques for odour classification with an array of gas sensors." *Systems, Man, and Cybernetics, Part B: Cybernetics, IEEE Transactions on* 29.5 (1999b): 626-632.

Gutierrez-Osuna, Ricardo. "Pattern analysis for machine olfaction: a review." *Sensors Journal, IEEE* 2.3 (2002): 189-202.

Gutierrez-Osuna, R., A. Gutierrez-Galvez, and N. Powar. "Transient response analysis for temperature-modulated chemoresistors." *Sensors and Actuators B: Chemical* 93.1 (2003): 57-66.

Haddi, Z., et al. "A portable electronic nose system for the identification of cannabis-based drugs." *Sensors and Actuators B: Chemical* 155.2 (2011): 456-463.

Hansen, Thomas, Mikael Agerlin Petersen, and Derek V. Byrne. "Sensory based quality control utilising an electronic nose and GC-MS analyses to predict end-product quality from raw materials." *Meat science* 69.4 (2005): 621-634.

Hatfield, J. V., et al. "Towards an integrated electronic nose using conducting polymer sensors." *Sensors and Actuators B: Chemical* 18.1 (1994): 221-228.

Haug, M., et al. "Chemical sensors based upon polysiloxanes: comparison between optical, quartz microbalance, calorimetric, and capacitance sensors." *Sensors and Actuators B: Chemical* 11.1 (1993): 383-391.

Harun, FK Che, et al. "An electronic nose employing dual-channel odour separation columns with large chemosensor arrays for advanced odour discrimination." *Sensors and Actuators B: Chemical* 141.1 (2009): 134-140.

Heeger, Alan J. "Semiconducting and metallic polymers: the fourth generation of polymeric materials." *The Journal of physical chemistry B* 105.36 (2001): 8475-8491.

Hierlemann, Andreas, et al. "Polymer-based sensor arrays and multicomponent analysis for the detection of hazardous oragnic vapours in the environment." *Sensors and Actuators B: Chemical* 26.1 (1995): 126-134.

Hildebrand, John G., and Gordon M. Shepherd. "Mechanisms of olfactory discrimination: converging evidence for common principles across phyla." *Annual review of neuroscience* 20.1 (1997): 595-631.

Hierlemann, Andreas, and Ricardo Gutierrez-Osuna. "Higher-order chemical sensing." *Chemical reviews* 108.2 (2008): 563-613.

Huang, Xingjiu, et al. "Gas sensing behavior of a single tin dioxide sensor under dynamic temperature modulation." *Sensors and Actuators B: Chemical* 99.2 (2004): 444-450.

Ide, Junichi, Takamichi Nakamoto, and Toyosaka Moriizumi. "Development of odour-sensing system using an auto-sampling stage." *Sensors and Actuators B: Chemical* 13.1 (1993): 351-354.

Ikohura, Kousuke, and Joseph Watson. "The Stannic Oxide Gas Sensor." (1994).

Johansson, Roland S., and Ingvars Birznieks. "First spikes in ensembles of human tactile afferents code complex spatial fingertip events." Nature neuroscience 7.2 (2004): 170-177.

Khlebarov, Zdravko P., Any I. Stoyanova, and Diana I. Topalova. "Surface acoustic wave gas sensors." *Sensors and Actuators B: Chemical* 8.1 (1992): 33-40.

Kirkpatrick, Scott, C. Daniel Gelatt, and Mario P. Vecchi. "Optimization by simulated annealing." *science* 220.4598 (1983): 671-680.

Kohonen, Teuvo. "Self-organized formation of topologically correct feature maps." *Biological cybernetics* 43.1 (1982): 59-69.

Korsching, Sigrun. "Olfactory maps and odor images." Current opinion in neurobiology 12.4 (2002): 387-392.

Kunt, Tekin A., et al. "Optimization of temperature programmed sensing for gas identification using micro-hotplate sensors." *Sensors and Actuators B: Chemical* 53.1 (1998): 24-43.

Lee, Andrew P., and Brian J. Reedy. "Temperature modulation in semiconductor gas sensing." *Sensors and Actuators B: Chemical* 60.1 (1999): 35-42.

Lee, Andrew P., and Brian J. Reedy. "Application of radiometric temperature determination methods to semiconductor gas sensors." *Sensors and Actuators B: Chemical* 69.1 (2000): 37-45.

Lin, Jie. "Near-IR calibration transfer between different temperatures." *Applied spectroscopy* 52.12 (1998): 1591-1596.

Mandayo, G.G., et al. "Liquid petroleum gas sensor based on zinc oxide nanorods" *Sensors and Actuators B: Chemical* 95.1 (2003): 221-228.

Mandenius, Carl Fredrik, Thomas Hedman, and Bo Mattiasson. "An online sensor for monitoring of ethanol in beer." Journal of the Institute of Brewing 90.2 (1984): 77-80.

Marco, Santiago, and Agustín Gutiérrez-Gálvez. "Signal and data processing for machine olfaction and chemical sensing: a review." *Sensors Journal, IEEE* 12.11 (2012): 3189-3214.

Michalewicz, Zbigniew. *Genetic algorithms+ data structures= evolution programs*. Springer Science & Business Media, 2013.

Miura, Keiji, Zachary F. Mainen, and Naoshige Uchida. "Odor representations in olfactory cortex: distributed rate coding and decorrelated population activity." Neuron 74.6 (2012): 1087-1098.

Moore, D. S. "Instrumentation for trace detection of high explosives." *Review of Scientific Instruments* 75.8 (2004): 2499-2512.

Morris, H., and Schaeffer, J. P. "The Nervous system-The Brain or Encephalon. Human anatomy; a complete systematic treatise". *New York* (1953): Blakiston.

Muezzinoglu, Mehmet K., et al. "A sensor conditioning principle for odor identification." *Sensors and Actuators B: Chemical* 146.2 (2010): 472-476.

Nagle, H. Troy, Ricardo Gutierrez-Osuna, and Susan S. Schiffman. "The how and why of electronic noses." *Spectrum, IEEE* 35.9 (1998): 22-31.

Nakamoto, Takamichi, et al. "Improvement of identification capability in an odor-sensing system." *Sensors and Actuators B: Chemical* 3.3 (1991): 221-226.

Narendra, Patrenahalli M., and Keinosuke Fukunaga. "A branch and bound algorithm for feature subset selection." *Computers, IEEE Transactions on* 100.9 (1977): 917-922.

Niebling, Gerhard, and Rudolf Mu. "Design of sensor arrays by use of an inverse feature space." *Sensors and Actuators B: Chemical* 25.1 (1995): 781-784.

O'Connell, Manuela, et al. "A practical approach for fish freshness determinations using a portable electronic nose." Sensors and Actuators B: chemical 80.2 (2001): 149-154.

Ohnishi, M., et al. "A molecular recognition system for odorants incorporating biomimetic gas-sensitive devices using Langmuir-Blodgett films." *Sensors and Materials* 1 (1992): 53-60.

Ortega, Arturo, et al. "An intelligent detector based on temperature modulation of a gas sensor with a digital signal processor." *Sensors and Actuators B: Chemical* 78.1 (2001): 32-39.

Padilla, M., et al. "Poisoning fault diagnosis in chemical gas sensor arrays using multivariate statistical signal processing and structured residuals generation." *Intelligent Signal Processing, 2007. WISP 2007. IEEE International Symposium on*. IEEE, 2007.

Padilla, Marta, et al. "Fault detection, identification, and reconstruction of faulty chemical gas sensors under drift conditions, using Principal Component Analysis and Multiscale-PCA." *Neural Networks (IJCNN), The 2010 International Joint Conference on*. IEEE, 2010.

Pan, Leilei, and Simon X. Yang. "An electronic nose network system for online monitoring of livestock farm odors." Mechatronics, IEEE/ASME Transactions on 14.3 (2009): 371-376.

Pardo, M., et al. "Monitoring reliability of sensors in an array by neural networks." *Sensors and Actuators B: Chemical* 67.1 (2000): 128-133.

Pearce, T. C. "Computational parallels between the biological olfactory pathway and its analogue 'The Electronic Nose': Part I. Biological olfaction." *BioSystems* 41.1 (1997): 43-67.

Pearce, Timothy C., and Julian W. Gardner. "Predicting organoleptic scores of sub-ppm flavour notes: Part 2. Computational analysis and results." *Analyst* 123.10 (1998): 2057-2066.

Pearce, Tim C. "Odor to sensor space transformations in biological and artificial noses." *Neurocomputing* 32 (2000): 941-952.

Pearce, Tim, et al. "Robust stimulus encoding in olfactory processing: hyperacuity and efficient signal transmission." *Emergent neural computational architectures based on neuroscience*. Springer Berlin Heidelberg, 2001. 461-479.

Pearce, Tim C., et al., eds. *Handbook of machine olfaction: electronic nose technology*. John Wiley & Sons, 2003.

Perera, Alexandre, et al. "A portable electronic nose based on embedded PC technology and GNU/Linux: Hardware, software and applications." Sensors Journal, IEEE 2.3 (2002): 235-246.

Persaud, Krishna, and George Dodd. "Analysis of discrimination mechanisms in the mammalian olfactory system using a model nose.". *Nature* 299 (1982):352-355.

Phillips, Michael, et al. "Detection of lung cancer with volatile markers in the breath." *Chest Journal* 123.6 (2003): 2115-2123.

Pudil, Pavel, Jana Novovičová, and Josef Kittler. "Floating search methods in feature selection." *Pattern recognition letters* 15.11 (1994): 1119-1125.

Sánchez-Montañés, Manuel A., and Tim C. Pearce. "Why do olfactory neurons have unspecific receptive fields?." *Biosystems* 67.1 (2002): 229-238.

Schaller, Emmanuelle, Jacques O. Bosset, and Felix Escher. "'Electronic noses' and their application to food." *LWT-Food Science and Technology* 31.4 (1998): 305-316.

Schiffman, Susan Stolte, and Robert P. Erickson. "A psychophysical model for gustatory quality." *Physiology & Behavior* 7.4 (1971): 617-633.

Scorsone, Emmanuel, Anna Maria Pisanelli, and Krishna C. Persaud. "Development of an electronic nose for fire detection." *Sensors and Actuators B: Chemical* 116.1 (2006): 55-61.

Shaham, Oded, Liran Carmel, and David Harel. "On mappings between electronic noses." *Sensors and Actuators B: Chemical* 106.1 (2005): 76-82

Shepherd, G.M. A molecular vocabulary for olfaction". *Annals of the New York Academy of Sciences* (1987).

Shier, AND., Butler, J. and Lewis, R. Hole's Human Anatomy & Physiology, Boston: McGraw Hill, 2004

Shih, Chung-Hung, et al. "Real-time electronic nose based pathogen detection for respiratory intensive care patients." *Sensors and Actuators B: Chemical* 148.1 (2010): 153-157.

Shurmer, Harold V., and Julian W. Gardner. "Odour discrimination with an electronic nose." *Sensors and Actuators B: Chemical* 8.1 (1992): 1-11.

Sjöblom, Jonas, et al. "An evaluation of orthogonal signal correction applied to calibration transfer of near infrared spectra." *Chemometrics and Intelligent Laboratory Systems* 44.1 (1998): 229-244.

Snopok, B. A., and I. V. Kruglenko. "Multisensor systems for chemical analysis: state-of-the-art in Electronic Nose technology and new trends in machine olfaction." *Thin Solid Films* 418.1 (2002): 21-41.

Raman, Baranidharan, et al. "Designing and optimizing microsensor arrays for recognizing chemical hazards in complex environments." *Sensors and Actuators B: Chemical* 137.2 (2009): 617-629.

Raman, Baranidharan, et al. "A statistical approach to materials and selection for chemical sensor arrays", *Computional Methods for Sensor Material Selection*, Eds. New York: Springer-Verlag, 2009.

Rumelhart, David E., Geoffrey E. Hinton, and Ronald J. Williams. *Learning internal representations by error propagation*. No. ICS-8506. CALIFORNIA UNIV SAN DIEGO LA JOLLA INST FOR COGNITIVE SCIENCE, 1985.

Rogers, Phillip H., and Steve Semancik. "Feedback-enabled discrimination enhancement for temperature-programmed chemiresistive microsensors." *Sensors and Actuators B: Chemical* 158.1 (2011): 111-116.

Rogers, Phillip H., and Steve Semancik. "Development of optimization procedures for application-specific chemical sensing." *Sensors and Actuators B: Chemical* 163.1 (2012): 8-19.

Sharaf, Muhammad A., Deborah L. Illman, and Bruce R. Kowalski. *Chemometrics*. Vol. 82. John Wiley & Sons, 1986.

Tauler, Romà, Beata Walczak, and Steven D. Brown. *Comprehensive chemometrics: chemical and biochemical data analysis*. Elsevier, 2009.

Therrien, Charles W. *Decision estimation and classification: an introduction to pattern recognition and related topics*. John Wiley & Sons, Inc., 1989.

Tomic, Oliver, et al. "Recalibration of a gas-sensor array system related to sensor replacement." *Analytica Chimica Acta* 512.2 (2004): 199-206.

Tran, Vanessa H., et al. "Breath analysis of lung cancer patients using an electronic nose detection system." *Sensors Journal, IEEE* 10.9 (2010): 1514-1518.

Turing, Alan M. "Rounding-off errors in matrix processes." *The Quarterly Journal of Mechanics and Applied Mathematics* 1.1 (1948): 287-308.

Van Deventer, D., and P. Mallikarjunan. "Optimizing an electronic nose for analysis of volatiles from printing inks on assorted plastic films." *Innovative Food Science & Emerging Technologies* 3.1 (2002): 93-99.

Vergara, A., et al. "Optimised temperature modulation of metal oxide micro-hotplate gas sensors through multilevel pseudo random sequences." *Sensors and Actuators B: Chemical* 111 (2005): 271-280.

Vergara, A., et al. "Quantitative gas mixture analysis using temperature-modulated micro-hotplate gas sensors: selection and validation of the optimal modulating frequencies." *Sensors and Actuators B: Chemical* 123.2 (2007): 1002-1016.

Vergara, Alexander, et al. "Information-theoretic optimization of chemical sensors." *Sensors and Actuators B: Chemical* 148.1 (2010): 298-306.

Vergara, Alexander, and Eduard Llobet. "Sensor selection and chemo-sensory optimization: toward an adaptable chemo-sensory system." *Frontiers in neuroengineering* 4 (2011).

Vermeulen, Arthur, et al. "Coding of odour intensity in a sensory neuron." *BioSystems* 40.1 (1997): 203-210.

Vinje, William E., and Jack L. Gallant. "Sparse coding and decorrelation in primary visual cortex during natural vision." *Science* 287.5456 (2000): 1273-1276.

Walczak, B., E. Bouveresse, and D. L. Massart. "Standardization of near-infrared spectra in the wavelet domain." *Chemometrics and intelligent laboratory systems* 36.1 (1997): 41-51.

Wang, Yongdong, David J. Veltkamp, and Bruce R. Kowalski. "Multivariate instrument standardization." *Analytical chemistry* 63.23 (1991): 2750-2756.

Wang, Yongdong, Michael J. Lysaght, and Bruce R. Kowalski. "Improvement of multivariate calibration through instrument standardization." *Analytical Chemistry* 64.5 (1992): 562-564.

Wilke, Stefan D., and Christian W. Eurich. "Representational accuracy of stochastic neural populations." *Neural Computation* 14.1 (2002): 155-189.

Wilson, Denise M., Thaddeus Roppel, and Ronald Kalim. "Aggregation of sensory input for robust performance in chemical sensing microsystems." *Sensors and Actuators B: Chemical* 64.1 (2000): 107-117.

Wilson, D. M., et al. "Array optimization and preprocessing techniques for chemical sensing microsystems." *Sensors Update* 10.1 (2002): 77-106.

Yasufuku, Sachio. "Electroconductive polymers and their applications in Japan." *IEEE Electrical Insulation Magazine* 5.17 (2001): 14-24.

Yinon, Jehuda. "Peer reviewed: detection of explosives by electronic noses." *Analytical Chemistry* 75.5 (2003): 98-A.

Zaromb, S., and J. R. Stetter. "Theoretical basis for identification and measurement of air contaminants using an array of sensors having partly overlapping selectivities." *Sensors and Actuators* 6.4 (1984): 225-243.

APPENDIX A

THE FISHER SCORE

We used the Fisher Score in Chapter IV as a figure of merit to measure the performance of our sensor in discriminating C odour classes. This measure of pattern separability is computed using the following expression:

$$F_S = tr(S_B S_W^{-1}) \tag{A.1}$$

where S_W and S_B are, respectively the within and between class scatter matrices. S_W is obtained as the summa of the individual within scatter matrices.

$$S_W = \sum_{i=1}^{c} \sum_{y \in i} (y - m_{D_i})(y - m_{D_i})^T \tag{A.2}$$

where *y* are the samples belonging a class *i*, and m_{Di} their corresponding sample mean. To obtain S_B, we first compute the position of the centroid of our pattern of response, *m*:

$$m = \frac{1}{N} \sum_{i=1}^{c} n_i m_{D_i} \tag{A.3}$$

being N the total number of samples of the dataset, and n_i the number of samples of the class i. Then S_B is computed as the sum of the individual between scatter matrices respect the position of the centroid.

$$S_B = \sum_{1=1}^{c} n_i (m_{D_i} - m)(m_{D_i} - m)^T \tag{A.4}$$

Basically, the Fisher Score increases directly with S_B, and inversely with S_W. We can see intuitively this idea in Fig. 65.

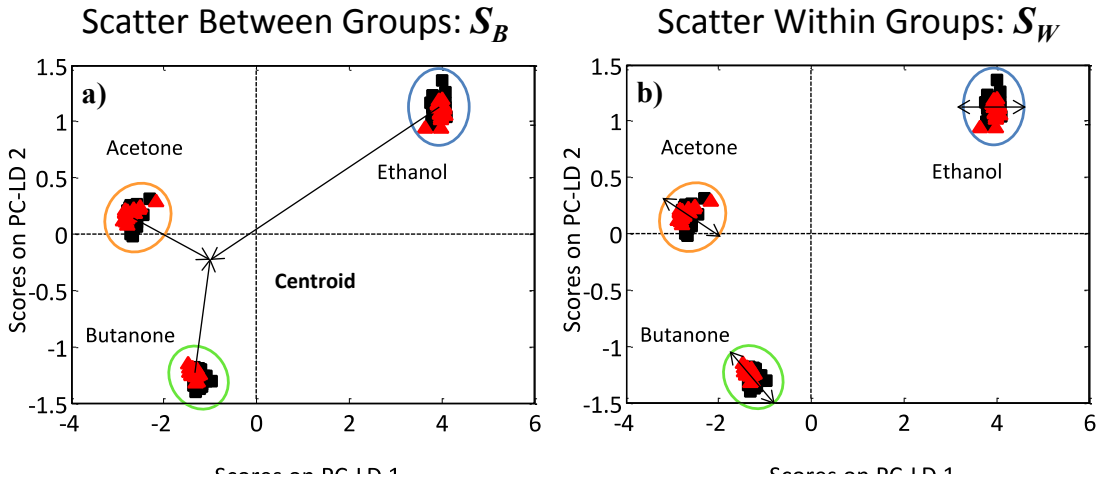

Fig. 65. Illustration of the measure of pattern separability using the FS. (a) Scatter between groups. (b) Scatter within groups.

APPENDIX B

LINEARIZATION OF THE SENSITIVITY MATRIX

Large arrays of sensors suffer from an inherent problem called 'the curse of dimensionality'. The origin of this problem is that the number of samples needed to accurately estimate the parameters of a random distribution on a given space grows exponentially with the dimensions of the space. In addition to this, chemical sensors (such as MOX sensors) usually show highly correlated responses when exposed to different odours. This fact gives rise to problems of collinearity on the array responses, which eventually can led to poorly discriminative datasets. To prevent these two problems, the dimensionality of the sensor space is generally deflated employing data decomposition algorithms, like Principal Component Analysis (PCA). An alternative approach, consist in the use of multivariate regression methods for dimensionality reduction, such as Partial Least Squares (PLS). The main advantage of this approach is that provides a linearized version of the sensitivity matrix $\hat{S}$ on this deflated sensor space.

In essence, what the PLS algorithm does is to seek the directions of maximum variance on the sensor space X (the latent variable scores, T) which are relevant for predicting samples of the odour space Y. Then, the concentrations of the pure compounds are regressed onto the latent variable scores:

$$TQ = Y \tag{B.1}$$

where Q is a regression matrix. The latent variable scores T can be considered as a new collection of sensors which mostly preserves the information of the original sensors space X. The relation between the previous regression matrix Q and the sensitivity matrix $\hat{S}$ on the reduced sensor space is obtained as follows: On the one hand, the linear transformation that relates the odour and the sensor scores spaces through the sensitivity matrix $\hat{S}$ is:

$$T^T = \hat{S}Y^T \tag{B.2}$$

On the other, an expression for the odour space samples Y^T in terms of the regression matrix Q and the latent variable scores T can be obtained by transposing both sides of equation (B.1):

$$Q^T T^T = Y^T \tag{B.3}$$

If we substitute the latter expression for Y^T in equation (B.2):

$$T^T = \hat{S}Q^T T^T \tag{B.4}$$

Thus, it is found that sensitivity matrix $\hat{S}$ in the latent variable space is the pseudo-inverse of the transposed regression matrix Q:

$$\hat{S} = (Q^T)^+ \tag{B.5}$$